

# **Finite Element-Based Computer Simulation of Motility, Sorting, and Deformation in Biological Cells**

By

Helen Hong Chen

A thesis  
presented to the University of Waterloo  
in fulfillment of the  
thesis requirement for the degree of  
Doctor of Philosophy  
in  
Civil Engineering

Waterloo, Ontario, Canada, 1998

© Helen Hong Chen 1998



**National Library  
of Canada**

**Acquisitions and  
Bibliographic Services**

**395 Wellington Street  
Ottawa ON K1A 0N4  
Canada**

**Bibliothèque nationale  
du Canada**

**Acquisitions et  
services bibliographiques**

**395, rue Wellington  
Ottawa ON K1A 0N4  
Canada**

*Your file Votre référence*

*Our file Notre référence*

**The author has granted a non-exclusive licence allowing the National Library of Canada to reproduce, loan, distribute or sell copies of this thesis in microform, paper or electronic formats.**

**The author retains ownership of the copyright in this thesis. Neither the thesis nor substantial extracts from it may be printed or otherwise reproduced without the author's permission.**

**L'auteur a accordé une licence non exclusive permettant à la Bibliothèque nationale du Canada de reproduire, prêter, distribuer ou vendre des copies de cette thèse sous la forme de microfiche/film, de reproduction sur papier ou sur format électronique.**

**L'auteur conserve la propriété du droit d'auteur qui protège cette thèse. Ni la thèse ni des extraits substantiels de celle-ci ne doivent être imprimés ou autrement reproduits sans son autorisation.**

0-612-30595-3

**The university of Waterloo requires the signatures of all persons using or photocopying this thesis.  
Please sign below, and give address and date.**

## **Abstract**

### **Finite Element-based Computer Simulation of Motility, Sorting and Deformation in Biological Cells**

Computer simulations are an efficient and powerful tool for investigating the complex processes involved in embryo morphogenesis. A survey of the literature shows that computer simulations have been applied at both the tissue level and the cell level. Here, a novel cell element is derived to model individual epithelial cells. Apical microfilament bundles, microtubules, intermediate filaments, adhesions and other cytoskeletal components are included in the model. The cell cytoplasm is assumed to be viscous. Each cell is allowed to undergo large deformations, but its area is kept constant using a Lagrange multiplier. Cells can rearrange and thus change the topology within the aggregate. This cell element is then used to model the behaviour of both homotypic and heterotypic cell aggregates.

In one set of simulations, a sheet of homotypic cells is subjected to large strains. Reaction forces on the edge of the sheet are calculated, and compared with analytical results. Significant shape changes and cell rearrangements are observed. The simulations show how bulk mechanical properties arise from sub-cellular structure, and provide a basis for sophisticated simulation models of an entire embryo.

In addition, heterotypic cell aggregates consisting of two kinds of cells are investigated. Important cell phenomena, including cell sorting, tissue spreading and checker-board formation, are simulated. Some hypotheses about the mechanisms of cell sorting and motility are tested. The simulation results agree with fundamental aspects of real cell behaviour. They also provide useful insights into the behaviour of embryonic cells during morphogenetic processes, and can serve as a guide to future experiments.

## **Acknowledgments**

To my supervisor, Dr. G. Wayne Brodland, for his profound knowledge in this discipline; for his inspiration and guidance during the time of this work, and for his true appreciation of the creation. Without him, I would not be possible to obtain this insight into the wonderful cell structure. I will never view the world in the same way.

To my father and mother, for their passion and devotion in seeking the truth and applying technology to make this world a better place to live; for their belief in me, their support, and mostly, their unconditional love. Without them, I would not be able to carry this far.

To my beloved husband, Richard, for his love, understanding and sacrifices; and for his support in every way. Without him, my life would not be complete.

To my brother, Pu, for his assistance and support in preparing this thesis, and for his companionship. To my colleague and special friend, Jim, for his great help during the past four years and for his friendship. Without them, my life would not be so colourful.

To all those who love me and support me so dearly in Canada and in China.

This research was funded by a Natural Science and Engineering Research Council (NSERC) grant to G. W. Brodland and an Ontario Graduate Scholarship grant to Helen Chen

**To The Creator and My Parents,  
From Whom Come Life, Love and Wisdom**

## TABLE OF CONTENTS

<b>Chapter 1 Introduction: Mechanics in Biology</b>	1
1.1 Embryos, Embryonic Tissues and Cells	2
1.1.1 Embryos	2
1.1.2 Embryonic Tissues	5
1.1.3 Cells	6
1.2 Mechanics of Biological Systems	9
1.2.1 Scales of Biological Systems	9
1.2.2 Computer Modeling of Biological Systems	11
1.3 Problem Statement and Main Results	14
<b>Chapter 2 Cell Micro-mechanics</b>	17
2.1 Plasma Membrane	18
2.2 Junctions	19
2.3 Adhesion Molecules	20
2.4 Cytoplasm	25
2.5 Circumferential Microfilament Bundles	27
2.6 Microtubules	28
2.7 Intermediate Filaments	29
2.8 Micromechanical Interactions	30
<b>Chapter 3 Simulation Models of Embryonic Tissues and Cells</b>	31
3.1 Tissue-level computer simulations	31
3.1.1 Studies of neurulation	31
3.1.2 Studies of gastrulation	35
3.1.3 Studies of cardiac looping	38
3.2 Cell-level computer simulations	41
3.2.1 Weliky and Oster model	42

3.2.2 Sulsky <i>et al.</i> model	44
3.2.3 Graner model	45
3.2.4 Graner and Glazier model	46
<b>Chapter 4 Finite Element Model of Cells</b>	<b>51</b>
4.1 Cell topology and Voronoi tessellation	51
4.2 Cell element	58
4.3 Rules of cell neighbour changes	65
4.4 Computer implementation	66
<b>Chapter 5 Cell Rearrangement and Bulk Mechanical Properties of Epithelial Cell Sheets</b>	<b>68</b>
5.1 Definition of parameters	69
5.2 Annealing process	72
5.3 Analytical formulation of the bulk mechanical properties	73
5.4 Simulation results	77
5.4.1 Cell sheet stretched at a constant strain rate	77
5.4.2 Factors affecting the bulk mechanical properties of cell sheet	81
Effect of the density	81
Effect of contractile force $F_c$	85
Effect of strain rate	85
5.4.3 Isotropy of the cell sheet	88
5.4.4 Necking phenomena	88
5.4.5 Cell sheet subjected to a constant lateral force	92
5.5 Discussion	93
<b>Chapter 6 Mechanisms of Cell Sorting and Tissue Spreading</b>	<b>96</b>
6.1 Reaggregate of dissociated cells	96

<b>6.2 Postulated cellular basis for cell sorting and tissue spreading</b>	<b>98</b>
<b>6.2.1 The differential adhesion hypothesis</b>	<b>99</b>
<b>6.2.2 Other hypothesis</b>	<b>100</b>
<b>The differential surface contraction hypothesis</b>	<b>102</b>
<b>The specific adhesion hypothesis</b>	<b>102</b>
<b>The differential chemotaxis hypothesis</b>	<b>103</b>
<b>6.3 Computer simulations of heterotypic cell aggregates</b>	<b>104</b>
<b>6.3.1 Definition of Parameters in a heterotypic cell aggregate</b>	<b>105</b>
<b>6.3.2 Rounding and protruding behaviour of cells</b>	<b>107</b>
<b>6.4 Simulations of cell sorting</b>	<b>109</b>
<b>6.4.1 Cell sorting without random variations</b>	<b>109</b>
<b>6.4.2 Cell sorting with random variations</b>	<b>110</b>
<b>6.5 Simulations of Tissue Spreading</b>	<b>115</b>
<b>6.6 Other Cell Phenomena Studied by simulations</b>	<b>115</b>
<b>6.7 Discussion</b>	<b>118</b>
<b>Chapter 7 Conclusions and Future Prospects</b>	<b>122</b>
<b>References</b>	<b>125</b>

## **List of Figures**

<b>Figure 1.1 Development Phase of Embryo Morphogenesis</b>	<b>3</b>
<b>Figure 1.2 Micrograph of Neural Plate Tissue</b>	<b>5</b>
<b>Figure 1.3 Different Cell Geometry</b>	<b>7</b>
<b>Figure 1.4 Characteristic Lengths Associated with Various Scales Relevant to Embryology</b>	<b>10</b>
<b>Figure 1.5 Science and Technology Essential to Computer Simulations of Morphogenesis</b>	<b>13</b>
<b>Figure 2.1 Cell Micro-components</b>	<b>18</b>
<b>Figure 2.2 Roles of Cell Adhesion in Embryo Morphogenesis</b>	<b>21</b>
<b>Figure 2.3 Micrograph of Circumferential bundles in Rat Retinal Pigment Epithelium</b>	<b>27</b>
<b>Figure 2.4 Micrograph of Microtubules in Glutaraldehyde-fixed Mouse 3T3 Cells</b>	<b>29</b>
<b>Figure 3.1 Amphibian Neurulation</b>	<b>32</b>
<b>Figure 3.2 Sequence of Shape Changes from a Simulation of Neurulation in an Embryo Cross-section</b>	<b>34</b>
<b>Figure 3.3 Sea Urchin Gastrulation (in Cross-section)</b>	<b>36</b>
<b>Figure 3.4 Shape Changes Within the Vegetal Plate</b>	<b>38</b>
<b>Figure 3.5 Schematic Diagram of the Cardiac Tube</b>	<b>39</b>
<b>Figure 3.6 Forces on a Vertex Node of Adjacent Cells</b>	<b>43</b>
<b>Figure 4.1 Image of Cellular Patterns of an Axolotl Embryo at Developmental Stages 7 and 9</b>	<b>52</b>
<b>Figure 4.2 Definition of Voronoi Tessellation</b>	<b>53</b>
<b>Figure 4.3 Parameters in the Calculation of Voronoi Tessellation</b>	<b>54</b>
<b>Figure 4.4 Computer Implementation of Voronoi Tessellation</b>	<b>55</b>

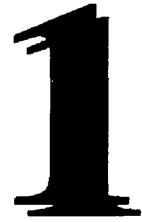
<b>Figure 4.5 Voronoi Tessellation</b>	<b>57</b>
<b>Figure 4.6 Cell Element</b>	<b>58</b>
<b>Figure 4.7 Two-dimensional Presentation of the Micro-components in a Cell</b>	<b>59</b>
<b>Figure 4.8 Neighbour Change in the Cell Sheet</b>	<b>65</b>
<b>Figure 4.9 Implementation of the Computer Simulation</b>	<b>67</b>
<b>Figure 5.1 Best-fit Shapes for a Polygon</b>	<b>71</b>
<b>Figure 5.2 Annealing Process of a Straight-edge Cell Sheet</b>	<b>72</b>
<b>Figure 5.3 Schematic Diagram of Forces in a Cell Sheet</b>	<b>74</b>
<b>Figure 5.4 Elongation of a Cell Sheet in X-direction at a Constant Rate</b>	<b>78</b>
<b>Figure 5.5a True Stress, Intra-cellular Pressure, Cell Shape Ratio, and Number of Neighbour Changes Versus Patch Elongation Ratio</b>	<b>79</b>
<b>Figure 5.5b Intra-cellular Pressure Versus Patch Elongation Ratio</b>	<b>80</b>
<b>Figure 5.6 Cell Patches of Different Densities</b>	<b>83</b>
<b>Figure 5.7 True Stress Versus Elongation Rate of Cell Patches with Different Densities</b>	<b>84</b>
<b>Figure 5.8 True Stress and Shape Ratio Versus Elongation Rate of Cell Patches with Different <math>F_C</math></b>	<b>86</b>
<b>Figure 5.9 True Stress and Shape Ratio Versus Elongation Rate of Cell Patches with Different Strain Rate</b>	<b>87</b>
<b>Figure 5.10 True Stress Versus Elongation Ratio of A Patch Stretched in Different Directions</b>	<b>89</b>
<b>Figure 5.11 Anisotropy of Cell Patches Without Annealing</b>	<b>90</b>
<b>Figure 5.12 Necking Phenomena</b>	<b>91</b>
<b>Figure 5.13 Elongation Rate of a Cell Sheet Subjected to Constant Lateral Stress</b>	<b>92</b>
<b>Figure 6.1 Tissue Reconstruction Through Cell Sorting and Tissue Spreading</b>	<b>97</b>
<b>Figure 6.2 Hierarchy of Final State of Cell Sorting</b>	<b>98</b>
<b>Figure 6.3 Relationship Between the Revisable Works of Cohesion</b>	

<b>and Cell Sorting</b>	<b>100</b>
<b>Figure 6.4 A Heterotypic Cell Aggregate</b>	<b>106</b>
<b>Figure 6.5 Rounding and Protruding behaviour of Cell Sheet</b>	<b>108</b>
<b>Figure 6.6 Simulation of Cell Sorting without Random Variations</b>	<b>112</b>
<b>Figure 6.7 Simulation of Cell Sorting with Random Variations</b>	<b>114</b>
<b>Figure 6.8 Tissue Spreading Simulation</b>	<b>116</b>
<b>Figure 6.9 Simulation of Checker-board Formation</b>	<b>117</b>
<b>Figure 6.10 Simulation Result Using DAH Values</b>	<b>120</b>
<b>Figure 6.11 Correlation Between Interfacial Forces and Cell Activities</b>	<b>121</b>

## **List of Tables**

<b>Table 2.1 Calcium-dependent Cell Adhesion Molecules and Their Distribution</b>	<b>22</b>
<b>Table 2.2 Methods of Adhesion Measurement, Their Uses and Drawbacks</b>	<b>24</b>
<b>Table 2.3 Methods of Measuring Mechanical Properties of Cytoplasm</b>	<b>26</b>
<b>Table 3.1 Simulation Models of Embryonic Tissues</b>	<b>40</b>
<b>Table 3.2 Simulation Models of Biological Cells</b>	<b>49</b>
<b>Table 4.1 Criteria Regulating the Characteristic of Voronoi Tessellation</b>	<b>55</b>
<b>Table 4.2 Neighbour Changes Within a Cell Sheet</b>	<b>66</b>
<b>Table 6.1 Interfacial Types in a Heterotypic Cell Aggregate</b>	<b>107</b>

# **Introduction: Mechanics in Biology**



Like conventional mechanics, which is about stresses, deformations and movements of structures such as bridges and machines made of concrete and steel, this thesis is about stresses, deformations and movements, — but of biological structures: cells, tissues and embryos. Compared to any man-made structures and machines, these biological systems are extremely complex. They are made of highly dynamic materials that have sub-components which are constantly assembling and disassembling, resulting in complicated constitutive relationships (Alberts *et al.*, 1989). Moreover, these structures are mostly imperceptible to human eyes. With the advent of new technologies, especially the arrival of the electron microscope, the structural details of embryos, tissues and cells have been revealed. Nevertheless, there are wide gaps in our knowledge of their morphologies and their behaviours. This is where the biomechanics comes into play, hoping to provide answers to fundamental questions such as:

1. How do cells, tissues and their micro-structures interact with each other and give rise to various vital processes leading to the formation of a normal embryo?
2. What are the driving forces behind these activities?
3. What are the consequences of changes in these driving forces?

The following sections elaborate the biological background and mechanical principles essential to this research.

## 1.1 Embryos, Embryonic Tissues and Cells

### 1.1.1 Embryos

An embryo is the juvenile stage of an animal. Within a short period of time after fertilization, the egg from which it started undergoes a series of very complicated developmental processes to form a new animal. In order to generate a healthy animal, a number of crucial events have to occur in the perfect place, at the perfect time, and in a precise manner. In embryology, the morphogenetic process leading to the birth of a new individual is divided into six phases (Balinsky, 1981; Bordzilovskaya *et al.*, 1989): **gametogenesis, fertilization, cleavage, gastrulation, organogenesis, and growth and historical differentiation** (Figure 1.1).

The first phase, **gametogenesis** begins with the ripening of an egg and the formation of the spermatozoon. It creates the conditions from which the subsequent embryogenesis starts. During the second phase **fertilization**, an egg is activated by a sperm and it involves a number of rather independent biological and physiological processes. The egg and the sperm from both parents are united through a very finely adjusted mechanism. The sperm finds the egg and fuses with it. A fertilized egg is then ready for further development. After a period of time, ranging from seconds to days, even years, depending on the species or conditions, the next phase, **cleavage**, takes place. It invokes a succession of cell divisions, which result in a large number of identical cells. The size of the embryo does not change, but the cells are smaller. Eventually, they form a hollow spherical body, a *blastula*, with a layer of cells, the *blastoderm*, surrounding a cavity, the *blastocoele*. During the fourth phase **gastrulation**, a large portion of the single-layered blastoderm enters the interior of the blastula, one side of which develops into three layers. The result is called a *gastrula*. The three layers of cells, — external layer *ectoderm*, intermediate one *mesoderm* and the innermost layer *endoderm*, become skin and brain, skeletal components and internal organs of the animal, respectively. The

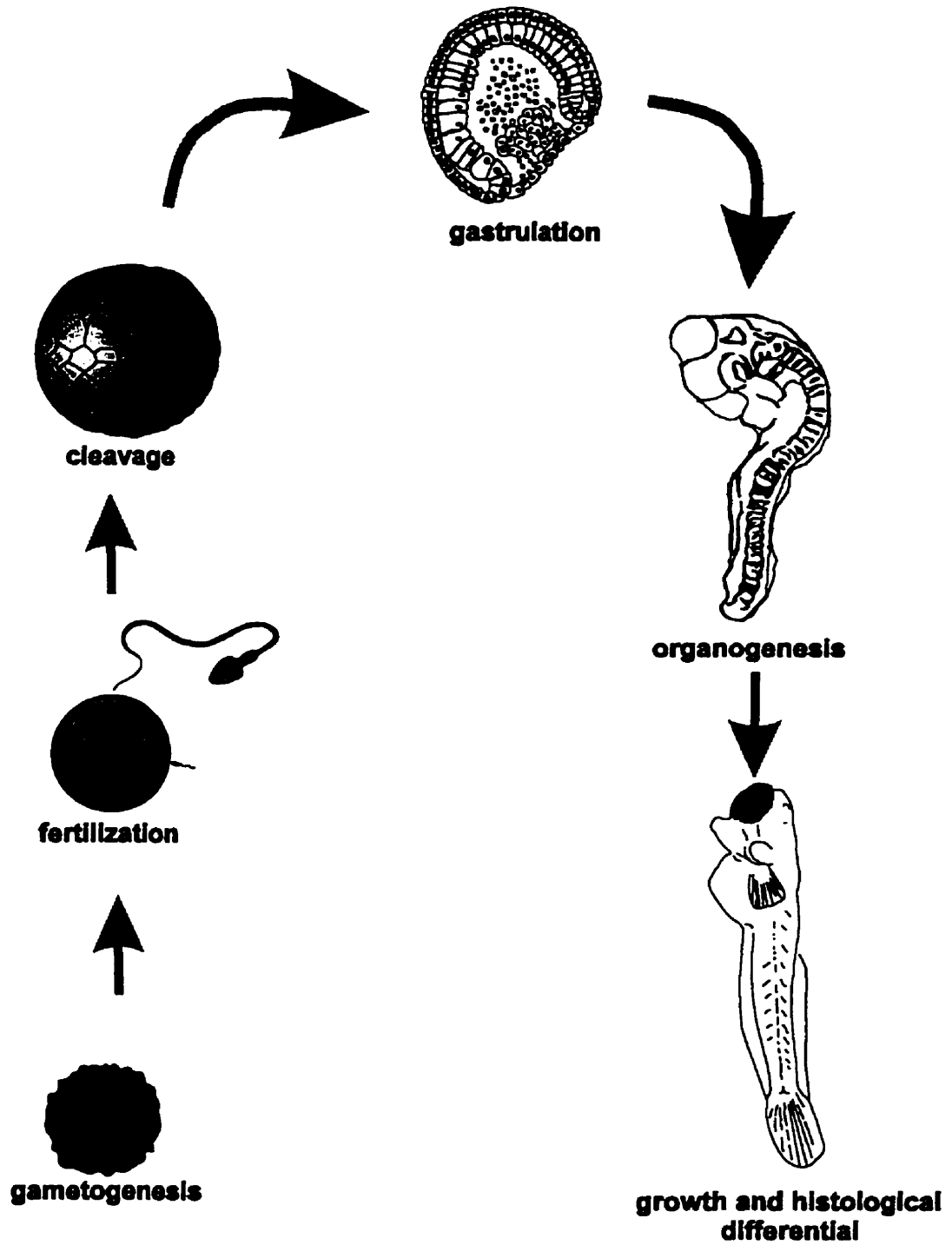


Figure 1.1 Development Phases of Embryo Morphogenesis

fifth phase **organogenesis**, commences immediately after the gastrula is formed. Cells become functionally differentiated from each other and begin to form specific organs. The group of cells that will form a particular organ, which is called the *rudiment* of that organ, is not always generated in its final anatomical location. The rudiment is able to move a long distance towards its final destination. Organ formation consists of many very complex processes. Large deformations of embryonic tissues are often required. Some imperfections in these processes may cause severe and irreparable birth defects such as spina bifida. With the appearance of primary and secondary organ rudiments, the embryo begins to show some similarity to the adult animal. The development of the embryo continues in the sixth phase of **growth and histological differentiation** to fully develop its organs and anatomical.

One intriguing feature of embryo morphogenesis is that many organs and anatomical structures possess considerable plasticity and may be able to repair injuries sustained from the environment. At the early stages of its development, if one type of rudiment is dislocated or generated at a place other than its final anatomical position, then it is able to go back to the right location and form a fully- functional organ (Keller and Speith, 1984; Jesuthasan, 1997). It may also change to another type of rudiment and develop into the right type of organ according to its location, developmental stages and the specie (Trinkaus, 1970). Most adult cells will lose this ability with time. Therefore, it is of great interest to human beings to understand the difference between the behavior of an embryonic cell and an adult cell in order to employ this great feature for wound healing, tissue reconstruction or organ repair.

Another interesting fact about embryo morphogenesis is that, between different species, or even different individuals of the same species, the results of embryo morphogenesis are easily distinguishable from each another. For example, the final shape of a human baby is very different from that of a baby chick, yet a large portion of their

embryo morphogenetic processes are similar. This provides the possibility of understanding human embryo development through studies carried out with other animals.

### 1.1.2 Embryonic Tissues

The term embryonic tissue here refers to assemblies of cells in an embryo. Cells in tissues are usually in contact with a filamentous network called extracellular matrix. This matrix holds cells and tissues together while allowing cells to migrate and interact with each other. In some tissues the extracellular matrix is a prominent component, while in other types such as epithelial tissues, it is a minor one.

Figure 1.2 is a scanning electron micrograph showing the three layers of a neural plate tissue. Embryonic tissue is usually treated as a viscoelastic material. However, microscopic mechanical interactions inside the tissue make it a very complicated and unique material (Brodland, and Clausi, 1995). For instance, during the process of neurulation, which is the formation of the neural tube in an embryo, the neural plate undergoes a sequence of in-plane movement, both sides move towards each other, while the neural ridge start to rise and the neural plate rolls up out-of-plane. Eventually the neural ridges meet in the midline and fuse to form the neural tube (Moury and Schoenwolf, 1995)



**Figure 1.2 Micrograph of Neural Plate Tissue**

(from Schoenwolf and Smith, 1990)

### 1.1.3 Cells

As the basic unit of life, biological cells can be described as “small membrane-bounded compartments filled with a concentrated aqueous solution of chemicals” (Alberts, *et al.*, 1989). With the rapid advances of modern technologies, more details of cell morphology and behaviors can be investigated. High resolution electron microscopes revealed an amazingly complex system inside each cell.

A cell is far more complicated and sophisticated than any machine ever built by human beings. Comprehension and duplication of its behaviour, have not been fully achieved. Nevertheless, certain patterns of behaviour have been revealed. Of the various cell properties leading to the formation of an animal, cell motility, cell rearrangement, cell sorting are among the most essential yet refractory behaviours to analyze. These behaviours are precisely timed, directed and limited, yet they appear to proceed in the absence of external stimuli or driving forces (Townes and Holtfreter, 1955; Sausedo and Schoenwolf, 1994; Moury. and Schoenwolf, 1995).

During embryo morphogenesis, the initially identical cells become differentiated into smaller groups. Each of these smaller groups will produce a certain organ or part of the animal. Over 200 types of cells are generated through successive cell differentiations, each with different shapes, components and functions. Figure 1.3 illustrates some typical geometric characteristic of cells.

In this research, the main focus is on epithelial cells. These cells have regular packed polygonal geometry and usually undergo large displacements and deformations during organogenesis. Also, epithelial cells are normally on the surface of the embryo and are easy to observe *in vitro*.

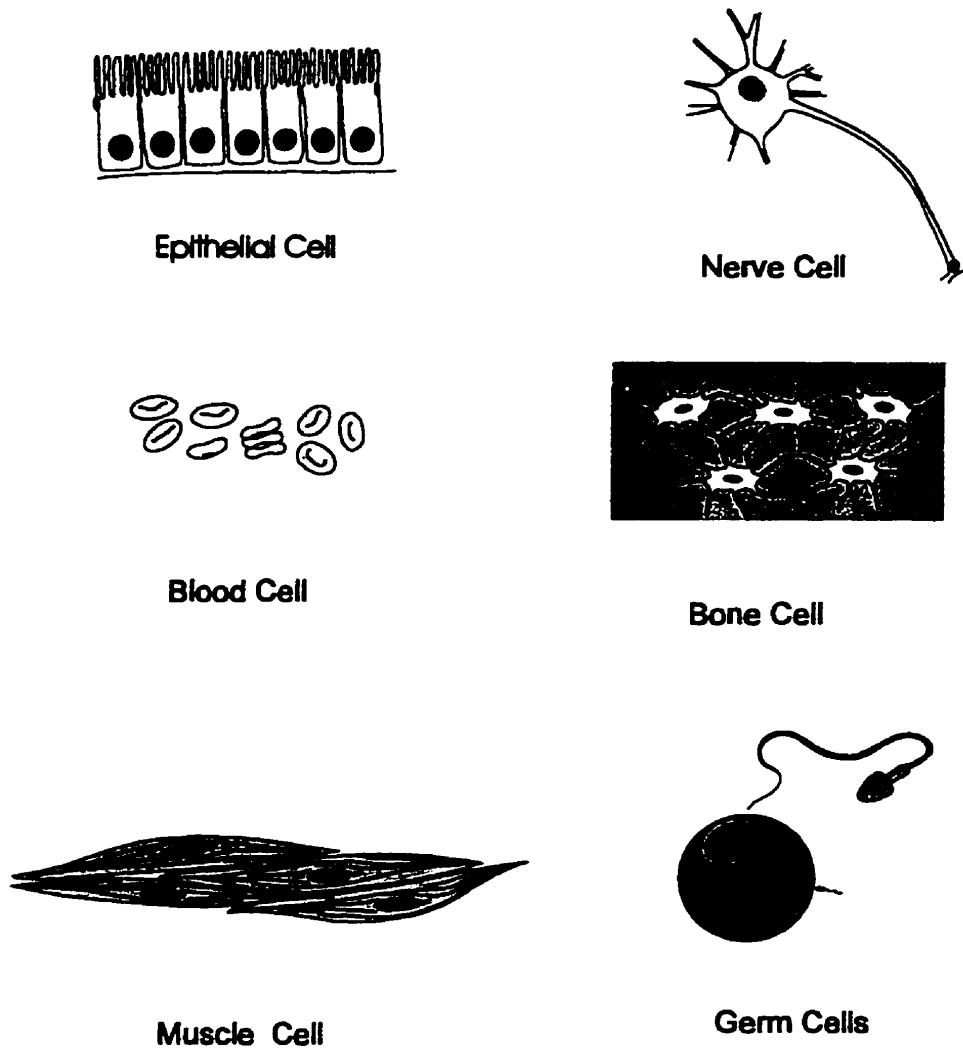


**Figure 1.3 Different Cell Geometry**

When cells are differentiated, specific types of cells do not always arise in their definitive location. A series of unique cell movements are then engaged during the following developmental stages. Cells move along a directed trajectory while recognizing cells of the same type. They can group together to form clusters of cells and move

towards their final destinations. These movements are essential to embryo morphogenesis (Townes and Holtfreter, 1955; Jacobson, 1985; Schoenwolf, 1991; Sausedo and Schoenwolf, 1994).

During organogenesis, in order to construct a certain organ, the perspective rudiment usually undergoes significant deformation. To accommodate these distortions, cells change their shapes as they rearrange their topology (Burnside and Jacobson; 1968; Wilson, et al., 1989; Schoenwolf, 1991). Furthermore, when heterogeneous dissociated cells are randomly mixed, they are able to sort out to form proper organs or the entire animal again (Wilson, 1907). One of the amazing observations made by Wilson which inspired the vastly developed research field of cell-cell recognition, is the regeneration of the marine sponge from largely dissociated cells. In his experiments, a marine sponge was cut into pieces, squeezed through bolting silk and placed into a glass dish. The suspended cell pieces coalesce with each other and gradually formed a small, functional sponge. Furthermore, it was discovered that when cells from different kinds of sponges, i.e. red sponge *microcina prolifera* and yellow sponge *Cliona celata* were placed together, they sorted out to form a red sponge and a yellow sponge. Further investigation show that cell sorting is not only species-specific, but also organ-specific. When heart cells and liver cells from the same embryo are place together, they sort out and liver cells eventually envelope heart cells (Steinberg and Takeichi, 1994).

Cell motility, rearrangement and sorting are basic phenomena of embryonic cells and are essential to successful embryo morphogenesis (Trinkaus, 1970). Given the precision and robustness of these cell behaviours, it appears to follow the blue prints of a master plan rather than random events. Can these same processes be utilized to repair a damaged or lost tissue, or even the entire organ? The following questions may come to mind:

1. How are the movements of embryonic cells directed?
2. How do they recognize other cells?

3. What forces drive these movements?
4. What makes embryonic cells different from adult cells with respect to cell sorting and tissue reconstruction?

These questions have been of interest to scientists and researchers in many research areas. Answers to these questions not only provide a better understanding of embryo morphogenesis, but also are of great importance in tissue reconstruction, wound healing and cancer metastasis, where tumor cells re-acquire motility and growth features of the embryonic cells.

## **1.2 Mechanics of Biological Systems**

### **1.2.1 Scales of Biological Systems**

The scale of living objects investigated in modern biomechanics ranges from  $10^{-10}$  m for atoms and simple molecules to  $10^2$  meter for large animals and trees. Figure 1.4 shows the hierarchy of the scale of life. Methodologies and technologies employed to study biological systems on different scale levels might vary greatly, yet they all obey the laws of chemistry and physics. The same forces that assembled matter eons ago from the dust of the big bang regulate life today. In the behavior of molecules, atoms and subatomic particles lies the key to such complex biological phenomena as the trapping and storing of solar energy by green plants, the extraction of usable energy from organic nutrients, the growth and development of organism, the patterns of genetic inheritance and the regulation of the activities of living cells. The fundamental principles in the study of biomechanics, as stated by Wilhem His (1888), are:

*Embryology and morphology cannot proceed independently of all reference to the general laws of matter, to the laws of physics and of mechanics.*

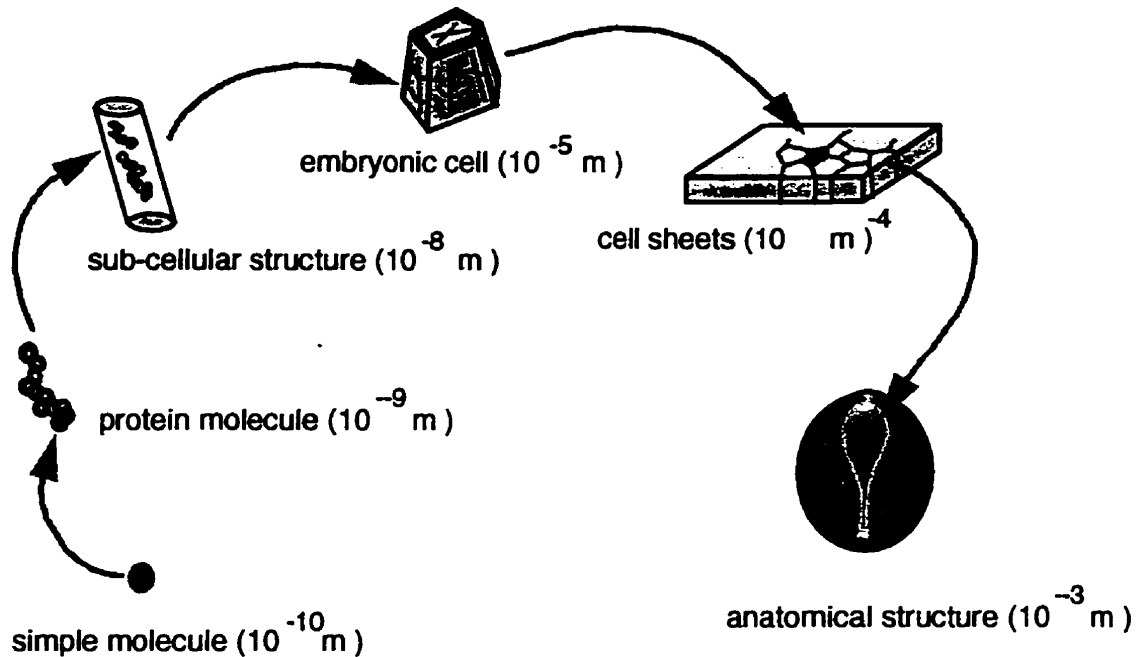


**Figure 1.4 Characteristic Lengths Associated with Various Scales  
Relevant to Embryology (after Brodland, 1997)**

It is becoming increasingly clear that embryo morphogenesis is regulated to a significant degree by mechanical interactions and that these interactions occur simultaneously at several different scales. For example, during neurulation, microfilaments act inside individual cells. The cells form part of a sheet that interacts with adjacent anatomical structures (Burnside, 1973; Brodland and Clausi, 1995). Pattern formation may sometimes have a mechanical basis that spans these same scales (Nardi, 1981; Odell, *et al.*, 1981; Ingber *et al.*, 1994). Mechanical interactions may, therefore, determine local and global morphogenetic shape changes, and ultimately affect individual cell behaviours. As a result, several important developmental questions arise:

1. How do forces generated at one scale affect what happens at the next?
2. Which forces are crucial and which are not?
3. What happens if specific sub-components are altered?

### **1.2.2 Computer Modelling of Biological Systems**

Even though many important processes in embryo development have been studied intensively and many details have been revealed during this century, there are still large gaps in our knowledge between the cause and the phenomena. To bridge these gaps, experiments are one of the approaches, however, there are many limitations to the methodology and materials presently available.

Computer simulations, however, can be carefully designed to bypass these drawbacks and have made possible breakthroughs in our understanding of the biological system. Simulations based on the known properties of biological components and well established physics principles make it possible to determine how actions at one scale affect behaviours at another, and hence provide correlation between causes and the morphogenetic phenomena. Moreover, simulations allow greater control of variables than do laboratory experiments on live embryos. This is because they are not subjected to the inherent variability of real embryos. Instead, multiple simulations can be identical in properties, geometry, and boundary conditions except for those precise changes made on purpose. Such changes can be made to individual cells or sub-cellular components or a global parameter. Thus, the effects of fine adjustment can be investigated. Another advantage offered by computer simulations, is that all variables can be specified arbitrarily. Therefore, all hypotheses regarding the driving forces behind the embryo morphogenetic processes and causes of certain classes of developmental abnormalities can be verified. Not only that, on a suitably formulated simulation platform, bio-chemical and bio-electrical factors can be incorporated into the model. Virtually, any kind of experiment that can be represented in mathematical terms can also be performed on the computer virtual embryo.

In order to develop a meaningful model of a physical system, it is essential to determine the behaviours of its basic units and the laws of their interaction. Eventually, these behaviours and interactions must be expressed mathematically. For instance, simulation modelling of embryonic cells requires the establishment of constitutive

equations for microfilament bundles, microtubules, and cytoplasm, etc. In addition, equilibrium and compatibility equations for these components must be written to describe how assemblages of these components interact with each other. To determine these mathematical relationships is a useful process in itself, as it forces a systematic consideration of the elements of the system, and often reveals where gaps in understanding exist.

Once the sub-component behaviours and relationship are described mathematically and a starting geometry of a specific system chosen, this information can be incorporated into a suitable "engine" — a computer program package. Many methods can serve this purpose, depending on the emphasis of the problem. The finite element method is a well-established method and has found wide application in many fields. It has been successfully applied to studies of embryonic tissue (Brodland and Clausi, 1995, 1996; Davidson, *et al.*, 1996) and, in the present work, to studies of individual cells. The output of the engine is a detailed description of how the individual components behave, as well as how they interact, and a description of how the system deforms as a whole. This is important information since the behaviour of a complex mechanical system is often not intuitive.

State-of-art computer simulations rely on a wide variety of scientific and technological advances, as shown in Figure 1.5 (Brodland, 1997). When the morphology and mechanical properties of sub-cellular components such as microfilaments, microtubules and cytoplasm are known, these can be input as known parameters. It is also desirable to know the geometry of the embryo as a whole in order that realistic initial configurations for simulations can be determined and deformed shapes produced by simulations can be compared with actual embryo shapes. Whenever possible, such embryo geometry should be based on accurate 3-D reconstructions. Shape comparisons should be based on surface geometry and other relevant mathematical descriptions of 3-D shapes. Then accurate and objective measures of surface curvature and in-plane strain can be derived and used to compare the shape changes that computer simulation produce with those that occur in live embryos.

At present, simulations of the embryo morphogenesis fall into one of the two categories: simulations on the tissue level, or, simulations on the cellular level. Simulations

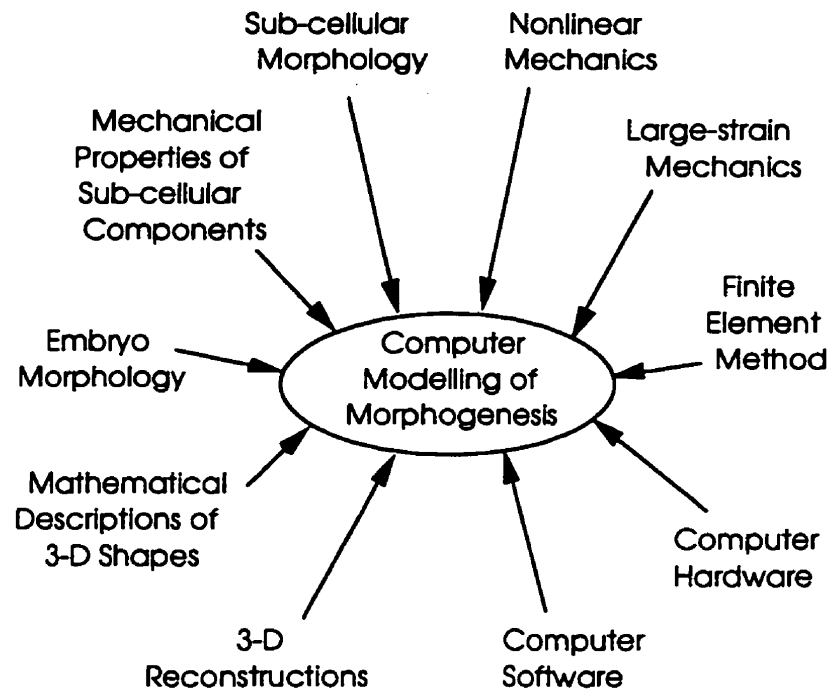


**Figure 1.5 Science and Technology Essential to  
Computer Simulations of Morphogenesis**  
(After Brodland, 1997)

on the embryo level model a specific portion of embryonic tissue or the whole embryo as a continuum. Various applications on this level include simulations of neurulation, invagination, cardiac looping, and are well addressed in Brodland's review paper (1997). The basic unit of analysis is a group of cells, in which the number of cells ranges from one cell to hundreds of cells. Some sub-cellular components might be presented in the formulation, yet behaviours of the cell aggregation is investigated rather than cellular activities. On the other hand, simulations on the cell level deal with individual cells. All sub-cellular components can be explicitly incorporated in the model and cell activities are

simulated. Singularities are permitted in the model to allow non-continuum phenomena such as cell division and cell rearrangement.

Whether tissue-level or cell-level simulations are appropriate depends on the morphology of the process studied. Cellular activities vary at different developmental stages, therefore, their effects on mechanical properties of embryonic tissues also change. When cellular effects do dominate, the continuum model is an accurate reflection of the true nature of the embryonic tissue, and simulations on the embryo level can yield good results. However, in some phenomena, cellular activities are very active and significantly affect the global mechanical properties of the tissue. For example, during cell cleavage, the daughter cells might line up along a certain axis and cause the axial elongation (Sausedo and Schoenwolf, 1994), or differences in the adhesiveness of cells might cause cells to change neighbours. These kinds of topological changes can alter the global mechanical properties. In such cases, cell-level simulations becomes a necessity. Thus, the development of the cell finite element model is presented in this work. Another motivation for cell-level simulation is to obtain insight into various mechanisms of cell motility, cell rearrangement and cell sorting.

### 1.3 Problem Statement and Main Results

Exciting advances in the application of finite element techniques to the solution of biomechanics problems have been witnessed in the last several years. Nowhere is this more apparent than in studies of embryo morphogenesis, where FE simulations have brought new depth of understanding regarding the driving forces of morphogenetic processes such as neurulation (Brodland and Clausi, 1993, 1995, 1996) and gastrulation (Davidson, *et al.*, 1996). A major drawback of the existing FE models is that they do not directly incorporate cell properties such as inter-cellular adhesions, cell motility, cell rearrangements and cell sorting — properties that are known to play a crucial role in certain tissue reshaping processes (Jacobson, 1984; Gumbiner, 1996; Schoenwolf and Alvarez, 1989). It is not clear whether characteristic shapes of cells during these processes are a cause or a consequence of associated shape changes. A FE simulation on the cell level, is therefore, of great importance in explaining how those essential cell activities occur and to what degree they change the overall material properties of embryonic tissues.

The purpose of this study is to determine, in quantitative terms, the effect of various micro-components and cell activities on the mechanical characteristics of epithelial cell sheets. The study will investigate the mechanisms of cell shape change, cell motility, sorting and rearrangement. These phenomena are of great interests not only in embryo morphogenesis, but in tissue reconstruction, wound healing and cancer cell migration.

Chapter 2 presents biological descriptions of cellular micro-components which are of mechanical significance to cell behaviour and which will be incorporated into the cell model. Chapter 3 reviews the existing computer simulation models for embryonic tissues and cells. Chapter 4 presents a detailed derivation of the cell element. Individual cells are modelled using special formulated cell finite elements, which incorporate sub-cellular structures including circumferential microfilament bundles (CMBs), microtubules, cytoplasm and cell adhesion molecules (CAMs). Each of these cell elements is subjected to large deformations and has been expressly formulated to allow cell rearrangements to occur. In Chapter 5, a thorough investigation is carried out on how cell properties such as CMBs strength, cell cytoplasm viscosity, internal cell pressures, cell rearrangement, and external loads or displacements give rise to the characteristic of the mechanical behaviour of a sheet of cells. The study shows that as a sheet of cells elongates, the initial stages of deformation are characterized by changes in average cell shape, while subsequent stages are governed by cell rearrangement. The instantaneous stress-strain relationship depends on current cell shape and size, circumferential force, and strain rate. Analytical expressions are also derived for the intra-cellular pressure and average cell sheet stress. At present, the cell shape data needed in these formulas must be provided by simulations or physical experiments since cell shape is a function of the deformation history of the sheet. These simulation results reveal many details of constitutive relationships of embryonic tissues, and thus can be directly incorporated into simulations on the tissue level.

The mechanisms of cell sorting and cell motility have been a very active research topic during the past decade. Heterotypic cell aggregates consisting of two cell types with different cell mechanical properties are modelled in Chapter 6. A variety of cellular phenomena including cell sorting, tissue spreading and checkerboard formation are simulated. These simulations show that the driving forces of these complex cell

behaviours can be caused by a combination of differential cell-cell and cell-medium adhesion forces and intracellular contractile forces. They also demonstrate that the final sorting configuration depends on a fine balance between adhesion forces which produce protrusions, and intracellular contractile forces that cause cell rounding. Chapter 7 outlines future prospects related to this work.

Simulations in this work provide, for the first time, a rigorous mechanical explanation for a variety of known cell behaviour and identify the parametric conditions under which each behaviour can occur. FE computer simulation on the cell level has proven to be an ideal means to study many remarkable developmental processes that occur during embryo development.

# Cell Micro-mechanics

# 2

In this century, the structure, behaviour and diversity of cells have been the subject of scientific scrutiny in a vast range of disciplines. Observations *in vivo* have revealed the structures of cells in great detail (Nagele and Lee, 1979; Alberts, *et al.*, 1989; Gordon and Essner, 1987; Thorp, 1984; Kalnins, *et al.*, 1995). Properties of various cell micro-components have also been measured and their functions identified (Hiramoto, 1969, 1982; Burnside, 1973; Schoenwolf, 1988; Ingber, *et al.*, 1994; Forty and Steinberg, 1995). Cell-cell and cell-environment interactions have also been intensively studied (Steinberg, 1963; Jacobson, 1985; Curtis and Lackie, 1991; Forgacs, 1995) and cell movements carefully tracked (Spratt, 1946; Jacobson, 1962; Burnside and Jacobson, 1968; Keller, 1982; Honda *et al.*, 1982; Sausedi and Schoenwolf, 1994; Schoenwolf, 1991; Brodland, *et al.*, 1996). These discoveries have not only deepened our comprehension of the biological cell itself, but have also provided a means to understand pathological phenomena such as the migration and invasiveness of cancer metastases (Takeichi, 1991), and the wound healing process (Kalnins *et al.*, 1995).

A cell is a very complicated device. Its internal structures and peripheral components form a sophisticated network in which a cell functions, reproduces, migrates and interacts. It is widely held that one of the regulators of cell behaviour is mechanical

forces (Belousov *et al*, 1994). However, the significance of other cell features such as signaling and ion balance in mediating cell behaviours should not be overlooked (Heldman and Goldschmidt-Clermont, 1993).

Figure 2.1 depicts some major sub-cellular structures found in epithelial cells. Each of these components is believed to have a significant effect on embryo morphogenesis. Each is described below.

### 2.1 Plasma Membrane

In animal cells, the cell surface consists of a plasma membrane. The plasma membrane forms a selective barrier, separating the cell contents from its environment. The pressure inside a cell results from surface tension in the membrane. This surface

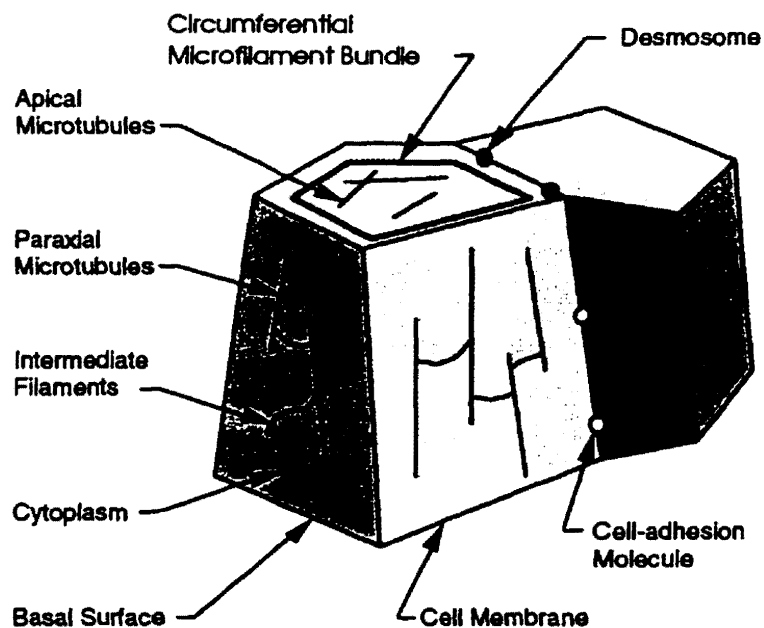


**Figure 2.1 Cell Micro-components**

tension is believed to be part of the contractile forces that drive various morphogenetic processes (Brodland and Shu, 1992). During the movement of a cell, its shape usually changes significantly. The substantial expansion of the membrane plays a pivotal role in the cell locomotion (Wolpert and Gingell, 1968).

Besides its mechanical roles in providing driving forces to various cell activities, the membrane is also a dynamic mosaic of proteins, lipids, and carbohydrates. Embedded in this membrane are receptors for a variety of extra-cellular molecules. Three major groups which are important to embryo morphogenetic movements are cell adhesion molecules (CAM), substrate adhesion molecules (SAM) and cell junctional molecules (CJM) (Edelman, 1985). These molecules act to establish cell specificity (Forgacs, 1995), mediate cell-cell, cell-substrate interaction (Steinburg, 1996), and information channels between cells or between cells and their environment (Revel, *et al.*, 1985). Functions of these molecules are further discussed in later sections.

## 2.2 Junctions

Cell junctions are very small structures on the cell surface attaching cells to other cells or to the extracellular matrix. They are particularly important and plentiful in epithelial cells. There are three functional groups of junctions: (1) occluding junctions, which seal the epithelial cell sheet in a way such that no molecules can leak from one side of the sheet to the other; (2) anchoring junctions, which mechanically attach cells and their cytoskeletons to their neighbours or to the extracellular matrix; and (3) communicating junctions, which pass chemical or electrical signals between interacting cells (Alberts, *et al.*, 1989). Desmosomes and hemidesmosomes are examples of anchoring junctions. They are button-like points which provide the connection site for intermediate filaments. Also, desmosomes function as special domains where the plasma membrane of the cell interacts with a corresponding domain of the plasma membrane of an adjacent cell, apparently

mediating intercellular adhesion in a stable way (Cowin, *et al.*, 1985). The abundant presence of cell junctions keep epithelial cells in contiguous sheets.

### 2.3 Adhesion Molecules

Strictly speaking, cell-cell and cell-substrate adhesions belong to the category of surface junctions. They are cell surface domains which provide physical bonding of cells to one another and to the extracellular matrices. They modulate the pathway by which cells differentiate, move, interact and form a mature tissue (Edelman, 1985; Gumbiner, 1996). The adhesion of cells is a phenomenon which affects all aspects of biology. Figure 2.2 lists the participation of the cell adhesion in some critical morphogenetic processes during organogenesis, as well as various cellular behaviours, including cell growth, cell-cell recognition, cell migration and cell sorting. Cell adhesion is identified as a fundamental property of cell tissues.

Adhesion molecules have been under intensive studies during the past few decades (for a review, see Steinberg, 1996; Ruoslahti and Öbrink, 1996). These studies lead to new discoveries and characterization of many types of adhesive proteins and several families of adhesion molecules, many with a large number of members. According to Hyne and Lander (1992), adhesion molecules are approximately classified into four families: (1) the calcium-dependent adherins; (2) the members of the immunoglobulin super-family; (3) the selectins and (4) the integrins. The molecules from the first three families are primarily responsible for direct cell-cell adhesion and are called cell adhesion molecules (CAM), whereas integrins provoke the cell-substrate adhesions and are referred to as substrate adhesion molecules (SAM). Among the numerous CAMs, calcium-dependent (CD) CAMs seem to play the most basic role in the construction of multicellular organs, since experiments demonstrate that tissues will be dissociated if the function of CD CAMs are disabled (Takeichi *et al.*, 1985; Steinberg and Takeichi, 1994).

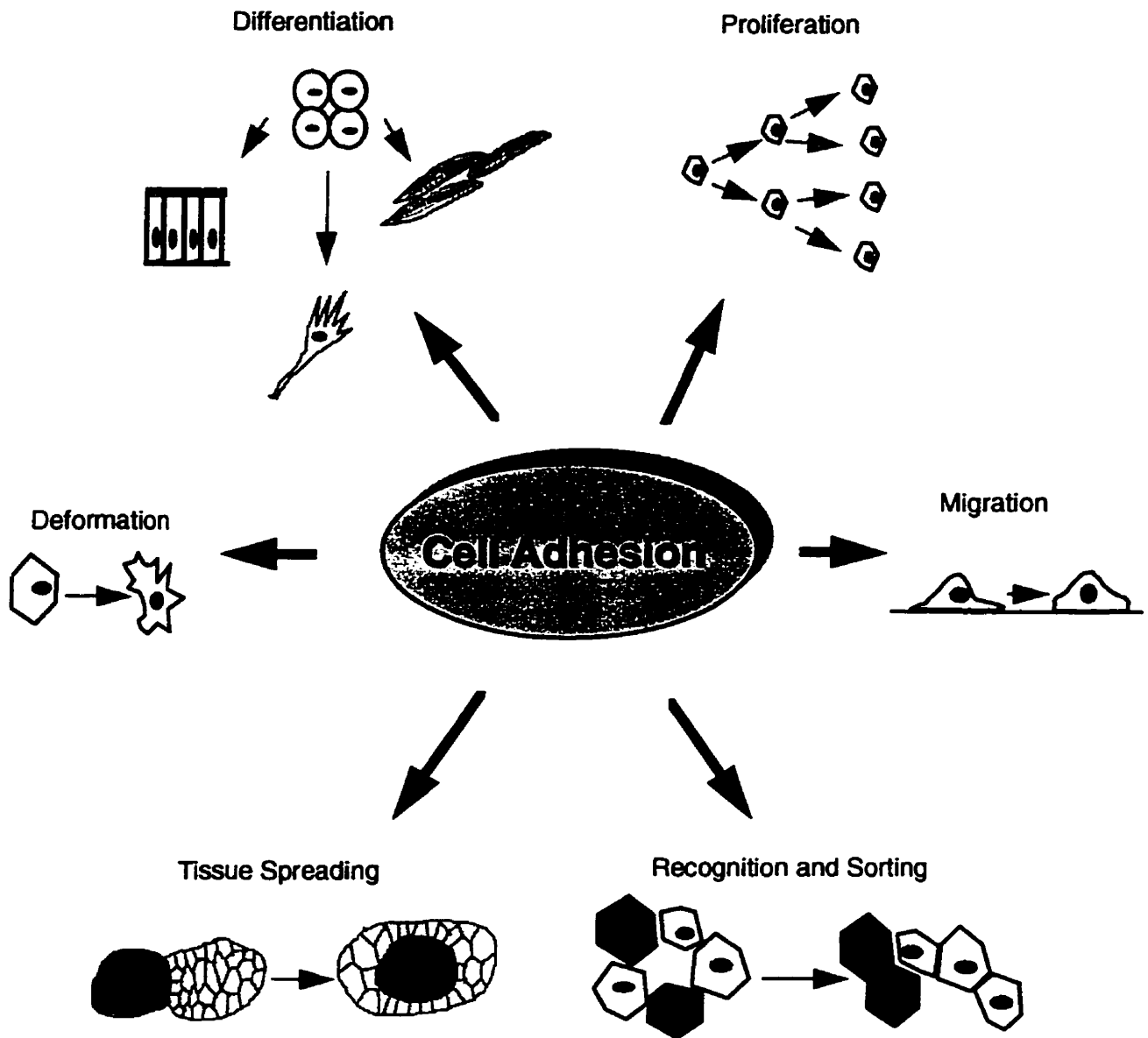


**Figure 2.2 Roles of Cell Adhesion in Embryo Morphogenesis**

Those who do not have this calcium-sensitivity are called CI CAMs. It is found that cells with either CD CAMs or CI CAMs can coaggregate but will not adhere to those which have the other kind of CAMs (Steinberg, et al., 1973). Therefore, CAMs possess cell recognition specificity.

The first vertebrate cell adhesion molecule was identified on the surface of neural cells and is called "N-CAM" (Brackenbury *et al.*, 1977). Liver cell adhesion molecules (L-CAM) and neuron-glia cell adhesion molecule (Ng-CAM) have been detected on the basis of their roles in calcium-dependent adhesion in a variety of tissues. Table 2.1 lists some common types of CD CAMs and their distributions. Nevertheless, this is not a place to review biochemical details of various adhesion molecules. The emphasis here is on the binding strength between cells and cell-substrate provided by CAMs and SAMs, and the mechanical effect of this adhesiveness on specific morphogenetic processes including cell sorting, motility and rearrangement.

**Table 2.1 Calcium-dependent Cell Adhesion Molecules and Their Distribution**

<b>CAM Name</b>	<b>Distribution</b>	<b>Sources</b>
N-CAM	brain tissue	Brackenbury <i>et al.</i> , 1977
L-CAM	liver tissue, epithelial tissue	Bertolotte <i>et al.</i> , 1980
Ng-CAM	neuron and glia	Grumet and Edelman, 1984
Cell-CAM 120/80	epithelial tissue	Caroline, <i>et al.</i> , 1985

Different CAMs and SAMs provide different binding strength among cells or between cells and their substrate. Different cells do display different adhesions, or so called specific cell adhesions. Even for the same type of cells, the cell adhesion changes with time (Ohmori and Meada, 1986). Therefore, cell adhesion serves as an agent of cell specificity and mediates cell activities (Edelman, 1985). It has even been postulated to be

one of the ways the body plan is carried out in the multicellular organ forming process (Gumbiner, 1996). Taking the cell sorting for example, when dissociated cells of different CAMs and thus of different interfacial adhesions are placed together, they adhere to each other to form a heterotypic cell aggregate. Spontaneous cell sorting follows and a final state is reached with a hierarchy of tissue engulfment analogous to the order of the cell adhesion (Steinberg, 1962b). Steinberg (1970) postulated the difference in the adhesions of heterotypic cells is sufficient for this type of cell sorting. However, there exists a quantitative dividing line to define the exact role of cell adhesions in a certain phenomenon. In the case of cell motility, as Ruoslahti and Öbrink (1996) pointed out, the cell-cell or cell-substrate adhesion “involved in the regulation of cell migration: ... can either promote or inhibit migration”. It depends on a delicate balance of the content of CAMs and on their milieu, including the amount of CAMs expressed on cell surfaces (Friedlander, *et al.*, 1989)

Identifying the role of cell adhesion requires measurement of adhesion. Theoretically, adhesion can be quantified in one of the following four ways (Curtis and Lackie, 1991):

1. the minimal energy required to break an adhesion of defined area, in a specific way (e.g. a peeling or a normal direction breakage)
2. the free energy of the bonding system
3. the energy obtained by integrating forces required to break an adhesion over time
4. the excess of forces of attraction over forces of repulsion which will lead to cells attracting each other (over a very short range)

Practically, there is no system yet to accurately measure any one of the above four quantities (Curtis and Lackie, 1991). The data are always mixed with other components arising from other mechanisms. The existing measurement methods are classified into three inherently different categories: distractive, kinetic and thermodynamic. The

distractive method measures the force required to separate adhering cells (Curtis, 1991); the kinetic method measures the aggregation rate of the labeled cell suspensions derived from embryonic tissue (Curtis, 1969; Roth and Weston, 1967; Jones, 1991); and the thermodynamic method measures the surface tension (Phillips and Steinberg, 1969, 1977, 1978; Foty et al., 1994, 1995). Each of these methods has its pros and cons, and serves a specific purpose in analyzing different morphogenetic processes (Table 2.2).

**Table 2.2. Methods of Adhesion Measurement, Their Uses and Drawbacks**

<b>Method</b>	<b>Quantity Measured</b>	<b>Purpose</b>	<b>Drawbacks</b>
distractive	force to separate adhering cells	to elucidate forces of cell motility	external force may alter intra-cellular structures
kinetic	aggregation rate of cells	to define adhesion in relative quantitative terms	Dissociated cells in the flow may not present the true cell behaviour <i>in vivo</i>
thermodynamic	surface tension	to define adhesion in relative and absolute quantitative terms	cell properties may change during the long experiment time

Since the observed behaviour of embryonic cell populations in sorting and spreading mimicks in detail the behaviour of immiscible liquids (Steinberg, 1962b), tissue surface tension becomes one of the popular measurable biological properties of cells (Forgacs, 1995). The traditional way of evaluating the surface tension in a cell is to measure the angle of the cell membrane at the attachment point (Belousov *et al.*, 1994). The other methods of surface tension measurement include the centrifuging method (Phillips and Steinberg, 1969, 1977, 1978) and the compression method (Foty, *et al.*, 1994). The centrifuging method measures the surface tension in relative terms, whereas

the compression method measures the absolute value of the surface tension. In a chick embryo, it is reported that the surface tension has an average value of 19.3 dyne/cm for limb bud tissues, 8.58 dyne/cm for heart ventricle tissues and 4.48 dyne/cm for liver tissues (Foty and Steinberg, 1995). It is worth noting that although the measurement is carefully carried out and is repeated for several times, great caution has to be taken to evaluate these “would-be” accurate numbers in other physical systems such as immiscible liquids. It is because during the process of the measurement, the external pressure might trigger some unknown cellular activities within the tested tissue and hence alter its surface tension. This concern exists in every method of adhesion measurement. Despite these limitations, the qualitative relationship  $\sigma_{\text{limb bud}} > \sigma_{\text{heart}} > \sigma_{\text{liver}}$  ( $\sigma$  denotes the surface tension) coincides with the result from the centrifugal method (Phillips and Steinberg, 1969), and provides direct evidence to validate Steinberg's differential adhesion hypothesis (DAH). This hypothesis deals with correlation between the adhesiveness of cells and various heterotypic cell population behaviour, and will be discussed in detail in Chapter 6.

The importance of the cell adhesion, as Foty and Steinberg (1995) put it, lies in its function in many cell activities as “an anatomical address code by generating forces which guide cells to adopt their preferred associations and positions”.

## 2.4 Cytoplasm

Cytoplasm is the material inside a cell, including cytosol and suspended organelles but excluding the nucleus. It is the site not only of protein synthesis but also of most of the cell's metabolism — that is, the many reactions by which some small molecules are degraded while others are synthesized to provide the building blocks of macromolecules. Cytoplasm was once thought to be relatively simple and structureless. However, observations via high voltage electron microscopes have shown that it contains solutes,

macromolecules and networks of fibers and filaments (Luby-Phelps, 1994). Destroyed and re-generated during various cellular activities (Mitcgison and Cramer, 1996), these networks provide the viscosity as well as relatively weak elasticity of the cytoplasm.

Understanding the structures and mechanical properties of the cytoplasm is basic for understanding various cellular functions. Listed in Table 2.3 are various methods of measuring the bulk viscosity of the cytoplasm. Usually, the strain rates are magnitudes higher than those that occur during morphogenetic movements. As a consequence, known estimates of cytoplasmic properties probably involve tearing the intermediate filaments meshwork that courses through the cells and do not provide numerical values that are applicable to the low strain rates typical of morphogenesis (Brodland and Gordon, 1990). As we should see in the next chapter, most simulation models represent cytoplasm, including any intermediate filament mesh that might be present, as a single isotropic material.

**Table 2.3 Methods of Measuring Mechanical Properties of Cytoplasm**

<b>Method</b>	<b>Quantity Measured</b>	<b>Constraints</b>	<b>Sources</b>
magnetic particle method	movement of the particle in cytoplasm and the force driving it	an artificial particle has to be inserted into the cell	Hiramoto, 1969; Valberg and Albertini, 1985 Kaneda, <i>et al.</i> , 1990
micropipet method	suction pressure required to aspirate a cell into a micropipet	cell undergoes large deformation	Needham and Hochmuth, 1990
TIR-FRAP* method	solute translational diffusion coefficient in cytoplasm	Only measure viscosity just beneath the cytoplasmic membrane	Swaminathan, <i>et al.</i> , 1996

\*Total Internal Reflection-Fluorescence Recovery After Photobleaching

## 2.5 Circumferential Microfilament Bundles

A maze of filamentous structures have been revealed within cells using fluorescence and high resolution electron microscopes. Microfilaments are one type of these filaments. They consist of helically intertwined chains of actin molecules that are about 6-7 nm in diameter. In epithelium cells, they form a band, which is approximately  $0.5\mu\text{m} \pm 0.2\mu\text{m}$  in width, at the apical regions just beneath the plasma membrane (Gordon and Essner, 1987). This band is called a circumferential microfilament bundle (CMB). Freeze-fracture studies confirm the presence of 30-nm electron particles around the CMBs. They are believed to be the "bandages" between the plasma membrane and CMBs. Figure 2.3 is a fluorescence micrograph of CMBs in a rat retinal pigment epithelium (Kalnins et al, 1995). Polygonal cell shapes are also clearly visible in the picture.

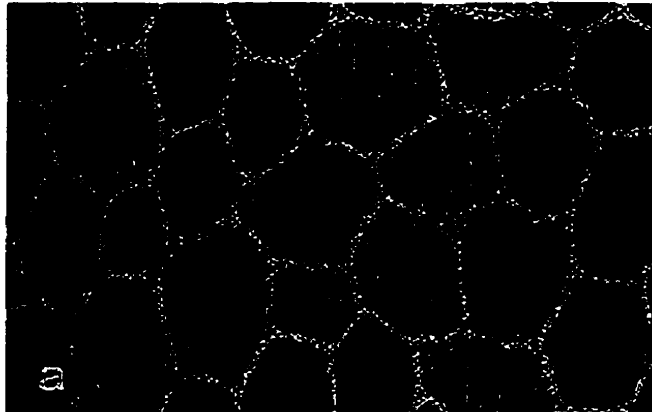


**Figure 2.3 Micrograph of Circumferential Microfilament Bundles in Rat Retinal Pigment Epithelium (from Kalnins *et al.*, 1995)**

The structural and functional characteristics of the microfilaments are very similar to those of muscle tissue. We assume that the contractile force  $F_{\text{CMB}}$  is constant and has a value of:

$$F_{\text{CMB}} = \sigma A_0 \quad (2.1)$$

where  $A_0$  is the original cross-sectional area and  $\sigma$  is the tonus of the CMBs (Rappaport, 1977; Gordon and Brodland, 1987).

Microfilament bundles are a primary component of the cytoskeleton and one of their roles is to provide contractile forces, which might be the reason for the name "stress fiber" for microfilament bundles (Ishikawa, 1986). The contractile forces are the driving forces for many embryonic morphogenetic movements (Brodland, 1997 for review). However, the role of the CMBs is far more complicated. They are one of the main regulators of cell growth, cell migration and even transdifferentiation (Harris, 1994b). Their roles in mediating cell motility, shape changes, sorting and rearrangement are further investigated using computer simulation in this work.

## 2.6 Microtubules

Microtubules exist singly or in groups depending on their functions in cells. They are responsible for a variety of internal dynamic events including chromosome movements, cytoplasmic streaming, mitosis and maintenance of cell shape (Fawcett, 1981; Grebecki, 1994). They are long, hollow, cylindrical structures about 24nm in diameter. Numerous apical microtubules are randomly placed in parallel with and immediately below the apical cell surface (Weber and Osborn, 1981). Figure 2.4 shows a micrograph of cytoplasmic microtubules. Based on their orientation, microtubules are thought to be serving the latter function by producing a constant outward force (Alberts, *et al.*, 1989). On the apical surface of a cell, the forces generated by the microtubules are in opposition to the forces produced by the microfilaments and are believed to be a constant value.

The intracellular microtubule network is highly dynamic, constantly forming and disappearing depending on cell activities (Thorpe, 1984). It has been shown that subtle changes in the microtubule system lead to a significant alteration of cell shapes (Bershadsky and Vasiliev; 1993). This dynamic behaviour is of great importance for several cell activities and shape changes.



**Figure 2.4** Micograph of Microtubules in Glutaraldehyde-fixed Mouse 3T3 Cells (from Weber and Osborn, 1981)

## 2.7 Intermediate Filaments

Another dynamic structure is formed by network of what are collectively known as intermediate filaments. These filaments form a complex three-dimensional network through the cell cytoplasm. They resist mechanical deformation and provide lateral support to compressively-loaded microtubules (Brodland and Gordon, 1989). They are also important to maintaining the general structural integrity of the cell (Galou *et al.*, 1997; Li *et al.*, 1997), the transmission of forces within the cell (Maniotis *et al.*, 1997), and aspects of cell signalling (Shyy and Chien, 1997). For purposes of modelling, we assume that the effective viscosity of the cytoplasm

includes not only the viscosity of the cytoplasmic fluids, but also the equivalent viscosity of the intermediate filament meshwork.

## 2.8 Micromechanical Interactions

In real cells, microfilament, microtubules, intermediate filaments and various organelles interact mechanically with each other (Brodland and Gordon, 1989; Maniotis *et al.*, 1997; Galou *et al.*, 1997). These interactions are important to the mechanical and biochemical functions of the cell (Ingber and Folkman, 1989; Khan and Sheetz, 1997; Li *et al.*, 1997). To conceptualize these interactions is not easy, and the recently popularized tensegrity model of Ingber (Ingber *et al.* 1994; Ingber *et al.*, 1994; Ingber, 1997) is at times helpful. A particular feature of that model is that it explains how mechanical signals can be transferred quickly from place to place in the cell using a minimal amount of structural material.

# **Simulation Models of Embryonic Tissues and Cells**

# **3**

With the rapid increase of computing capability, more variety and more complicated biological systems are being studied using computer simulations. In this chapter, two groups of computer simulation models are reviewed: models of embryonic tissues and models of biological cell.

## **3.1 Tissue-Level Computer Simulations**

In current tissue-level computer simulations, embryonic tissues are modelled as a continuum. Special morphogenetic processes have been investigated, and various hypotheses about the forces which drive these processes have been tested. Listed below are three major areas studied using computer simulations (Brodland, 1997 for review).

### **3.1.1 Studies of Neurulation**

Neurulation is the process that forms the neural tube in all vertebrate embryos. During this process a sheet of tissue called the neural plate undergoes a series of in-plane motions and rolls up out-of plane to form the neural tube. Figure 3.1 illustrates the process of amphibian neurulation. It shows a dorsal view in which the head end of the embryo is towards the top of the figure. Amphibian embryos are approximately spherical

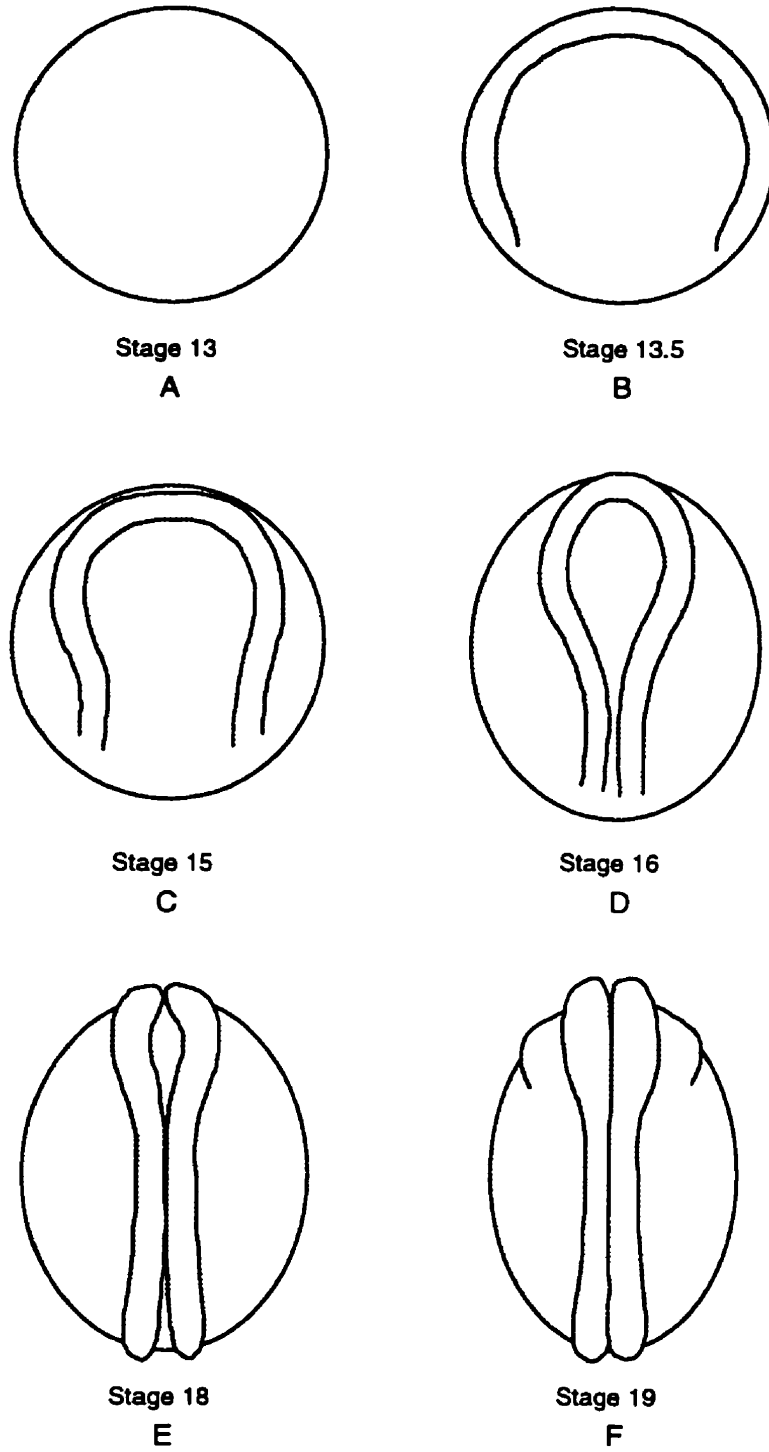


**Figure 3.1 Amphibian Neurulation**

(from Brodland, 1997)

at the beginning of neurulation (Figure 3.1A). Neural ridges then rise and move towards the embryo midline (Figures 3.1B to F). The neural plate, bounded by the neural ridges, undergoes significant in-plane strains as it deforms. As the ridges continue to move, the narrowed plate rolls up to form a closed tube. The middle part of the tube closes first (Figure 3.1E), followed by the cephalic and caudal ends (Figure 3.1F).

One of the features of neurulation that has made it a favorite subject of fundamental studies of morphogenesis, is that it occurs on the surface of the embryo and can be observed easily *in vivo*. The neural tube is the precursor of the brain and spinal cord. Any imperfection in the neural tube closure may result in serious malformation birth defects such as spina bifida and anencephaly.

The forces that drive this process have been the subject of intense investigation for more than a century (Lewis, 1947; Jacobson, 1962; Burnside and Jacobson, 1968; Hifler, and Hifler, 1983; Lee and Nagele, 1988; Brodland and Shu, 1992). To date, experimental studies have provided reasonably detailed descriptions of the shape changes that occur in the neural plate and its cells during neurulation (Burnside, 1973; Nagele and Lee, 1979; Brun and Garson; 1983; Schoenwolf, *et al.*, 1988; Moury and Schoenwolf, 1995). They also identified the primary force-generating structures such as cytoplasm, circumferential microfilament bundles, microtubules, and have provided considerable data about the mechanical properties of these force generators, as elucidated in the previous chapter (Figure 2.1).

However, how do these forces give rise to the distinctive sequence of shape changes of neural plate? Many theories have been proposed to explain the mechanics of neurulation (Schoenwolf and Smith, 1990). Brodland and Clausi investigated the driving forces and tested various hypotheses using finite element computer simulations (Brodland and Clausi, 1994, 1995).

A strip that represents a cross-section of the neural plate, together with some attached epidermis, was modeled using 8-node brick elements (Figure 3.2A). CMBs are put on the

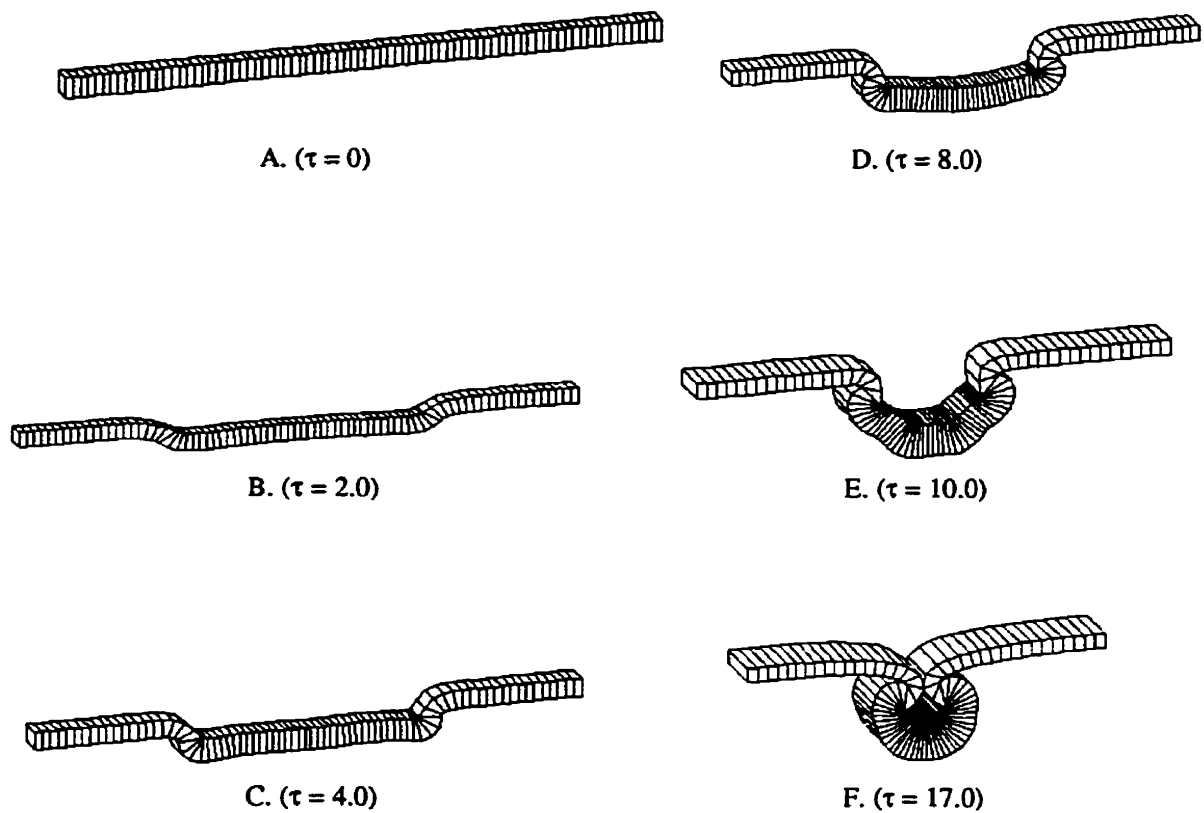


**Figure 3.2 Sequence of Shape Changes from a Simulation of Neurulation in an Embryo Cross-section**

(from Brodland and Clausi, 1995)

apical surface of the neural plate (the middle half of the strip) and exert a contractile force:

$$F_{\text{CMB}} = \sigma A_0 \frac{L_0}{L} \quad (3.1)$$

where  $\sigma$  is the microfilament stress,  $A_0$  its initial cross-sectional area,  $L_0$  the original length and  $L$  the current length. There are no CMBs on the adjacent epidermis. The effects of notochord elongation is also incorporated in the model.

The simulation yields a sequence of shape changes that match the biological phenomenon remarkably well. Both general reshaping and distinctive, detailed characteristics were reproduced (Figure 3.2 B-F). The simulation results explain the mechanism of neurulation from a mechanical perspective. These studies use measured mechanical properties and initial geometry as input, and output can be compared with shape changes in live embryos. The engine of the simulation program is the finite element method, which is well established. The simulations are quite sophisticated, realistic, and trustworthy. These simulations of neurulation have made it possible to model and understand a wide variety of important phenomena associated with neural tube closure.

### 3.1.2 Studies of Gastrulation

The morphogenetic process of gastrulation has also been the subject of several computer studies (Odell, *et al.*, 1981; Davidson, *et al.*, 1996). The simulations have focused primarily on sea urchin invagination or gastrulation, shown schematically in Figure 3.3. Before gastrulation, the embryo is a hollow sphere of packed cells called the blastula (Figure 3.3A). During gastrulation, a dimple appears at the vegetal end of the embryo (Figure 3.3B) and, subsequently, a fraction of the surface invaginates into the

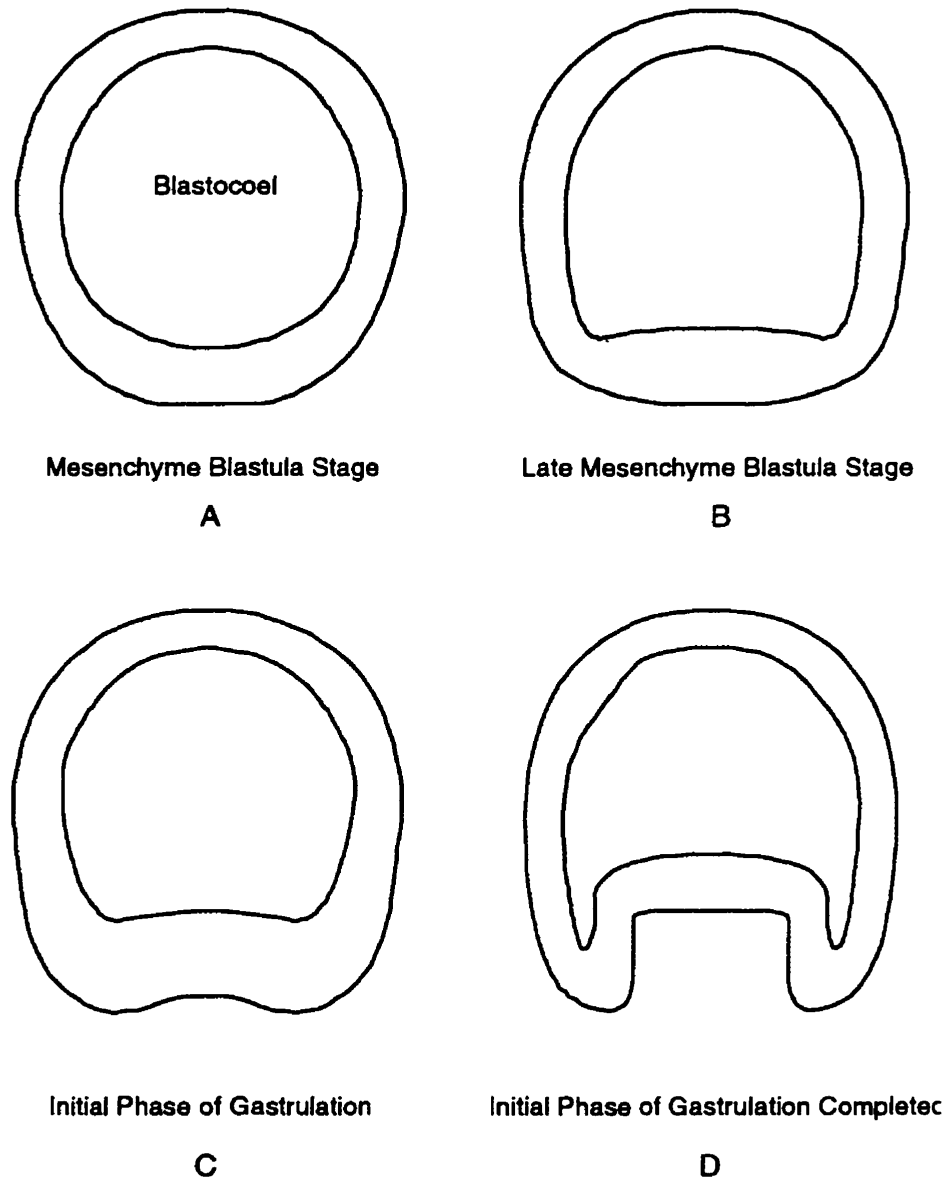


**Figure 3.3 Sea Urchin Gastrulation (in Cross-section)**  
(from Brodland, 1997)

embryo (Figure 3.3C-D). In vertebrates, a significant portion of the surface invaginates inside the cavity of the blastula through a small hole called the blastopore.

Dimpling of the blastula, the first step in gastrulation, might be caused one or a combination of the following mechanisms: (1) buckling due to reduced internal (blastocoel) pressure; (2) buckling due to autonomous expansion or in-plane growth of a localized region; (3) buckling of a region that is surrounded by a ring of contractile material; (4) localized contraction of the apical (outside) surface.

In their recently work, Davidson *et al.*(1996) employ a commercial finite element package NASTRAN to simulate the dimpling of the blastula. The initial geometry of the simulation is digitized from the image of a *Lytechinus pictus* embryo. The finite element model of the blastula consists of two layers of brick finite elements. Elastic material properties are assumed and contractile forces are distributed on the apical surface of the blastula.

Five hypotheses are investigated using this model: apical constriction; cell tracting; perimeter ring contraction; apico-basal contraction; and swelling (Figure 3.4). The paper shows the mechanical plausibility of each of these mechanisms, along with the biological evidence for and against each of them. It does not prove or disprove any one of these hypotheses. Instead, it identifies ranges of mechanical properties compatible with each mechanism, and the general cell shapes to be expected from each if it operates alone. The simulations of gastrulation, therefore, provides an important mechanical basis for the design of further experiments to differentiate between hypothesized gastrulation mechanisms.

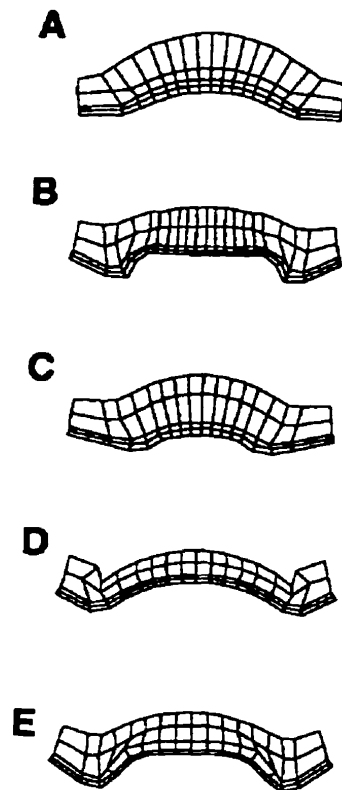


**Figure 3.4 Shape Changes Within the Vegetal Plate** (from Davidson, *et al.*, 1996)

Deformation of the finite elements in a sagittal section of the vegetal plate. The two top layers of finite elements are the cell layer, the top layer is the hyaline, the bottom is the apical lamina.

- (A) apical constriction
- (B) cell tractor
- (C) annular ring contraction
- (D) apicobasal contraction
- (E) gel swelling

### 3.1.3 Studies of Cardiac Looping

The process of cardiac looping is another area studied using computer simulations, with the finite element method. During early embryogenesis, at about the same time as neurulation occurs, a muscle-wrapped tube called the cardiac tube forms. Figure 3.5 is a schematic diagram of the cardiac tube before the looping starts. The dorsal mesocardium (DM) is a longitudinal ridge that connects the cardiac tube to the embryo, which detaches from the rest of the embryo right before the looping process begins. The tube then undergoes a series of specific bending motions, such that the DM lies along the inner radius of curvature. The DM is resorbed before looping finishes. The myocardium (MC) is a two-cell-thick cylinder that surrounds the balance of the cardiac tube.

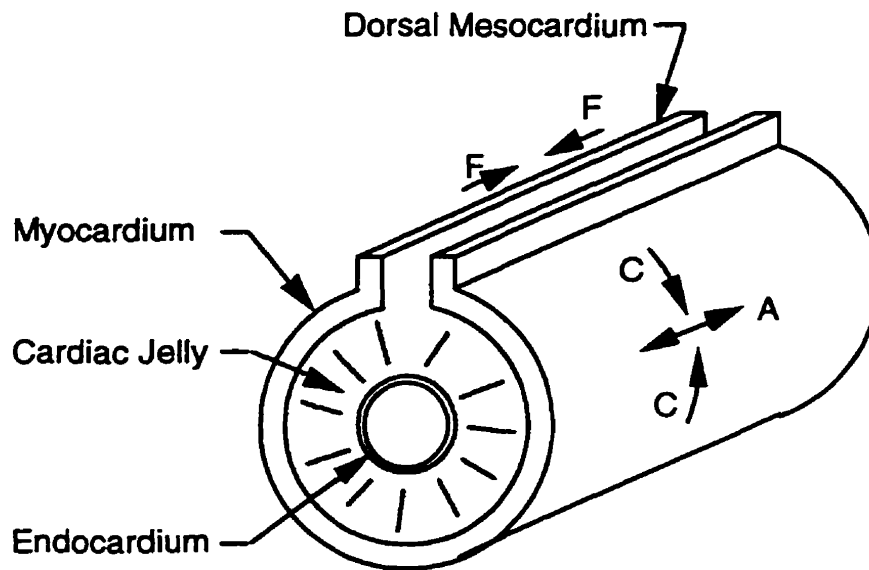


**Figure 3.5 Schematic Diagram of the Cardiac Tube**  
(from Brodland, 1997)

It contains CMBs. Between the MC and the one-cell-thick endocardium (EC), is a thick layer of extracellular matrix called cardiac jelly (CJ). With the progress of looping, parts of the tube fuse, and eventually forms a multi-chamber heart with valves and a specialized electrical conduction system (vanMierop *et al.*, 1978).

A section of the cardiac tube is modeled as a section of beam, subjected to either CMBs contraction (force  $C$  in Figure 3.5) (Itasaki *et al.*, 1991), or a residual tension in DM (force  $F$ ) (Taber *et al.*, 1993), representing two basic hypotheses about the driving forces of cardiac looping. Analytical bending deformations are calculated in both cases (Taber *et al.*, 1993, 1995). The first case is further simulated using a finite element beam

model (Taber *et al.*, 1996). These studies confirm that both mechanisms can give rise to bending of isolated cardiac tube fragments. Even though the present beam model is a far too simplified representation of the real cardiac tube, these investigations lay a foundation for future studies that might incorporate the actual boundary conditions of the cardiac tube, and studies that might compare model driving forces magnitudes with those that can occur in real embryos.

Table 3.1 is a summary of the tissue-level simulation models mentioned above. These simulations bring new depth in the understanding of neurulation, gastrulation and cardiac looping. They also show that realistic computer simulations of basic morphogenetic processes are now possible. The finite element method has proven to be a

**Table 3.1 Simulation Models of Embryonic Tissues**

<b>Name</b>	<b>Biological Process</b>	<b>Features</b>	<b>Engine</b>	<b>Simulation Results</b>	<b>Drawbacks</b>
Brodland and Clausi Model	neurulation of the neural plate	realistic mechanical properties of micro-structures	specialized finite element simulation package	shape change of the neural plate and closure of the neural tube	can not model the real geometry of the whole embryo
Davidson <i>et al.</i> Model	gastrulation in the blastula	realistic initial geometry for simulation	commercial finite element package	dimpling of the blastula subjected to five kinds of forces	unable to distinguish the real mechanism
Taber <i>et al.</i> Model	cardiac tube looping	major force-generating apparatus and idealized initial geometry	analytical solutions and finite element method	bending of the cardiac tube	unrealistic boundary conditions

powerful tool in simulating embryonic structures, for it provides the ability to handle complicated geometry, forces and boundary conditions, which are typical of morphogenetic processes.

### 3.2 Cell-Level Computer Simulations

Simulations of the cell level can investigate details of cell micro-components and cell activities, and have made use of more diversified models of cells. Much literature has dealt with such simulations (Jacobson, 1980; Stein and Gordon, 1982; Sulsky, *et al.*, 1984; Honda and Yamanaka, 1986; Weliky and Oster, 1990; Graner and Glazier, 1992; Glazier and Graner, 1993; Graner, 1993). These models can be classified into two categories. The first includes models of monotypic cells and the simulations are carried out to investigate the mechanism of cell movement and cell rearrangement, and their effect on the tissue reshaping process. These include the models proposed by Jacobson (1980), Stein and Gordon (1982), Honda and Yamanaka (1986) and Weliky and Oster (1990). The second type of cell model is dedicated to verification of the various hypotheses of cell sorting, especially Steinberg's differential adhesion hypothesis. Heterotypic cells, normally two kinds which are characterized by different adhesiveness, are randomly mixed in the starting configuration and cell sorting, tissue engulfment and other cellular phenomena are simulated. In most of these models, a cell is reduced to a two-dimensional polygonal territory. Such polygonal cells occupy the full calculating plane without gaps in between. Each cell-cell, or cell-medium interface is then assigned certain properties, such as the intracellular pressure or "affinity value" analogous to adhesive intensity or energy. Imbalance forces are calculated at each node. On the next simulation step, the node moves according to this imbalance force at a certain rate, usually governed by an assumed resistance from the media or the cytoplasm of the cell. The process is then set in motion and the trend and extent of configuration changes observed. This process usually takes many simulation steps and can be very time consuming.

Simulations using these models produce cell movements and configurations mimicking experimental observations of cell behaviours. Even though assumed values of cell properties are used in all these models, the results have qualitatively provided some insights into the mechanisms of cell behaviour and suggested the quantitative range of cell property values necessary for certain cell behaviour to take place. Moreover, these works have laid a foundation for future models. The following section reviews some typical cell models.

### 3.2.1 Weliky and Oster Model

To simulate the cell shape changes and rearrangement of a Fundulus during epiboly, a number of evenly distributed points are set up on a hemisphere (Weliky and Oster, 1990). A Voronoi tessellation scheme is then employed to generate convex polygons on the hemisphere, where each polygon represents a cell. Contractile forces from the circumferential microfilament bundles are exerted on each node. Two pressures  $P_{osm}$ , denoting the osmotic pressure which tend to expand the cell, and  $P_{elas}$ , denoting the restraining elastic pressure generated by the filamentous fiber of the cytoskeleton, are assumed within each cell. The resulting "swelling pressure  $P_{swell}$ ", which is the difference between  $P_{osm}$  and  $P_{elas}$ , is acting on each side of the cell. The mechanical equivalents of this pressure act on each node and produce the protrusion of the apex. The forces acting on a vertex node of a cell is illustrated in Figure 3.6.

At each step, once the imbalance force of each node is determined., the finite difference method is employed to determine the successive position  $(x_{n+1}, y_{n+1})$  by the following equations:

$$\begin{aligned} \mathbf{x}_{n+1} &= \mathbf{x}_n + \mathbf{F}(\mathbf{x}) \frac{\Delta t}{\mu} \\ \mathbf{y}_{n+1} &= \mathbf{y}_n + \mathbf{F}(\mathbf{y}) \frac{\Delta t}{\mu} \end{aligned} \quad (3.2)$$

where  $\Delta t$  is the time step interval between successive iterations, and  $\mu$  is the viscosity.

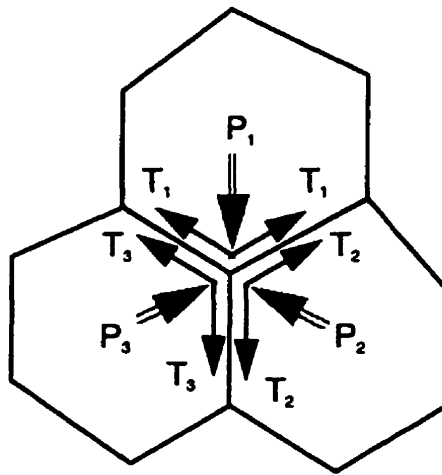


**Figure 3.6 Forces on a Vertex Node of Adjacent Cells**  
(from Weliky and Oster, 1990)

A scheme is designed to allow cells to change neighbours when one shared side of two adjacent cells becomes too short (Jacobson, 1980). The simulation results mimic some essential features of epiboly including cell shape changes, reduction in the number of marginal cells, and the dynamic pattern of cell rearrangements (the experimental observations were done by Keller and Trinkaus, 1987). However, this model excludes the

fundamental fact that a cell is part of a continuum field, rather they are simply an assembly of vertices. This drawback prevents true cell shape changes from being reproduced.

### 3.2.2 Sulsky et al Model

In order to verify Steinberg's differential adhesion hypothesis, many attempts have been made to simulation the sorting of heterotypic cell aggregates (Steinberg, 1975 for review). Sulsky et al (1984) proposed a cell model which is based on the minimization of the interfacial free energy theory. They also generate the Voronoi tessellation to represent a group of monotypic cells. A characteristic surface tension  $e_{ij}$  is assigned to pairs of cells, which will remain constant through out the simulation. The free energy of the aggregate then can be written:

$$V = \sum_{\langle i,j \rangle} l_{ij} e_{ij} \quad (3.3)$$

where  $\langle i,j \rangle$  denotes a sum over pairs of cells and  $l_{ij}$  is the length of the edge between adjacent cells  $i$  and  $j$ . Area constancy of every cell in the plane  $dA_i/dt = 0$  is enforced in the simulation process. To find the path in which cells move, a variation is considered:

$$0 = \delta \left[ \frac{dV}{dt} + \lambda \Phi - \sum_i p_i \frac{dA_i}{dt} \right] \quad (3.4)$$

where  $\Phi$  is a quadratic function of the velocities, which can be obtained from Newtonian incompressible fluid theory;  $\lambda$  and  $p$  are multipliers. A set of governing equations can be derived from Equation 3.4 and the displacement of each cell can be found by solving these equations. In this model, a cell moves through the configuration space of steepest descent along the surface  $V(x_i, e_{ij})$  with a given dissipation  $\Phi$ . Neighbour change is also allowed and partial sorting is obtained.

The initial configuration is a mesh of squares with the same areas. Three kinds of cells are distributed in certain patterns. By assigning different combinations of adhesive energies to cell interfaces, the simulation results reproduce various cellular phenomena including cell sorting, engulfment and inter-mixing of heterotypic cells. This model, however, fails to portrait the true behaviour of cell shape change since each cell is represented only by the location of its so called “nucleus”, which is actually the centroid of the polygon in the model. In the initial configuration, cells are not randomly mixed, as they are in the experiments. Another constraint of this model is that it excludes the other force-generating intra-cellular components which are known to be important to cell activities.

### 3.2.3 Graner Model

In his model, Graner (1993) started from a simple idea that cell-cell adhesion is associated with an energy per unit area and defined the total adhesion energy  $E_{adh}$  as a function of the cell configuration. He further assumed that this adhesion energy depends only on the relative positions of the objects. Thus it behaves like a potential energy for the cell aggregate, being invariant under spatial translation and rotation as well as exchanging positions between adjacent cells. As a result, a force  $F$  analogous to gravity can be defined as the derivative of  $E_{adh}$ , respect to the relative position vector  $r_{ij}$  of any pair of cells:

$$\bar{F}_i = \bar{\nabla}_i E_{adh} = \sum_j \frac{\partial E_{adh}(\bar{r}_{12}, \dots, \bar{r}_{ij}, \dots)}{\partial r_{ij}} \frac{\bar{r}_{ij}}{r_{ij}} \quad (3.5)$$

This force exists between any two cells, regardless whether they share the common boundary or not. It tends to propel two cells move towards each other. The velocity of the cell movement is governed by the following equation of motion:

$$\frac{d\bar{\mathbf{r}}_i}{dt} = \frac{1}{\mu_c} \left( -\bar{\mathbf{F}}_i + \bar{\mathbf{F}}_{\text{others}} \right) \quad (3.6)$$

where  $\bar{\mathbf{F}}_{\text{others}}$  are all forces not arising from surface adhesion, and  $\mu_c$  is the viscosity of the media in which a cell moves.

Initially a set of forming points are distributed on a plane, according to which a Voronoi tessellation is generated representing a cell aggregate. It is assumed that this cell aggregate consists of two types of randomly mixed cells, one is more adhesive than the other. At each iterative step, new positions of forming points are determined using Equation 3.6. A updated topology of the cell aggregate is achieved by a Voronoi tessellation according to the current positions of forming points. However, in order to keep the area constancy of each cell, the Voronoi tessellation used here allows gaps within the aggregate, and thus cells may not be simple-connected.

Given different values of the surface energy, various activities of cells including cell sorting, dissociation, checker-board formation and tissue engulfment are reproduced. However, the basic assumption of this model, which assumes there are mutual attraction forces across the long distance between non-adjacent cells, is quite disputable due to lack of experimental evidences.

### 3.2.4 Glazier and Graner Model

Inspired by the success of the large-Q Potts model in the simulation of the topological changes in cellular patterns in metal and soap froths (Glazier, 1989), Glazier

and Graner (1992, 1993) used an extended large-Q Potts model to simulate differential adhesion-driven cell sorting. Unlike all the above models which use packed polygons in a plane to represent the cell aggregate, cells in the large-Q Potts are defined by  $N$  degenerate spins,  $\sigma(i,j) = 1, 2, \dots, N$ , where  $i,j$  identify a lattice site. A cell  $\sigma$  consists of all sites in the lattice with the same spin. Cells might have different the number of sides at different steps, and need not be simply connected. Two types of cells: dark cells denoting stronger adhesiveness and light cells denoting lesser adhesiveness, are randomly mixed at the beginning. The medium is also considered as one cell type. No cellular properties other than the cell-cell, cell-medium interfacial energies  $J$  are assigned to the entire cell aggregate. Therefore, there are four independent parameters of interfacial energy:  $J(d,d)$  is the interfacial energy between two dark cells;  $J(l,l)$  between two light cells;  $J(d,l) = J(l,d)$  is the interfacial energy between a dark cell and a light cell;  $J(d,M) = J(l,M)$  is the interfacial energy between a dark or light cell and the medium. At each step, a lattice site is selected randomly and its spin is changed from  $\sigma$  to  $\sigma'$  with Monte Carlo probability. Simulations with a wide range of the energy parameters are carried out. It was found that spontaneous cell sorting can occur when the values of  $J$  satisfy the following inequalities:

$$0 < J(d,d) < (J(d,d) + J(l,l))/2 < J(d,l) < J(l,l) < J(l,M) = J(d,M) \quad (3.7)$$

Over a long period of simulation time, complete cell sorting is obtain under the assumption  $J(d,d) = 2$ ,  $J(d,l) = 11$ ,  $J(l,l) = 14$ ,  $J(d,M) = J(l,M) = 16$ . It is worth pointing out that Equation 3.5 is only a necessary condition for complete cell sorting but not a sufficient one. Small differences between  $J(d,d)$  and  $J(l,l)$  prevent the complete sorting configuration (i.e., cluster of dark cells is completely engulfed by light cells) from being reached. Sulsky's simulation results (1984) also support this statement. By varying these interfacial energy values, other important cell behaviours including checkerboard formation, tissue spreading, position reversal and dispersal are reproduced from the simulations.

Since differential adhesion is the only driving force in this model, the simulation results suggest that the energy landscape is important to biological cell sorting and that not only active cells can rearrange, slightly fluctuating or possibly even purely passive cells, lacking autonomous motile apparatus, can sort partially or completely, engulf, disperse, or form checkerboards. It serves as a verification of Steinberg's differential adhesion hypothesis.

This study carries out a systematic investigation of various cell properties related to the cell interfacial free energy, and defines qualitative free energy relationships between different types of interfaces within a heterotypic cell aggregate associated with each of those phenomena (cell sorting, engulfing, etc.). Although the simulations yield good cell sorting patterns, like Sulsky *et al.* model, there are no other morphogenetically important intracellular structures presented, since the methodology of this model is purely from statistics point of view. Table 3.2 summarizes the existing models of biological cells.

Inspired by the existing models both on the tissue-level and cell-level, and by the need of for better model to combine a good simulation engine and the feasibility of incorporating cell micro-components, a novel finite element cell model is proposed in the following chapter.

**Table 3.2 Simulation Models of Biological Cells**

<b>Name</b>	<b>Biological Process</b>	<b>Features</b>	<b>Engine</b>	<b>Simulation Results</b>	<b>Constraints</b>
<b>Weliky and Oster Model</b>	<b>Fundulus epiboly</b>	<b>VT* monotypic cell population, CMB contractile forces and intracellular pressure; elastic material property; CNC allowed</b>	<b>finite difference method to calculate cell movement caused by nodal imbalance force</b>	<b>cell shape changes; reduction in the number of marginal cells; the dynamic pattern of cell rearrangement</b>	<b>cells are treated as mere vertices, not a continuous unit with visco-elastic material properties, no area-constancy preserved</b>
<b>Sulsky et al Model</b>	<b>differential adhesion-driven cell sorting</b>	<b>VT* heterotypic cell aggregate consisting three kinds of cells; different adhesive energy is assigned; viscous material properties; CNC allowed</b>	<b>iterative scheme to calculate cell movement to minimize free energy</b>	<b>cell sorting; engulfment; intermixing</b>	<b>no other force-generating intracellular structures included; initially cells are not randomly mixed; can not portrait the real cell shape changes</b>
<b>Graner Model</b>	<b>differential adhesion-driven cell sorting</b>	<b>VT* heterotypic cell aggregate consisting two kinds of cells; different adhesive energy is assigned</b>	<b>iterative scheme to calculate cell movement along the gradient of free surface energy</b>	<b>cell sorting; engulfment; intermixing, cell dissociation</b>	<b>basic assumption lacks of experimental evidence</b>

**Table 3.2 Simulation Models of Biological Cells (continue)**

<b>Name</b>	<b>Biological Process</b>	<b>Features</b>	<b>Engine</b>	<b>Simulation Results</b>	<b>Constraints</b>
Graner and Glazier Model	differential adhesion-driven cell sorting	heterotypic cell aggregate consisting of two kinds of cells; temperature and membrane type-dependent surface energy is assigned; CNC allowed	extended high-Q Potts method (statistics) to calculate cell movement according to Monte Carlo probability	a systematic study of cell sorting, engulfment, intermixing, dispersing, checker-board forming in terms of surface energy	based on hypothetical values of cell surface-energy; no mechanical analyses presented; can not portray the real cell shape changes

\*VT: Voronoi Tessellation; \*\*CNC: cell neighbour changes

# Finite Element Model of Cells



## 4.1 Cell Topology and Voronoi Tessellation

As shown previously in Figure 1.3, a cell can take various shapes depending on its location and function. Most epithelial cells in a living embryo typically form sheets of convex polygons with 3 to 7 sides. The size of an embryonic cell is a couple of micrometers which is invisible to human eyes. Figure 4.1 shows two micrographs of embryonic cells. Stage numbers are according to the classification of Bordzilovskaya, *et al.*, (1989). During these stages, significant cell divisions and position changes occur, thus at stage 9, a smaller cell size and greater number of cells are observed. However, there is no significant volume change of the embryo.

Two embryos are never exactly the same, and two cell sheets are unique when mapped bit by bit. Yet the same type of cells do possess very similar properties. The first challenge of the simulation of such materials is to find a general geometric representation of the cell sheet, which is independent of the individual shapes of the cells. Voronoi Tessellation is found to give a close representation of this type of cell topological pattern [Bowyer, 1981; Honda and Yamanaka, 1986]. The definition of Voronoi Tessellation is described as this: given the positions of  $n$  distinct points  $a, b, c, \dots$ , namely forming points,

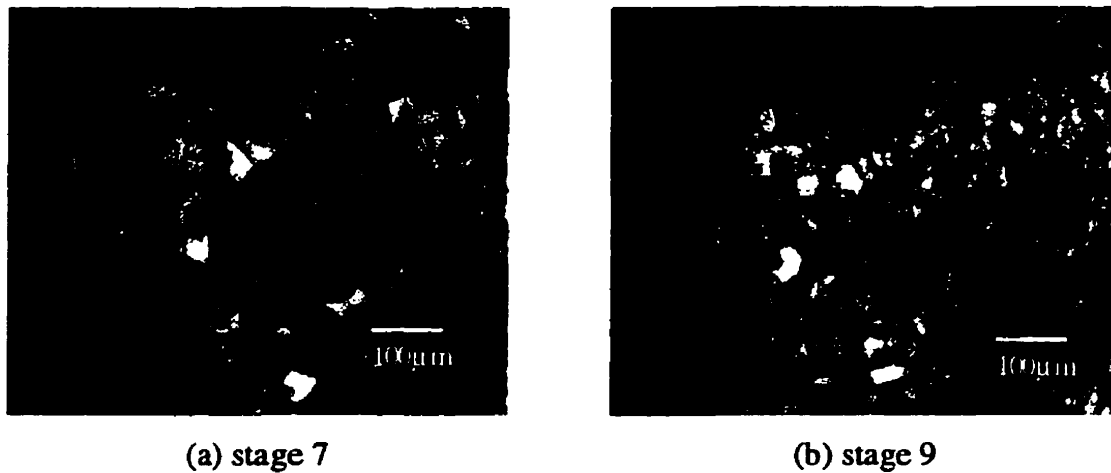


**Figure 4.1 Image of Cellular Patterns of an Axolotl Embryo at Development Stages 7 and 9.**

(after Brodland and Veldhuis, 1996)

in the plane, around a point  $O$ , a territory can be found such that every point within this territory is nearer to this forming point than to any other forming point. The resulting territories will form a pattern of packed convex polygons covering the entire plane (Figure 4.2).

The process of obtaining a Voronoi Tessellation is illustrated in Figure 4.3. First, a set of forming points are generated within a given region  $w$  by  $h$ . In this study, a machine-dependent random number generating algorithm is employed to find the coordinates of forming points. The minimum distance between distinct points is  $d$ . When a new point is generated, the distances from this new point to every existing point in the region are calculated and compared with  $d$ . If any of these distances is shorter than  $d$ , the new point will be discarded. Thus, the smaller  $d$  is, the more forming points are generated. Around a forming point  $O$ , a circular region with the radius  $r$  is defined. This

is called the searching circle, containing all eligible points to form a Voronoi tessellation cell around that forming point. Among all points in the searching circle, the closest point to point  $O$ , which is indicated by  $a$ , is chosen to be the starting point. The perpendicular line  $v_0-v_1$  lies in the middle of line  $O-a$  and consists one side of a cell. A counter clockwise research is carried out to find the next point  $b$ , and the perpendicular line  $v_1-v_2$  at the middle point between  $O$  and  $b$  will be another side of the cell. The intersection point  $v_1$  is a vertex of the cell. The same procedure is repeated until all sides of the cell are found. The resulting pattern can be a straight edge or a free boundary depending on the nature of the simulation. If a straight edge pattern is required, then reflections of the points along the edges within the bandwidth of  $b$  are needed, as indicated by the gray dots in Figure 4.3.

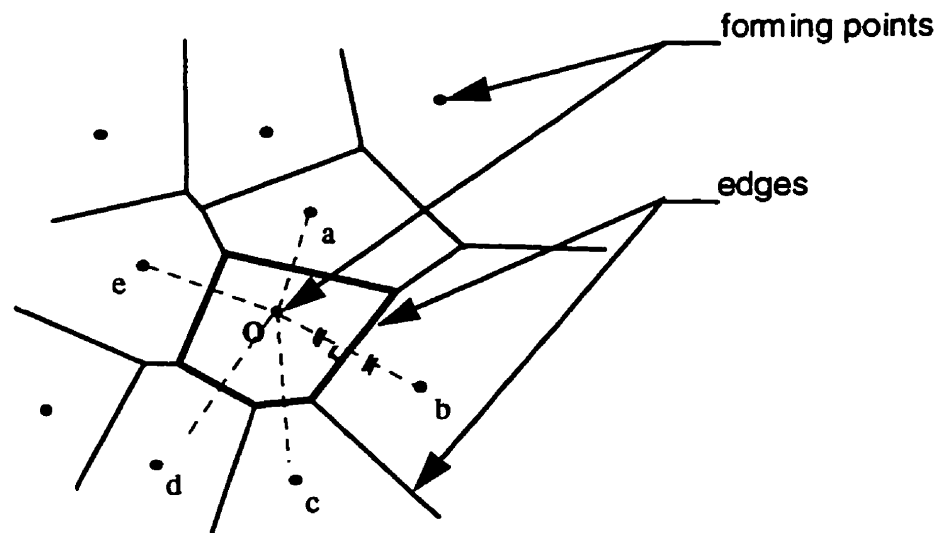


**Figure 4.2 Definition of Voronoi Tessellation**

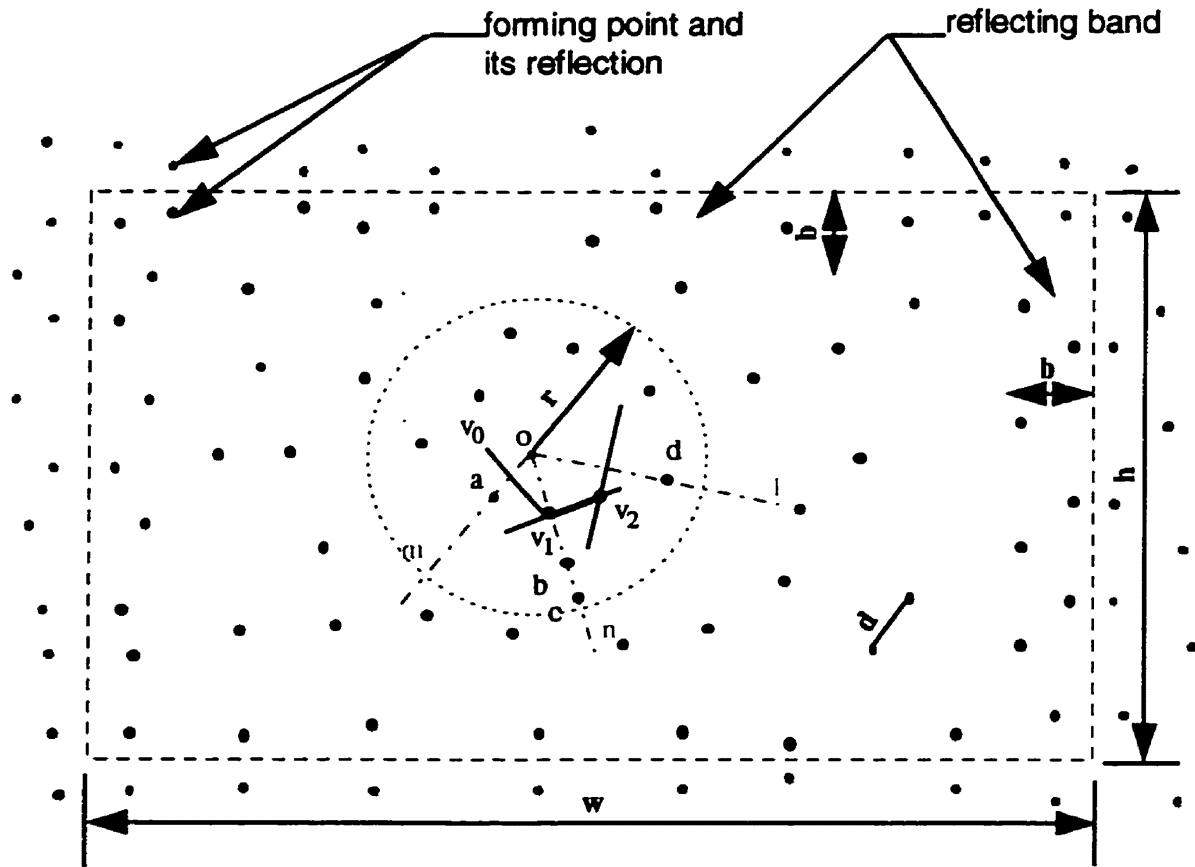


**Figure 4.3 Parameters in the Calculation of Voronoi Tessellation**

The density and regularity of the tessellation depend on a combination of certain criteria, as summarized in Table 4.1. Figure 4.4 depicts the flow chart of the computer implementation.

Two straight-edge and two free-edge Voronoi tessellation patterns are presented in Figure 4.5. The irregular pattern (a) is similar to a cell sheet at its early stage of development with very active cell division. The pattern (b) is an evenly distributed pattern common at later stages of the development. (c) and (d) are two free-edge tessellation, with more evenly distributed patterns, representing more mature cell aggregates. Great

similarity exists between the cell sheet shown in Figure 4.1 and the Voronoi Tessellation patches.

**Table 4.1 Criteria Regulating the Characteristics of a Voronoi Tessellation**

<b>Parameter</b>	<b>Description</b>	<b>Function</b>
<b>d</b>	minimum distance between two distinctive forming points	density of the tessellation
<b>MAX_TRY</b>	maximum number of attempts to find a new forming point before stopping	regularity of the patch
<b>r</b>	the searching range	regulate points selected in the process of finding all vertices for a polygon
<b>b</b>	bandwidth of the region within which points are reflected	generate a straight edge of the patch

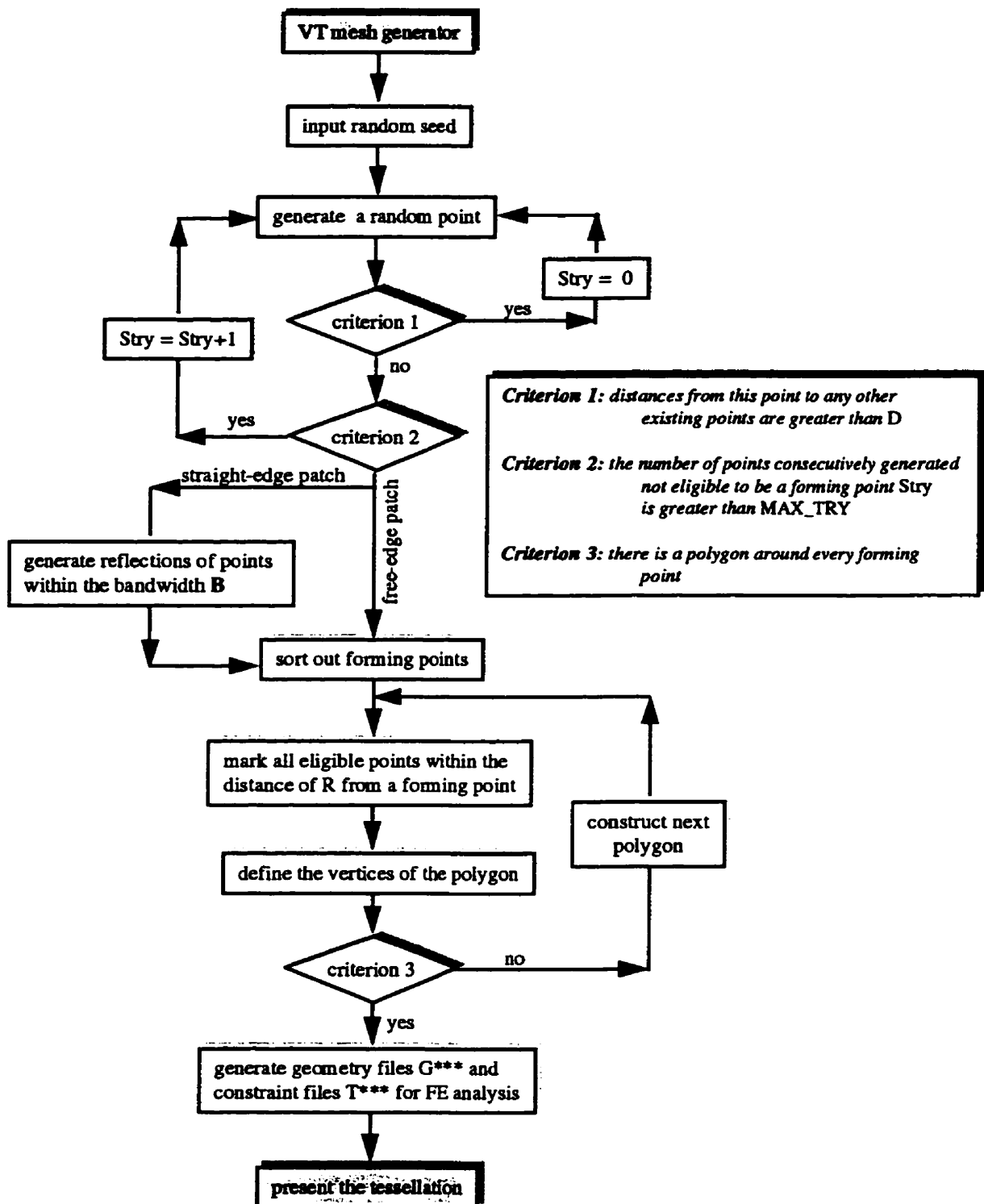
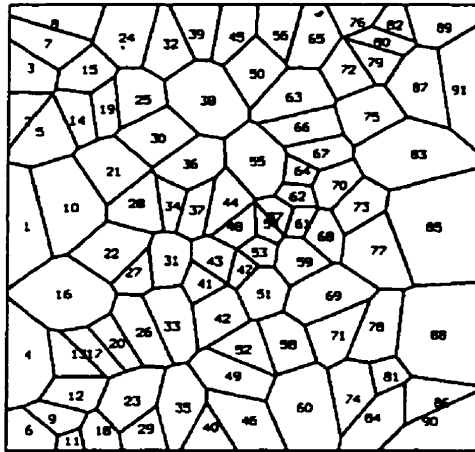
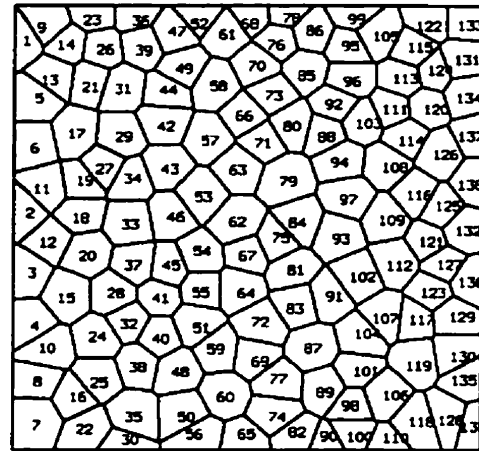


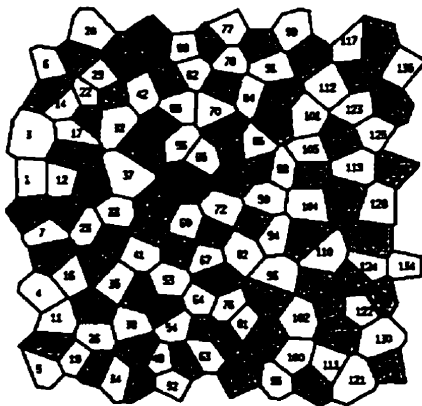
Figure 4.4 Computer Implementation of Voronoi Tessellation



(a) uneven straight-edge mesh



(b) even straight-edge mesh



(c) intermixed free-edge cell aggregate



(d) heterotypic cell tissues

Figure 4.5 Voronoi Tessellation

## 4.2 Cell Element

A key to meaningful simulations on the cellular level is a successful numerical model of a living cell, which incorporates cell geometry, cell micro-structures and most of all, cellular activities. A cell sheet consists of numerous cells and is treated as a plane strain problem.

In this study, each cell is modeled individually. As shown in Figure 4.6, a  $n$ -sided cell is broken into  $n$  triangular elements as indicated by the dash lines. An auxiliary node (shown solid black) is placed in the centroid of each cell. It is not a physical node but a division reference point to produce reasonable aspect ratios in the triangular elements. Each triangular sub-element has viscosity  $\mu$  and Poisson's ratio,  $\nu = 0$ , permitting the cytoplasm to freely shift from one place to another within the cell. Although each

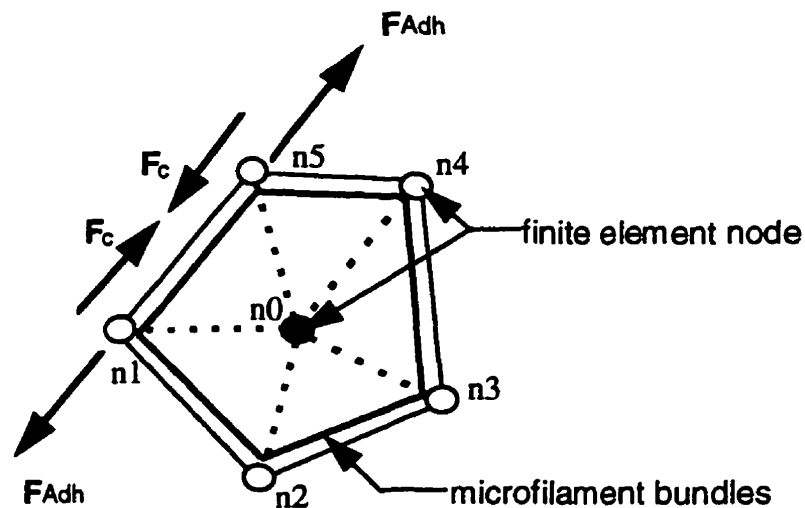
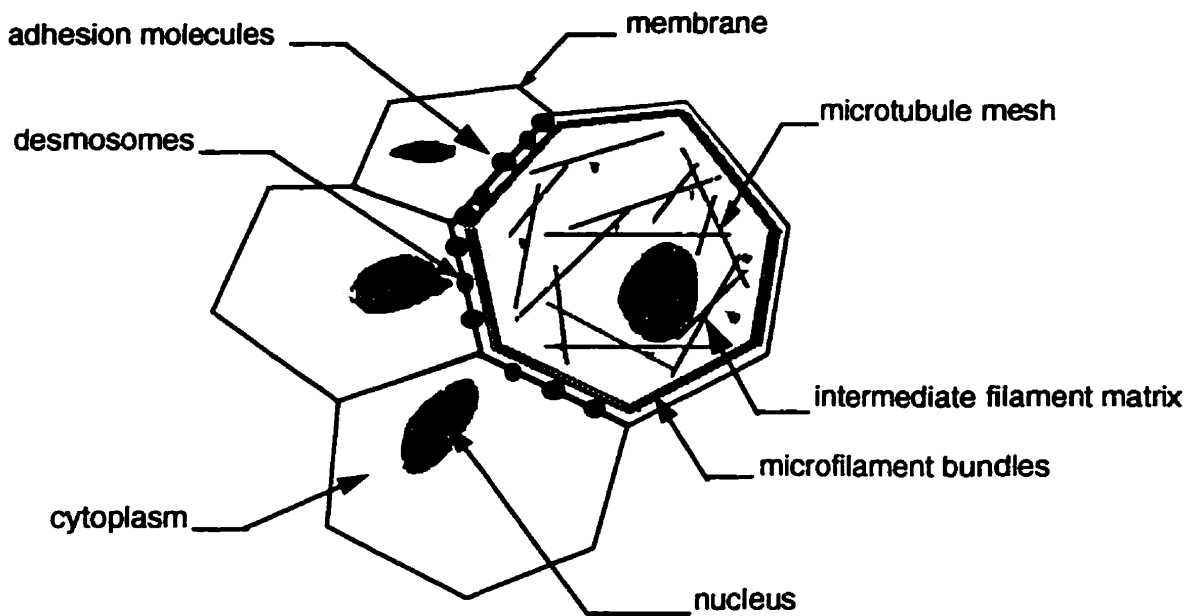


Figure 4.6 Cell Element

triangular sub-element can change in area, the total volume of the cell is kept constant using a Lagrangian side condition. Therefore, an n-side cell is treated as a bulk element called a cell element. Note that n can be an arbitrary number.

A variety of structural components are thought to have mechanical significance inside of these cells and between adjacent cells (Figure 4.7).



**Figure 4.7 Two-dimensional Presentation of the Micro-components in a Cell**

Several of these generate forces along cell boundaries. These include circumferential microfilament bundles (CMBs) which inscribe the apical end of the cell and generated a contractile force

$$F_{\text{CMB}} = \sigma A, \quad (4.1)$$

where  $A$  is the cross-sectional area of the CMBs and  $\sigma$  is the contractile stress or tonus in the bundle. A contractile force  $F_{\text{Mem}}$  is also produced by the cell membrane itself. In contrast to these contractile forces, surface adhesions between two adjacent cells  $i$  and  $j$  produce forces  $F_{\text{Adh}}$  that tend to make their common boundary increase in length. Randomly oriented microtubules which lie immediately below and parallel to the apical surface of the cell also generate an equivalent force  $F_{\text{MT}}$  along the boundaries. This force also acts in opposition to the CMBs and membrane tension. Some of these forces are transferred directly from cell to cell by cell junctions. Collectively, these forces produce a total equivalent contractile force,

$$F_c = F_{\text{CMB}} + F_{\text{Mem}} - F_{\text{Adh}} - F_{\text{MT}} \quad (4.2)$$

along each interior cell edge (Figure 4.6). Cell edges along the boundary of a patch are assumed to generate a force of  $F_c/2$ . The cytoplasm in each cell generates forces due to its viscosity  $\mu$ , and forces due to any intra-cellular pressure  $p$  it carries.

With time, the entire cell sheet undergoes large deformations. An updated Lagrange algorithm is employed to calculate the deformations. Within a sufficiently small time interval, an infinitesimal linear theory can be applied to solve the system equations. The configuration is updated at the end of each time step.

The area of an  $n$ -sided polygon is obtained through its nodal coordinates:

$$A = \frac{1}{2} \sum_{i=1}^n \begin{vmatrix} x_i & y_i \\ x_{i+1} & y_{i+1} \end{vmatrix} \quad (4.3)$$

Note that in the above formulation, the index numbers 1 and  $n+1$  both indicate the first node since the polygon is a closed object. Within time interval  $\Delta t$ , when the displacement of each node,  $\Delta u_i$  and  $\Delta v_i$ , are infinitesimal, the change of the area is:

$$\begin{aligned}\Delta A &= \frac{1}{2} \sum_{i=1}^n \left\{ \frac{\partial A}{\partial x_i} dx_i + \frac{\partial A}{\partial y_i} dy_i \right\} \\ &= \Phi \Delta U\end{aligned}\quad (4.4)$$

where

$$\begin{aligned}\Delta U &= \left\{ \Delta u_1, \Delta v_1, \dots, \Delta u_i, \Delta v_i, \dots, \Delta u_n, \Delta v_n \right\}^T \\ \Phi &= \left\{ \alpha_1, \beta_1, \dots, \alpha_i, \beta_i, \dots, \alpha_n, \beta_n \right\} \\ \alpha_i &= \frac{y_{i+1} - y_{i-1}}{2} \quad \beta_i = \frac{x_{i-1} - x_{i+1}}{2}\end{aligned}$$

Since a pure viscous material property is assumed within each triangular element, the stress depends on the strain rate. The constitutive equation is:

$$\dot{\epsilon} \equiv \frac{d\epsilon}{dt} = \mathbf{D}\sigma \quad (4.5)$$

here  $\mathbf{D}$  is the stress-strain rate operator matrix related to Poisson's ratio and viscosity of the material. The subsidiary condition  $\Delta A = 0$  which preserve the area constancy of a cell can be introduced into the functional of the principle of minimum potential energy  $\prod_p$  using a Lagrange multiplier  $p$ . Denoting the strain energy of the system by  $E$ , the body force by  $\bar{f}_i$ , and the force on the boundaries by  $\bar{T}_i$ ,  $\prod_p$  takes the form:

$$\Pi_p = \iint_{\Omega} [\mathbf{E}(\boldsymbol{\sigma}, \boldsymbol{\varepsilon}, \dot{\boldsymbol{\varepsilon}}) - \bar{\mathbf{f}}_i] d\Omega - \int_{\sigma_e} \bar{\mathbf{T}}_1 ds + p\Delta A \quad (4.6)$$

Linear shape functions are used in each triangular element. The stationary conditions of  $\Pi_p$  with respect of  $u_i, v_i, \dot{u}_i, \dot{v}_i$  and  $p$  provide system equations as follows:

$$\sum_{i=1}^n \mathbf{c}_i^e \dot{\mathbf{u}}_i^e + \sum_{i=1}^n \mathbf{k}_i^e \mathbf{u}_i^e + p\Phi\Delta\mathbf{U} = \sum_{i=1}^n \mathbf{f}_i^e \quad (4.7)$$

and

$$\Phi^T \Delta\mathbf{U} = 0 \quad (4.8)$$

where

$$\mathbf{u}_i^e = \{u_0, v_0, u_i, v_i, u_{i+1}, v_{i+1}\}^T$$

$$\dot{\mathbf{u}}_i^e = \{\dot{u}_0, \dot{v}_0, \dot{u}_i, \dot{v}_i, \dot{u}_{i+1}, \dot{v}_{i+1}\}^T$$

The symbol  $\Sigma$  denotes the assembling of all triangular elements in one cell. The damping and stiffness matrices of the  $i^{\text{th}}$  triangular element are  $\mathbf{c}_i^e$  and  $\mathbf{k}_i^e$ , respectively. The displacement and velocity vectors are  $\mathbf{u}_i^e$  and  $\dot{\mathbf{u}}_i^e$ . Since the time interval  $\Delta t$  is small, the velocity can be approximated by

$$\dot{\mathbf{u}} = \frac{\Delta \mathbf{u}}{\Delta t} \quad (4.9)$$

in which  $\Delta \mathbf{u}$  is the change of the displacement within the current step  $t$ . Combining the change of the displacements and the multiplier  $\lambda$  into one vector  $\Delta\mathbf{U}^T$ :

$$\Delta \mathbf{U}^t = \{\Delta u_0, \Delta v_0, \Delta u_1, \Delta v_1, \dots, \Delta u_n, \Delta v_n, \lambda\}^T \quad (4.10)$$

equations 4.7 and 4.8 can be written in matrix form as:

$$\mathbf{S}^t \Delta \mathbf{U}^t = \mathbf{F}_{\text{cell}}^t - \left\{ \sum_{t=0}^{t-1} \mathbf{K}^t \Delta \bar{\mathbf{U}}^t, 0 \right\}^T \quad (4.11)$$

where

$$\mathbf{F}_{\text{cell}}^t = \{ 0, 0, f_1, f_2, \dots, f_{2n-1}, f_{2n}, 0 \}^T$$

$$\Delta \bar{\mathbf{U}}^t = \{\Delta u_0^t, \Delta v_0^t, \Delta u_1^t, \Delta v_1^t, \dots, \Delta u_n^t, \Delta v_n^t\}^T$$

and

$$\mathbf{S}^t = \begin{bmatrix} S_{1,u_0} & S_{1,v_0} & S_{1,u_1} & S_{1,v_1} & \dots & S_{1,u_n} & S_{1,v_n} & 0 \\ S_{2,u_0} & S_{2,v_0} & S_{2,u_1} & S_{2,v_1} & \dots & S_{2,u_n} & S_{2,v_n} & 0 \\ \hline S_{3,u_0} & S_{3,v_0} & S_{3,u_1} & S_{3,v_1} & \dots & S_{3,u_n} & S_{3,v_n} & \alpha_1 \\ S_{3,u_0} & S_{4,v_0} & S_{4,u_1} & S_{4,v_1} & \dots & S_{4,u_n} & S_{4,v_n} & \beta_1 \\ \vdots & \vdots & \vdots & \vdots & \ddots & \vdots & \vdots & \vdots \\ S_{2n+1,u_0} & S_{2n+1,v_0} & S_{2n+1,u_1} & S_{2n+1,v_1} & \dots & \cdot & \cdot & \alpha_n \\ S_{2n+2,u_0} & S_{2n+2,v_0} & S_{2n+2,u_1} & S_{2n+2,v_1} & \dots & \cdot & \cdot & \beta_n \\ 0 & 0 & \alpha_1 & \beta_1 & \dots & \alpha_1 & \beta_1 & 0 \end{bmatrix}$$

where

$$S_{i,j} = \frac{c_{i,j}}{\Delta t} + k_{i,j}$$

By rewriting partitioned Equation 4.11 as

$$\begin{bmatrix} S_{oo} & S_{oc} \\ S_{co} & S_{cc} \end{bmatrix} \begin{Bmatrix} x_o \\ x_c \end{Bmatrix} = \begin{Bmatrix} 0 \\ f_c \end{Bmatrix} \quad (4.12)$$

where

$$x_o = \{u_o \ v_o\}^T$$

$$x_c = \{u_1 \ v_1 \ \dots \ u_n \ v_n \ \lambda\}^T$$

Furthermore, the degree-of-freedom of the internal node can be eliminated by being condensed to the nodes on the cell edges. Note that in Equation 4.12, the force vector includes the recovery forces from the last term of Equation 4.11 at the right hand side. Here  $S_{oo}$  is a  $2 \times 2$  matrix,  $S_{oc}$  is a  $2 \times (2n+1)$  matrix,  $S_{co}$  is a  $(2n+1) \times 2$  matrix and  $S_{cc}$  is a  $(2n+1) \times (2n+1)$  matrix. Two equations can be derived from Equation (12):

$$S_{oo} x_o + S_{oc} x_c = 0 \quad (4.13)$$

$$S_{co} x_o + S_{cc} x_c = f_c \quad (4.14)$$

Eliminating  $x_o$  from Equations 4.13 and 4.14 gives the condensed cell element equations:

$$\left( S_{cc} - S_{co} S_{oo}^{-1} S_{oc} \right) x_c = f_c \quad (4.15)$$

Thus in the simulations herein, no degrees-of-freedom related to internal nodes are explicitly calculated.

### 4.3 Rules of Cell Neighbour Changes

During neurulation, cell division is not a dominant phenomenon and will be excluded from this study. On the other hand, cell neighbour changes are one of the most common activities and play a significant role especially when large deformations of the cell sheet are involved. The sides of cells will lengthen or shorten. When a side is shorter than a minimum length, the connection between two cells is finally broken, and the two contiguous cells separate. For instance, in Figure 4.8 (a), adjacent cells 1 and 3 share the side a-b (highlighted by the circle). When the minimum specified length is reached (b), side a-b rotates 90°, resulting in the separation of cells 1 and cell 3 (c).

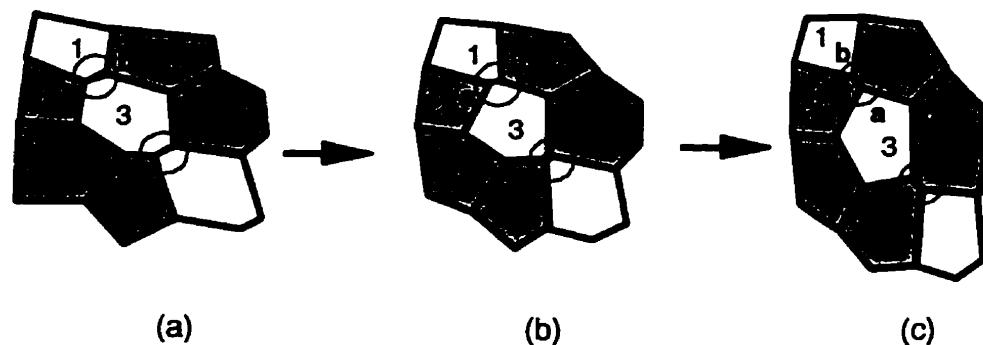


**Figure 4.8 Neighbour Change in the Cell Sheet**

A computing algorithm permits this crucial cellular behaviour in our model. When a straight edge cell sheet is considered, special attention need to be paid to the nodes on the cell sheet edge when they change neighbours. Table 3.1 is a detailed summary of all possible cases in neighbour changes between cells.

Table 4.2 Neighbour Changes Within a Cell Sheet

Position	Before NC	After NC	Position	Before NC	After NC
straight edge			free-edge		
left top			left bottom		
right top			right bottom		

\*NC: Neighbour Changes

#### 4.4 Computer Implementations

A program called **FECSEM** (Finite Element Computer Simulation of Embryo Morphogenesis) was developed in the programming language C to implement the above cell model. There are three major sections of **FECSEM**: **vmesh**, **cell2d**, and **fastdraw**. Both straight-edge and free-edge Voronoi tessellation meshes are generated using **vmesh**. A different set of random points will result in a different cell patch. Various cell activities are simulated using **cell2d**. An updated Lagrangian iterative scheme is used. The cell element formulation is applied to each cell, and all forces at each node are calculated. After applying constraints and boundary conditions, the system equations are solved and a new configuration is obtained. Based on this new configuration, the same procedure is repeated. Simulation results can be played back and forth step by step using **fastdraw**. The flowchart in Figure 4.9 illustrates the detail computer implementation of the cell model.

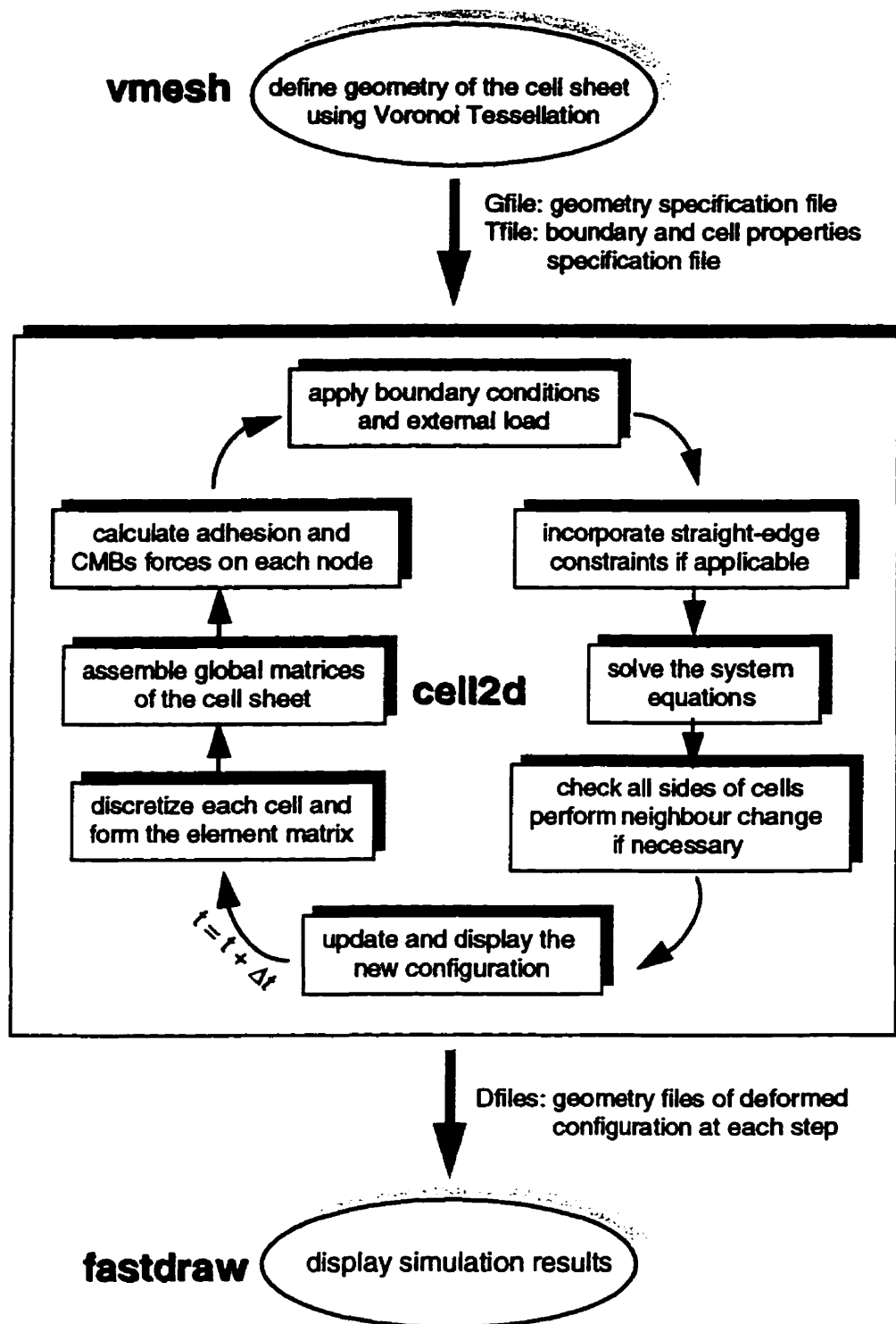


Figure 4.9 Implementation of the Computer Simulation

# **Cell Rearrangement and Bulk Mechanical Properties of Epithelial Cell Sheets**

# **5**

Unlike materials such as steel or cement which have properties that can be tested using established methods and expressed in well-known constitutive equations, the mechanical properties of the biological cell sheet are still largely unknown. Since the mechanical properties are greatly affected by the active behaviour of cells, none of the traditional testing methods are feasible for measuring these mechanical properties because they will interfere with the cell activities, thus altering the true mechanical characteristic of the cell sheet. Nevertheless, computer simulations using the cell element derived previously, keep cell micro-structures intact and permit simulation of critical living cell activities during the deformation of the cell sheet. They thus provide an ideal and systematic way to study the mechanical properties of the cell sheet in a systematic way.

In this chapter, straight-edged epithelial cell sheets subjected to various external stimuli are simulated. Active cell rearrangements occur during the deformation of the cell sheet. The external stresses acting on the cell sheet generate the movement of the cell sheet and the internal pressures inside the cell sheet caused by the deformation of cells are calculated. Moreover, an analytical expression for these stresses and pressures are derived and the results are compared with the numerical values. The purpose of this simulation is

to determine, in quantitative mechanical terms, the mechanical effect of circumferential microfilaments bundles, cell cytoplasm viscosity, internal cell pressures, cell rearrangement, and external loads or displacements on the mechanical behaviours of epithelial cell sheets.

### 5.1 Definition of Parameters

Morphogenetic processes in embryos are a dynamic phenomenon, which can be described in terms of a developmental time  $\tau$ , which can be a real time  $t$  or a development stage. Thus a dynamic procedure ( an iterative scheme in this study), is adapted for the computer simulations. In a meaningful simulation, the time  $t$  in the iterative solving process should possess a linear relationship with the development time  $\tau$ .

In the simulation of neurulation, for example, Brodland and Clausi (1995) defined a time scaling factor  $\theta$  with a unit of  $\text{time}^{-1}$ , where

$$\tau = t \theta. \quad (5.1)$$

By setting  $\theta$  to 0.5, the simulation results match the real sequence of neurulation embryo *in vivo* reasonably well. In this current work, the same convention is followed. The value of  $\theta$  varies from case to case depending on the process simulated and the properties assigned to the cell sheet.

Once the geometry and the size of the cell sheet are determined, the amplitude of the contractile forces  $F_C$  and the viscosity  $\mu$  of the cytoplasm are assigned to the cell sheet. From a mathematical point of view, it is the ratio of these values that decides the movement of each node and thus defines the deformation of the cell sheet, rather than the absolute values of  $F_C$  or  $\mu$ . In other words, different cell properties, different cell sheet sizes, and different iterative time steps can yield exactly the same deformed configuration of the cell sheet, as long as the ratio between these parameters remain the same. To

simplify the analysis, we define a sheet characterization parameters  $Q_x$  as the ratio of the microfilament forces,  $S_{c_x}$ , in  $x$  direction per unit of sheet width, to the viscous forces produced by the cytoplasm, namely:

$$Q_x = \frac{S_{c_x}}{\mu \delta \dot{\epsilon}_x}, \quad (5.2)$$

where  $\delta$  is the thickness of the cell sheet. The value of  $S_{c_x}$ , can be found experimentally by counting the number of cell boundaries that cross a unit cross-section of the sheet and multiplying that number by the average cosine of the angle that they make with the cross-section, or it can be found theoretically by a similar procedure based on statistical mechanics. The parameter  $S_c$  is proportional to  $F_c$  and to the boundary density. It is also affected by cell shape in as much as cell shape affects the angles at which the cell boundaries cross an arbitrarily oriented section through the sheet.

The dimensionless internal pressure,  $P$ , is defined as

$$P = \frac{\bar{p}}{\mu \delta \dot{\epsilon}_x}, \quad (5.3)$$

where  $\bar{p}$  is the average intracellular pressure. The dimensionless stress,  $S_x$ , is defined as

$$S_x = \frac{r_x}{\mu \delta \dot{\epsilon}_x}, \quad (5.4)$$

where  $r_x$  is the total applied load divided by the dimension along which it acts. In the case of a cell sheet stretched in the  $y$ -direction, parameters  $Q_y$  and  $S_y$  are similarly defined.

A cell might take an arbitrary, n-sided polygonal shape. In order to describe it in a general quantitative manner, a simple geometric parameter has to be defined to describe the basic shape of the polygonal geometry. A conventional way is to approximate a polygon with an "best-fit" ellipse (Figure 5.1a). This ellipse and the original polygon will have the same principal moments of inertia  $I_1$  and  $I_2$ . As the cell sheet deforms, each cell elongates in the same direction and the principal axis remain aligned in x and y directions. Therefore, in this study, for each cell, a rectangle of size of  $a \times b$  (Figure 5.1b) is defined such that it will have the same momentum of inertia  $I_{xx}$ ,  $I_{yy}$  as the original polygon. The shape ratio of a cell is defined as the ratio of a to b, and is given by:

$$\kappa = \frac{a}{b} = \sqrt{\frac{I_{xx}}{I_{yy}}}, \quad (5.5)$$

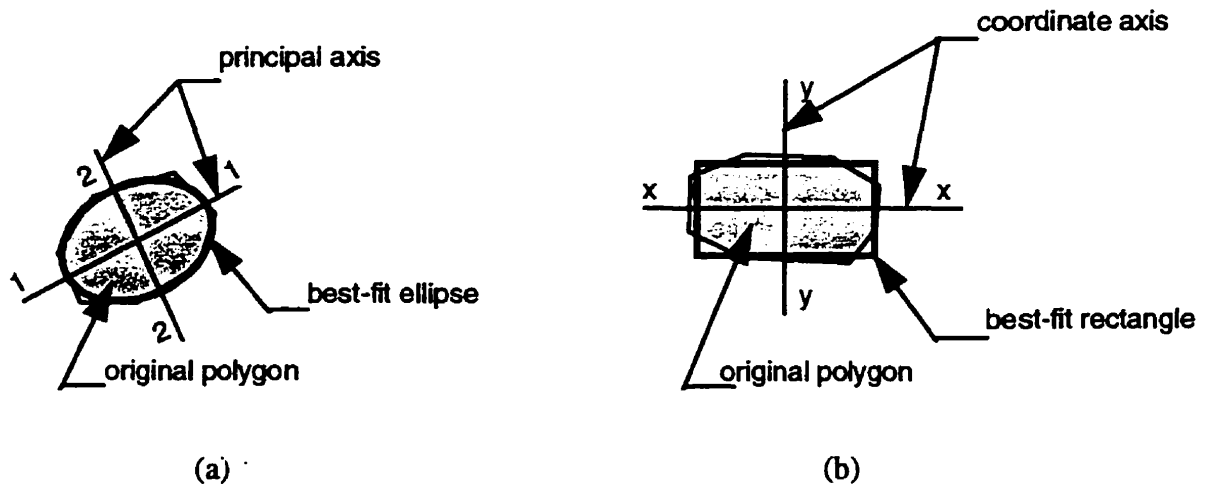


**Figure 5.1 Best-Fit Shapes for Polygon**

## 5.2 Annealing Process

In general, the nodal forces associated with the starting configuration ( a Voronoi tessellation) are not in balance. An annealing process is used to establish an equilibrated starting configuration. This is done by fixing all nodes along the boundaries so that they cannot move normal to their respective boundaries. Nodes are then allowed to move under the action of internal forces until an equilibrium state is obtained. Figure 5.2(a) is a Voronoi tessellation before annealing and Figure 5.2(b) is the annealed configuration. Some cell rearrangements occur, as might be expected, and cells tend to form equal angles

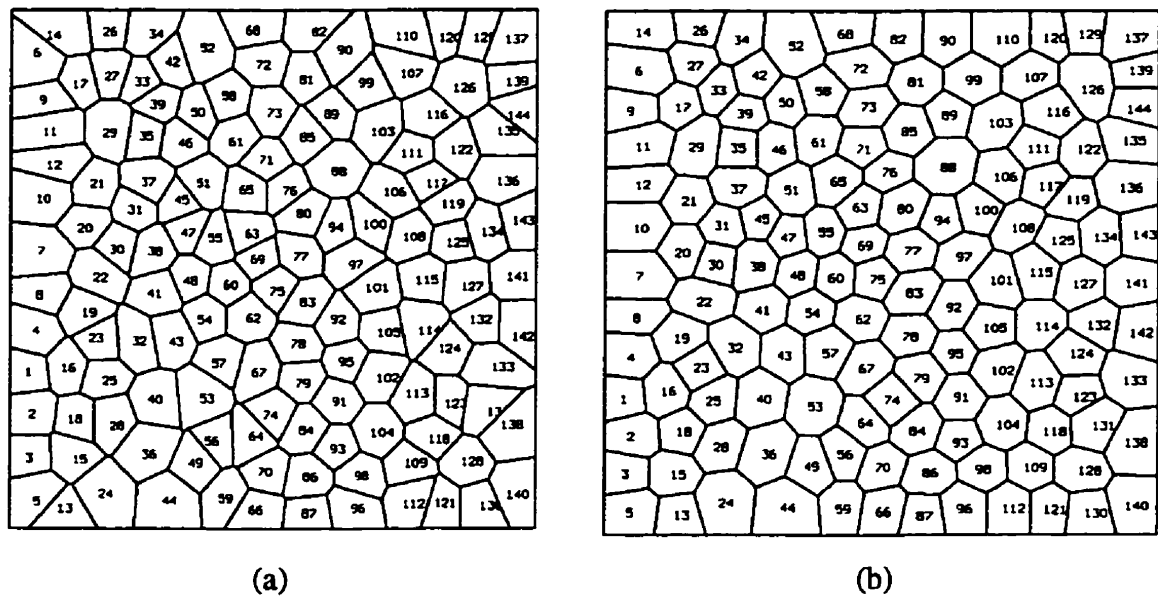


Figure 5.2 Annealing Process of a Straight-edge Cell Sheet

of  $120^\circ$  at all internal nodes. An intra-cellular pressure is also produced in each cell by the contraction forces  $F_C$  around their respective boundaries. Further tests prove that the final annealed configuration is independent of the parameters  $Q_x$  and  $Q_y$ . However, the smaller the magnitude of  $Q$ , the longer the time it takes to reach the annealed state. The annealing process ensures isotropy of the initial configuration. All sheets used hereafter are annealed before they are subjected to any external stimuli.

### 5.3 Analytical Formulation of the Bulk Mechanical Property

Consider a rectangular area with dimensions  $w$  and  $h$ , as shown in Figure 5.3. The area may consist of many cells as suggested by the dashed lines, or it may consist of a single (hypothetical) rectangular cell. The patch is assumed to have a thickness  $\delta$ , to be filled with a viscous material having viscosity  $\mu$ , and to have an (initially unknown) average internal pressure of  $p$ . The patch is further assumed to be stretched at a constant true strain rate, and to be acted on by an external true stress  $\sigma_x$ . No external stress is applied in the vertical direction.

The patch will be in equilibrium in the  $x$ -direction when

$$\sum F_x = 0 = F_{C_x} + \mu \delta h \dot{\epsilon}_x - p \delta h - \sigma_x \delta h \quad (5.6)$$

where  $F_{C_x}$  is the total force in the  $x$ -direction due to contraction forces along the cell boundaries. Similarly, there will be equilibrium in the  $y$ -direction when

$$\sum F_y = 0 = F_{C_y} - \mu \delta w \dot{\epsilon}_y - p \delta w \quad (5.7)$$

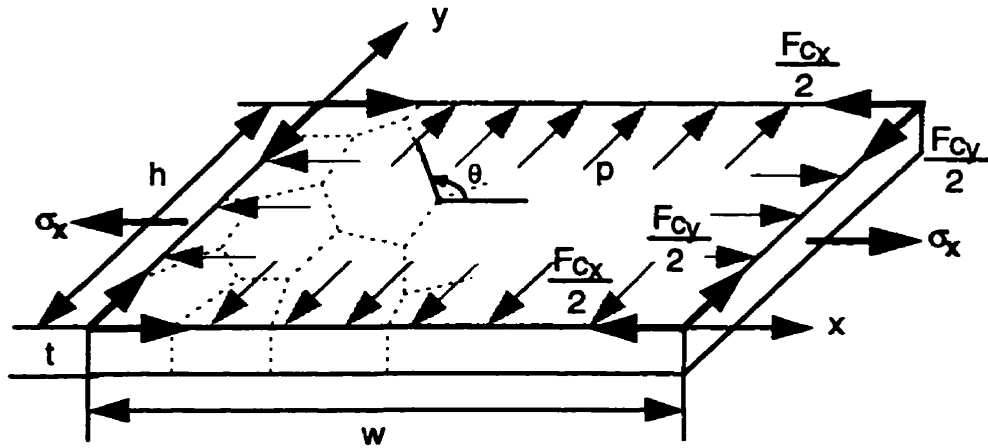


Figure 5.3 Schematic Diagram of Forces in a Cell Sheet

These equations can be combined to find the dimensionless internal pressure

$$p = \frac{F_{Cy}}{wt} - \mu \dot{\epsilon} \quad (5.8)$$

and the tensile resultant or stress

$$\sigma_x = \frac{F_{Cx}}{h\delta} - \frac{F_{Cy}}{w\delta} + 2\mu \dot{\epsilon}_x \quad (5.9)$$

or

$$\sigma_x = \frac{F_{Cx}}{h\delta} - \left( \frac{F_{Cy}}{w\delta} - \mu \dot{\epsilon}_x \right) + \mu \dot{\epsilon}_x \quad (5.10)$$

Following the same procedure as those in Equation 5.2-5.5, the dimensionless pressure and stress are defined as the following:

$$P = \frac{S_{C_x}}{\mu \delta \dot{\epsilon}_x} - 1 \quad (5.11)$$

$$S_x = \frac{S_{C_x}}{\mu \delta \dot{\epsilon}_x} - \frac{S_{C_y}}{\mu \delta \dot{\epsilon}_x} + 2 \quad (5.12)$$

Note that the internal pressure arises from contraction of the cell boundary in the y-direction and from an interaction of the viscosity with the constant-volume constraint. This is more readily apparent in Equation 5.10. The three terms of which show how the stress  $\sigma_x$  results from 1) the direct stress produced by the horizontally-oriented microfilaments, 2) a stress caused by the induced internal pressure, and 3) the direct viscous effect of the cytoplasm, respectively.

If the sheet is composed of many cells, as suggested by the dashed lines in Figure 5.3, the total force in the x-direction due to the action of force  $F_c$  along the cell boundaries can be estimated using statistical mechanics. If, for example, a cell sheet starts in an isotropic (annealed) condition, so that its  $q$  boundaries of average length  $d$  are distributed uniformly with respect to their angle  $\theta$  counter-clockwise from the x-axis, then the force across any cross-sectional normal to the x axis is given by

$$F_{c_x} = \int_0^{2\pi} \frac{qd}{w} \cos \theta F_c \cos \theta d\theta = \frac{qdF_c}{2w} = \frac{DhF_c}{2} \quad (5.13)$$

where

$$D = \frac{qd}{wh}, \quad (5.14)$$

is the area density of cell boundary. This can be expressed as an equivalent resultant

$$\sigma_x = \frac{DFc}{2}. \quad (5.15)$$

Force and resultant in the y-direction  $F_{Cy}$  and  $\sigma_y$  are defined in a similar fashion.

If the patch deforms, or if for some other reason, the cells in the patch and their boundaries are not isotropic, but stretched to a ratio of  $\gamma$  in the x-direction and  $1/\gamma$  in the y-direction (to maintain area constancy), then the angles of the cell boundaries that were not in the coordinate directions will change. The component of the force in the x-direction will now depend on the cosine of the new orientation angle and will produce a new net force of

$$F_{C_x} = \int_0^{2\pi} \frac{qd}{w} \frac{\gamma \cos \theta}{\sqrt{(\gamma \cos \theta)^2 + (\sin/\gamma)^2}} Fc \cos \theta d\theta \quad (5.16)$$

where the term with the square root ratio is the cosine of the new angle of a side which has been at angle  $\theta$  in the initial configuration. Equation 5.11 is a special case ( $\gamma = 1$ ) of Equation 5.14.

Equations 5.6 through 5.16 allow pressure and stress to be calculated provided that the cell shape is known. The cell shape parameter is dependent on the loading history and, at present, must be determined from numerical simulations or physical experiments which provide cell shape data via the shape ratio  $\kappa$  defined in Equation 5.5. An estimate of  $\gamma$  can be obtained by assuming that it is related to  $\kappa$  by

$$\gamma = \sqrt{\kappa_{\text{avg}}} , \quad (5.17)$$

as it is for a single, rectangular cell.

## 5.4 Simulation Results

In this section, 7 cases are presented. These cases systematically investigate the mechanical properties of cell sheets with different CMBs forces, viscosity, of different densities, boundaries, subjected to different external stimuli are investigated.

### 5.4.1 Cell Sheet Stretched at a Constant Strain Rate (Case 1)

Figure 5.4 (a) shows a cell sheet consisting of 144 cells. The sheet is stretched horizontally at a constant true strain rate. This is accomplished by constraining nodes along the left side of the cell patch from moving horizontally and nodes along the bottom side from moving vertically. Nodes along the right side are moved horizontally at an increasing speed so as to produce a constant true strain rate. Nodes along the top edge are constrained so that they all move in the vertical direction by the same amount. The dimensionless parameter  $Q_x$  is 12.

Figure 5.4 (b) and (c) show the patch as it is stretched in the x-direction. The solid curve in Figure 5.5 (a) is  $S$  versus stretch ratio  $\lambda$  curve for the patch. The average cell shape as measured by  $\kappa$  is also shown. The vertical bars show the number of neighbour changes that occur at each step of the simulation. By the time the patch is stretched to  $\lambda = 5$ , 322 simulation steps have been used. During the initial stages of elongation ( $1 \leq \lambda \leq 2$ ), few neighbour changes occur, and the deformation is accommodated almost entirely by cell shape change. Beyond approximately  $\lambda = 3$ , significant neighbour changes occur and the average cell shape changes little. This is because it becomes energetically

Chapter 5 - Cell Rearrangement and Bulk Mechanical Properties

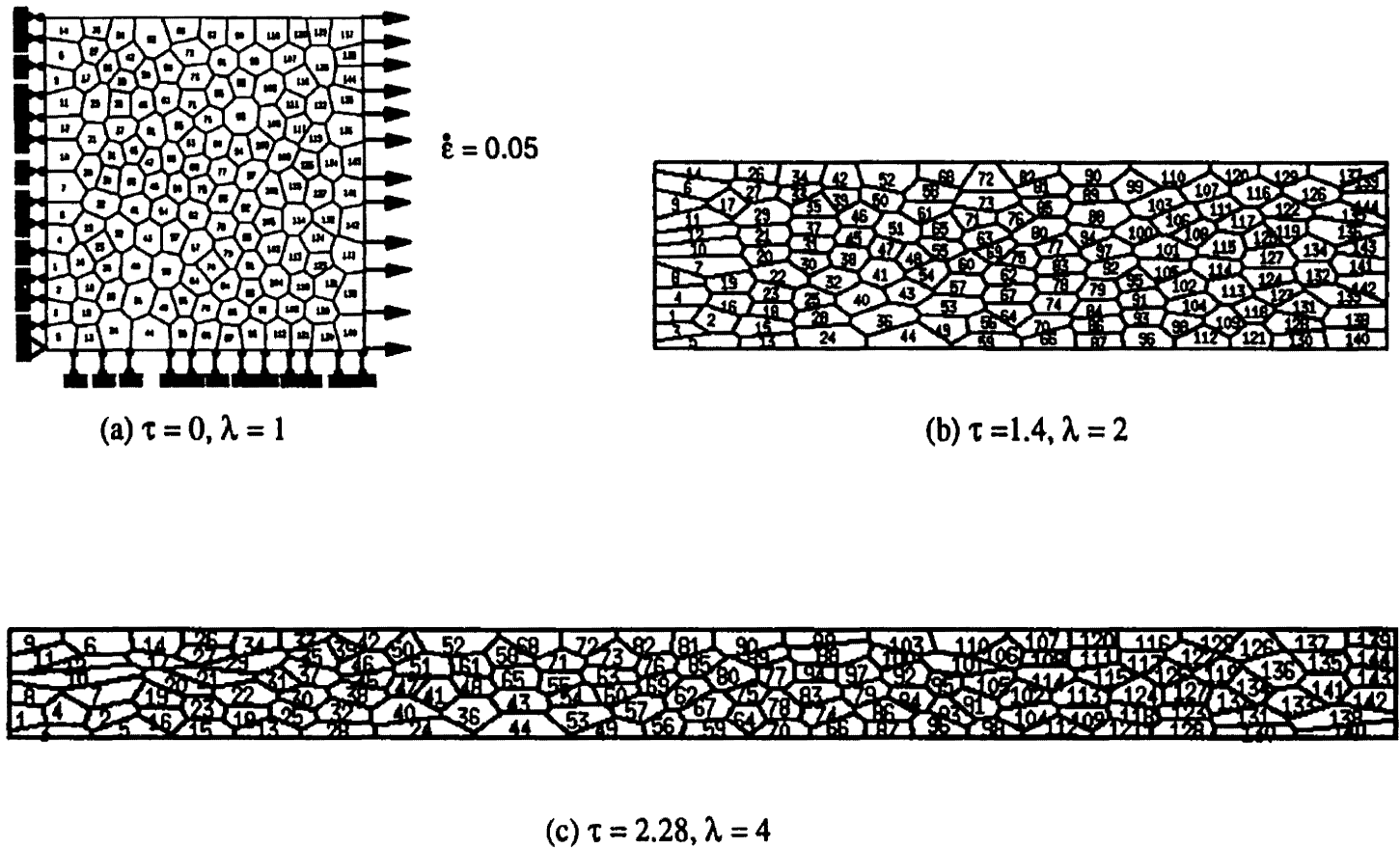


Figure 5.4 Elongation of a Cell Sheet in X-direction at a Constant Rate

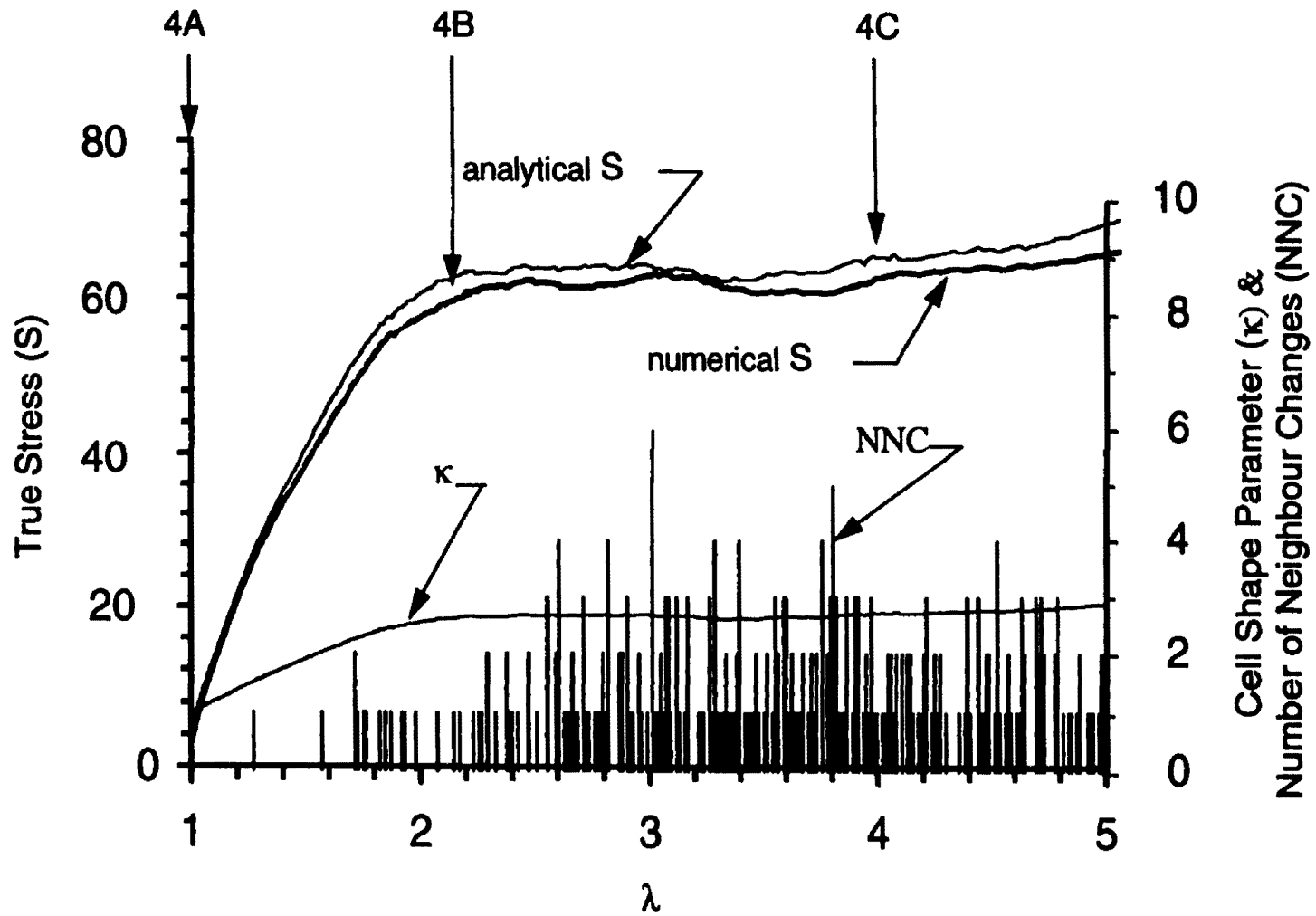


Figure 5.5 (a) True Stresses ( $S$ ), Cell Shape Ratio ( $\kappa$ ), and Number of Neighbour Changes (NNC) Versus Patch Elongation Ratio( $\lambda$ )

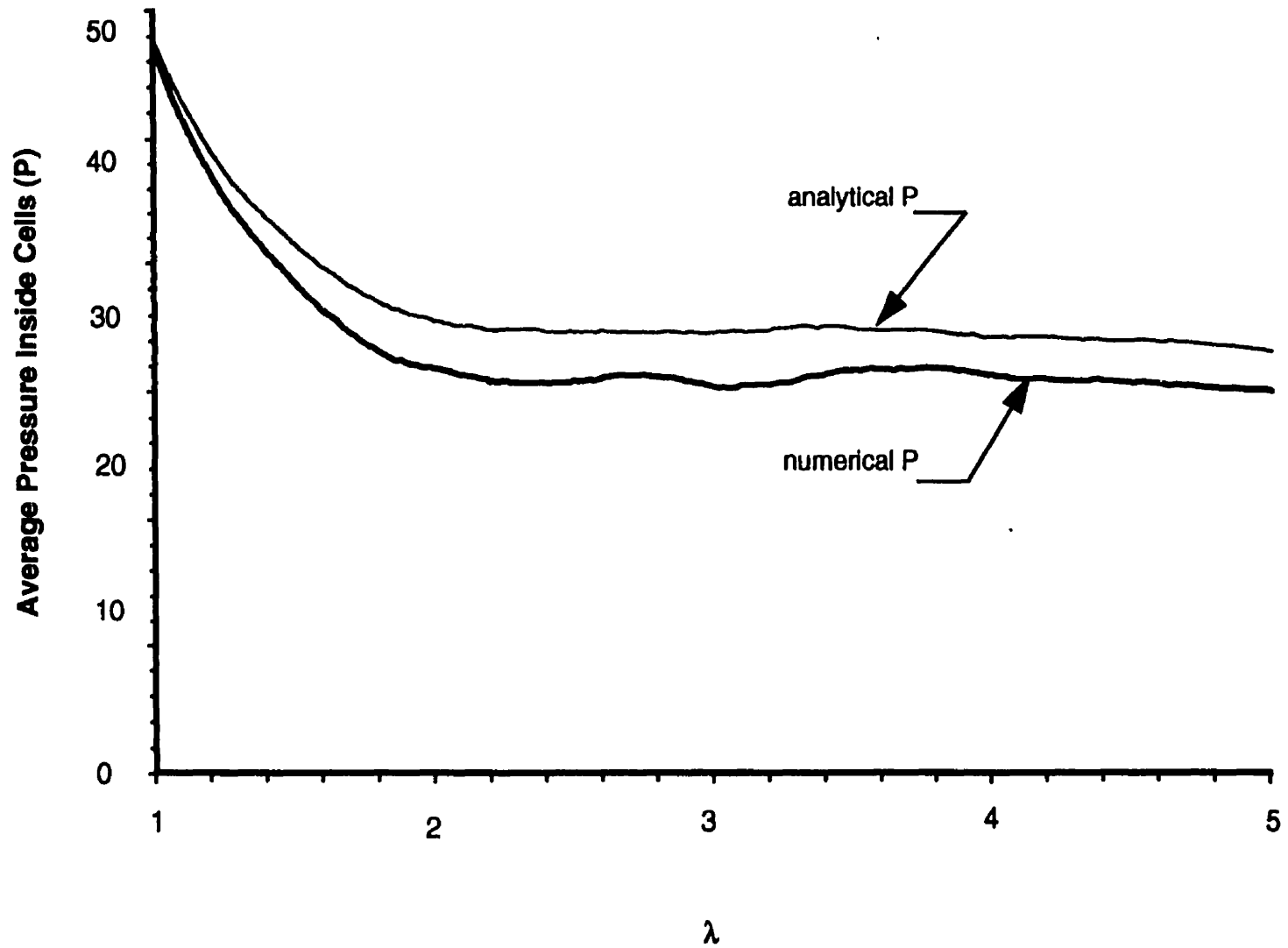


Figure 5.5 (b) Intra-cellular Pressure Versus Patch Stretch Ratio ( $\lambda$ )

preferable for a neighbour change to occur than for the cells to become further elongated. Also shown in Figure 5.5 (a), is a plot of the stress resultant  $S$  calculated using Equations 5.6 to 5.16. Theoretical pressure estimates (made using Equation 5.10) and average numerical pressures are shown in Figure 5.5 (b). In both graphs, numerical and theoretical curves are in good agreement.

#### 5.4.2 Factors Affecting the Bulk Mechanical Properties of Cell Sheets

There are many factors affecting the shape of the stress-strain curve of a cell sheet. Among them are the density of the cell patch, cell properties such as contractile forces and viscosity inside each cells, and the rate of deformation.

##### Effect of the Density (Case 2)

For a  $w$  by  $h$  patch consisting of  $n$  cells, the directional edge densities of the cell sheet  $\psi_x$  and  $\psi_y$  are defined as follows:

$$\psi_x = \frac{w}{\sqrt{\frac{w \times h}{n}}} = \sqrt{\frac{w}{h}n}, \quad (5.18)$$

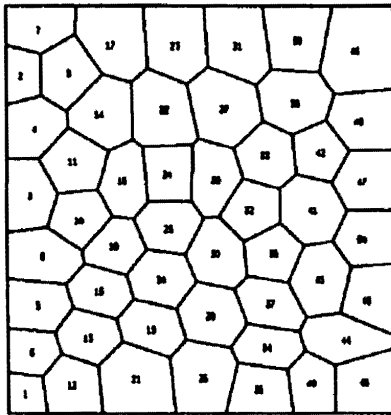
$$\psi_y = \frac{h}{\sqrt{\frac{w \times h}{n}}} = \sqrt{\frac{h}{w}n}. \quad (5.19)$$

When the cell sheet is annealed, the density parameters are approximately equal to the average number of cells distributed along  $x$  and  $y$  directions respectively.

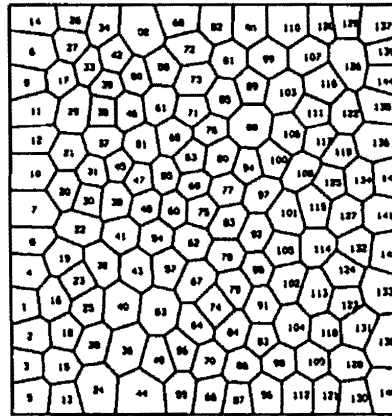
The following simulations are designed to study the effect of the density of the cell sheet on the shape of the stress-strain curve. Three cell patches with the same sizes but different number of cells are shown in Figure 5.6. Patch B is the

same patch in the reference case, with 144 cells and a density of 12.00; while Patch A consists 50 cells and had a lower density of 7.07. Patch C has more cells (275 cells), thus has the highest density of 16.58 among the three patches. Each of them is subjected to a constant strain rate at its right edge. The left edge is restrained to move horizontally and the bottom edge is fixed vertically. The top edge is kept straight during the deformation. The parameters  $Q_x$  in the three patches are 24, 12 and 7 respectively. Curves in Figure 5.7 demonstrate the relationship between true stresses ( $S_x$ ) versus elongation ratio ( $\lambda$ ) of the three patches, along with their deformed configuration at  $\lambda = 4$ . Patch A is stiffer than the other two patches, because a larger fraction of the cells are constrained by the straight edge condition. Increasing the cell density gradually (more tests not shown here) minimizes this kind of "edge-effect" and the curve approaches the shape of that for Patches B and C. The curve of Patch C takes a very similar shape of Patch B, suggesting that the patch of density 12 is sufficient that boundary conditions are negligible. The differences in the stress values between Patch B and C are due to the strength of  $F_c$  per cross-sectional length inside the cell sheets. Since Patch C has more cells along each direction, resulting in stronger total contractile force acting at the edge, larger forces are needed to cause the same amount of deformation in Patch C as that of Patch B.

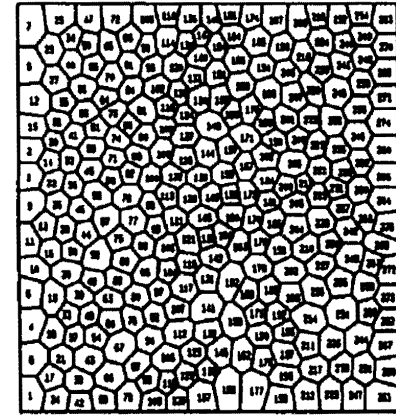
*Chapter 5 - Cell Rearrangement and Bulk Mechanical properties*



(a) Patch A (50 Cells)



(b) Patch B (144 Cells)



(c) Patch C (275 Cells)

**Figure 5.6 Cell Patches of Different Densities**

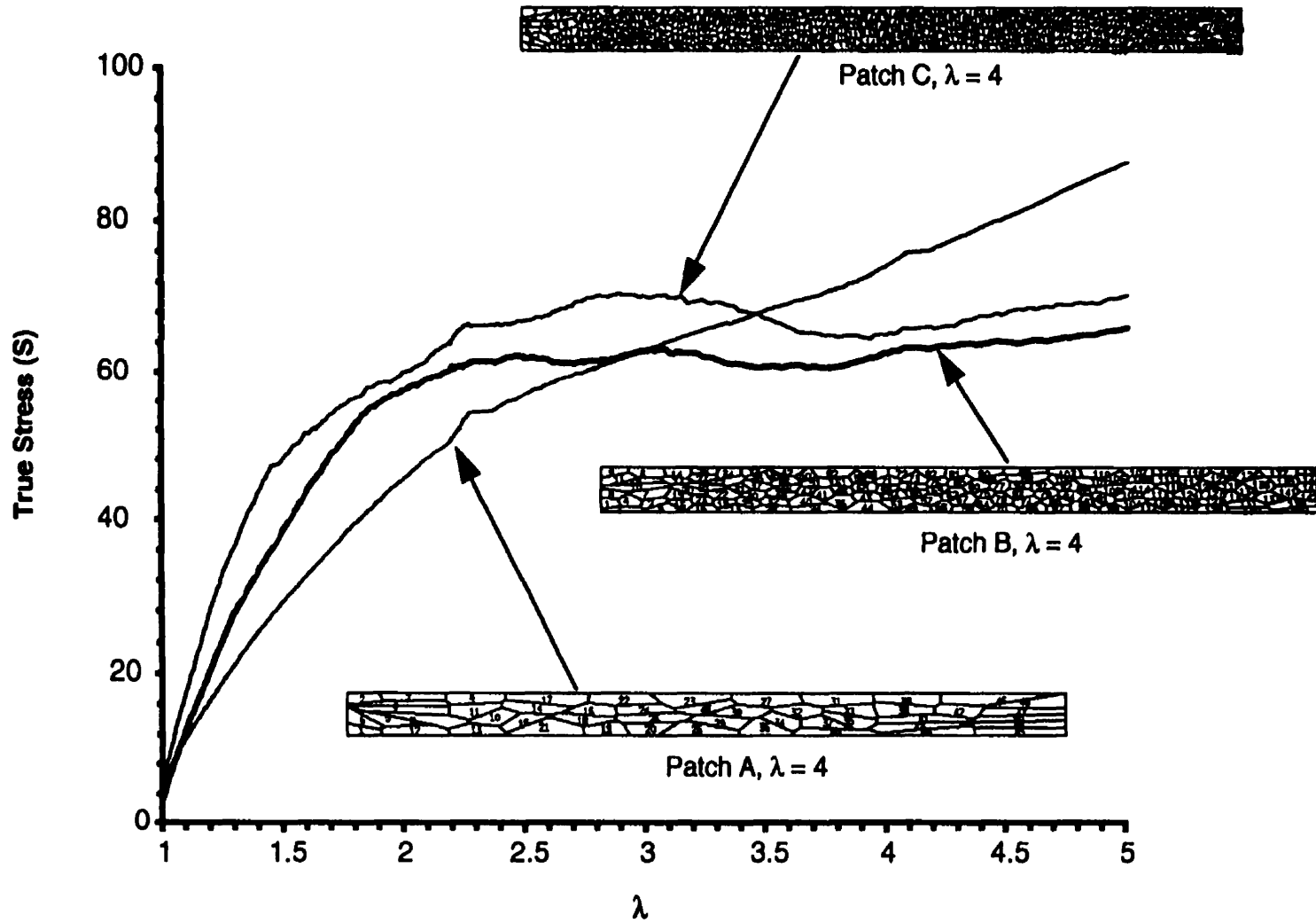


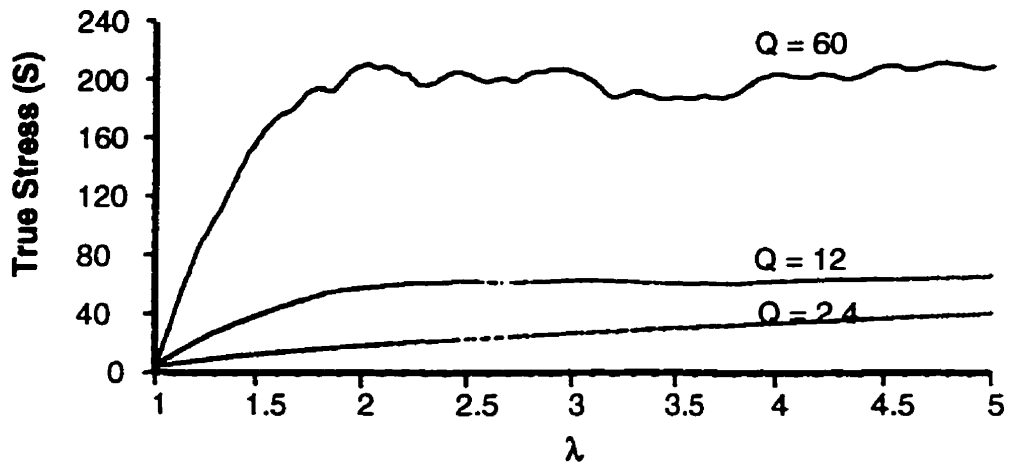
Figure 5.7 True Stress ( $S_x$ ) Versus Elongation Rate ( $\lambda$ ) of Cell Patches with Different Density

### **Effect of Contractile Force $F_c$ (Case 3)**

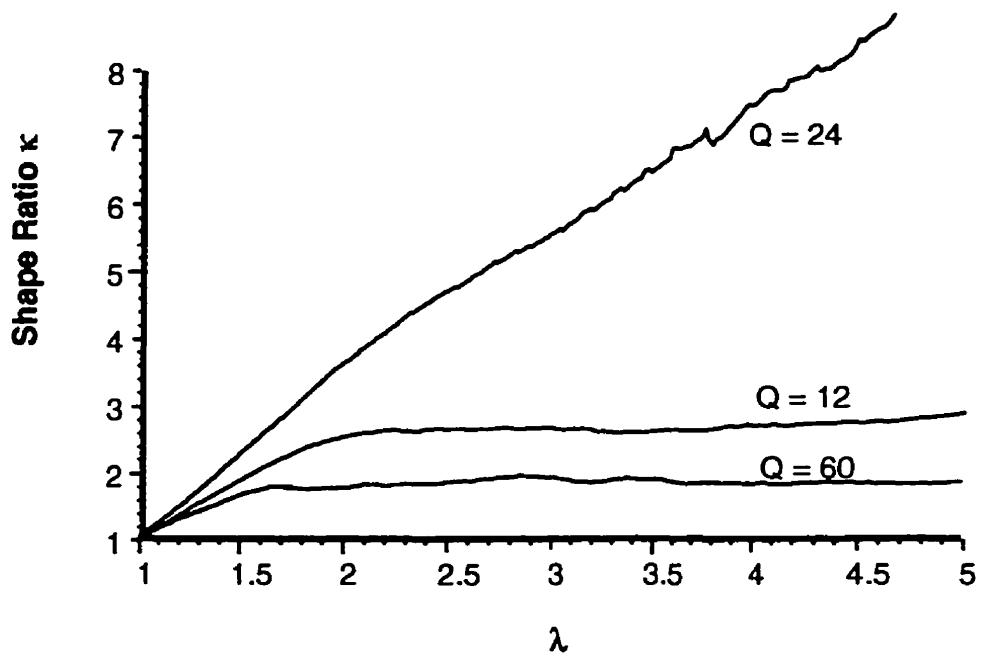
The strength of the contractile force  $F_c$  has a direct impact on the shape of the cells and the stress-strain curve. Three values of contractile forces were assigned to the geometry of the patch in the reference case (Figure 5.4 (a)), resulting in the dimensionless parameter  $Q_x$  equals to 2.4, 12 and 60 respectively. The stress-strain curves that resulted are shown in Figure 5.8 (a). Evidently, stronger  $Q_x$  causes a higher stress level and more vigorous cell rearrangements inside the cell sheet. As a result, the shape ratio curves in Figure 5.8 (b) show that in patches with stronger  $Q_x$ , cells remain rounder in shape than those with smaller  $Q_x$ . The roughness in the stress-strain curve of  $Q_x = 60$  is caused by cell rearrangements. In an extreme case, where  $Q_x$  approaches 0, the cell sheet behaves more like a pure viscous material and the stress remains constant as the cell sheet elongates. Very few, if there is any, neighbour changes occur in this case and the cell shape  $\kappa$  equals the elongation ratio  $\lambda$ .

### **Effect of Strain Rate (Case 4)**

The reference patch was then stretched at three strain rates, giving the value of 24, 12 and 6 to  $Q_x$ . Since the cytoplasm inside each cell is viscous, higher strain rates cause stronger resistance from the cell sheet and higher stresses result, as shown in Figure 5.9 (a). Moreover, the higher strain rate allows less time for the cells to change their shapes and neighbours. Hence cells intend to elongate more than those subjected to a lower strain rate. The effect of strain rate on the shape ratio is demonstrated in Figure 5.9 (b). As predicted, the shape ratio versus elongation curves are similar to those of Figure 5.9 (a).

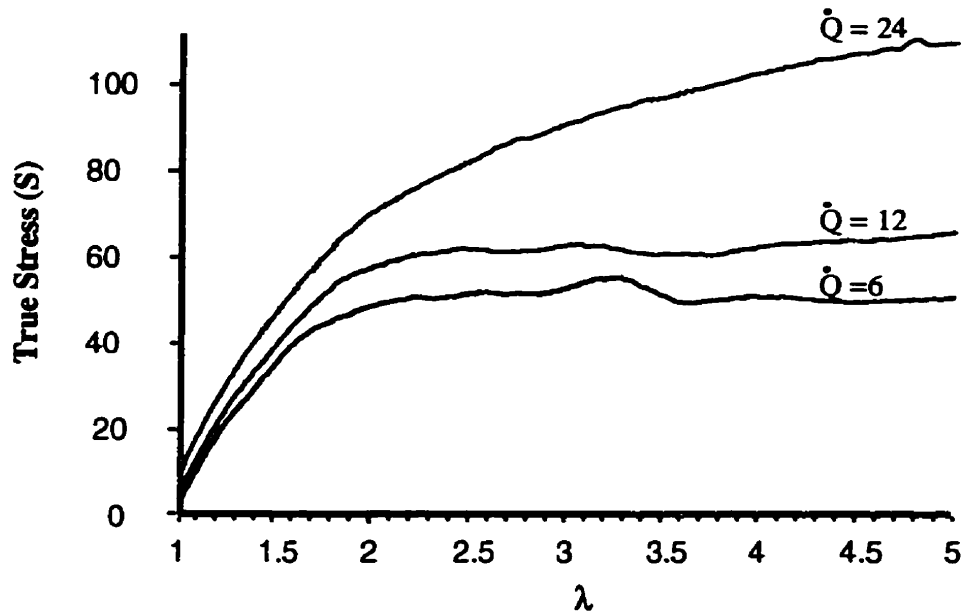


(a) True Stress (S) Versus Elongation Ratio ( $\lambda$ )

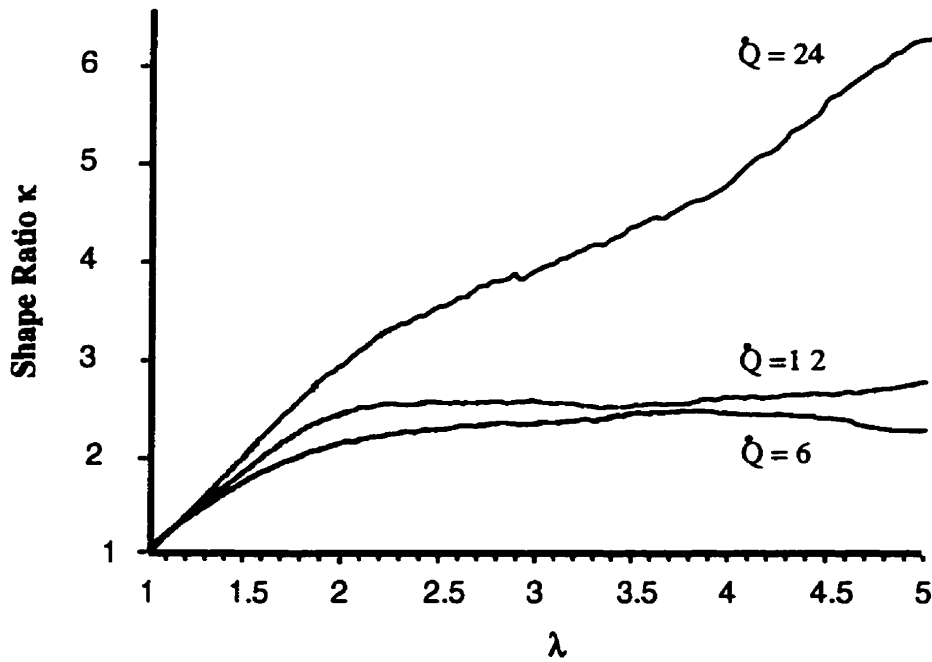


(b) Shape Ratio ( $\kappa$ ) Versus Elongation Ratio ( $\lambda$ )

**Figure 5.8 True Stress (S) and Shape Ratio ( $\kappa$ ) Versus Elongation Ratio ( $\lambda$ ) of Cell Sheets with Different  $F_c$**



(a) True Stress (S) Versus Elongation Rate ( $\lambda$ )



(b) Shape Ratio ( $\kappa$ ) Versus Elongation Rate ( $\lambda$ )

**Figure 5.9 True Stress (S) and Shape Ratio ( $\kappa$ ) Versus Elongation Ratio ( $\lambda$ ) of Cell Sheets with Different Strain Rate**

### 5.4.3 Isotropy of the Cell Sheet (Case 5)

In a living embryo, most mature epithelial cells are in a regular polygonal shape and are evenly distributed. A sheet consisting of such cells possesses isotropic mechanical properties during its deformation. The stress-strain curves shown in Figure 5.10 resulted from simulations of patches with the same density. Testing cases include stretching the same patch (patch in reference case) in the  $x$  and  $y$  direction respectively, and stretching a patch which doubles the size in length. The values of  $Q_x$  in these three cases are the same. The good agreement of these three curves confirm the isotropic properties characteristic of an initially annealed cell sheet.

However, in some morphogenetic or wound healing processes, cells are aligned along a certain axis (Sausedo and Schoenwolf, 1994). Simulations reveal that a sheet of such cells displays anisotropic characters. Case A in Figure 5.11 is the reference case, where the patch is annealed and elongates in  $x$ -direction at a constant rate ( $Q_x = 12$ ). Patch B is the elongated configuration of the reference case when  $\lambda = 2.58$ . The initial configuration of Patch B is not annealed. The patch is then set to elongate in  $y$ -direction at the same constant rate as Patch A. The differences between the case A and B are obvious. At the beginning, since Patch B is severely deformed initially, the forces in the sheet is not balanced. Contractile forces from CMBs and other cytoskeletal structures tend to pull cells back to rounder shapes. This explains the negative values of stress-strain curve of Patch B.

### 5.4.4 Necking Phenomena (Case 6)

In the course of elongation, if the edges of a cell sheet are not properly restrained, or not kept straight, the mechanical properties of the cell sheet can be significantly affected. Patch B in Figure 5.12 is the same patch as Patch A (reference case) except that the top edge does not have the straight-edge constraint. When the cell sheet is stretched at a degree, for example,  $\lambda > 1.5$  in this case, the value of the stresses start to differ at an

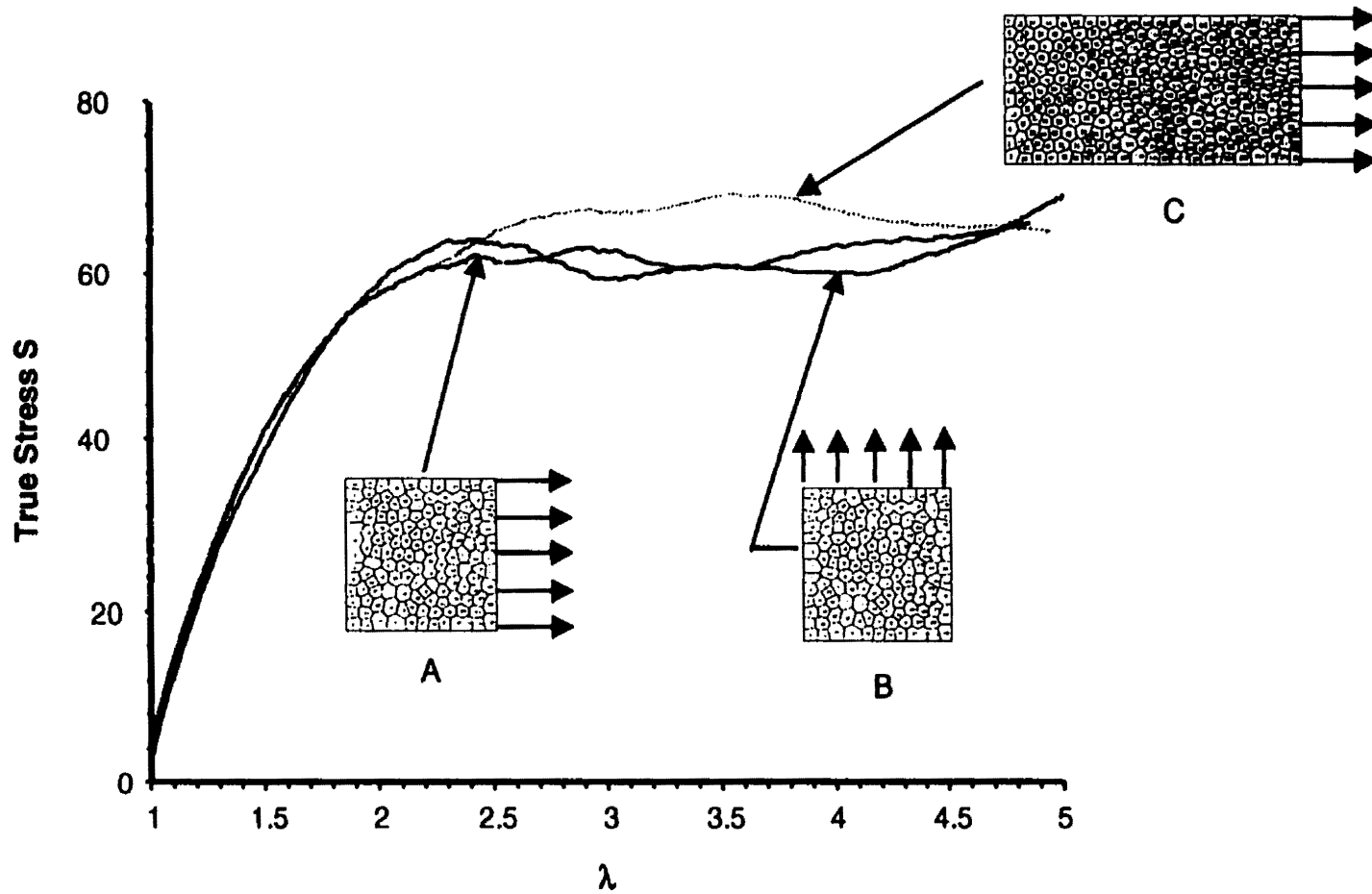


Figure 5.10 True Stress Versus Elongation Ratio of A Patch Stretched in Different Direction

Chapter 5 - Cell Rearrangement and Bulk Mechanical Properties

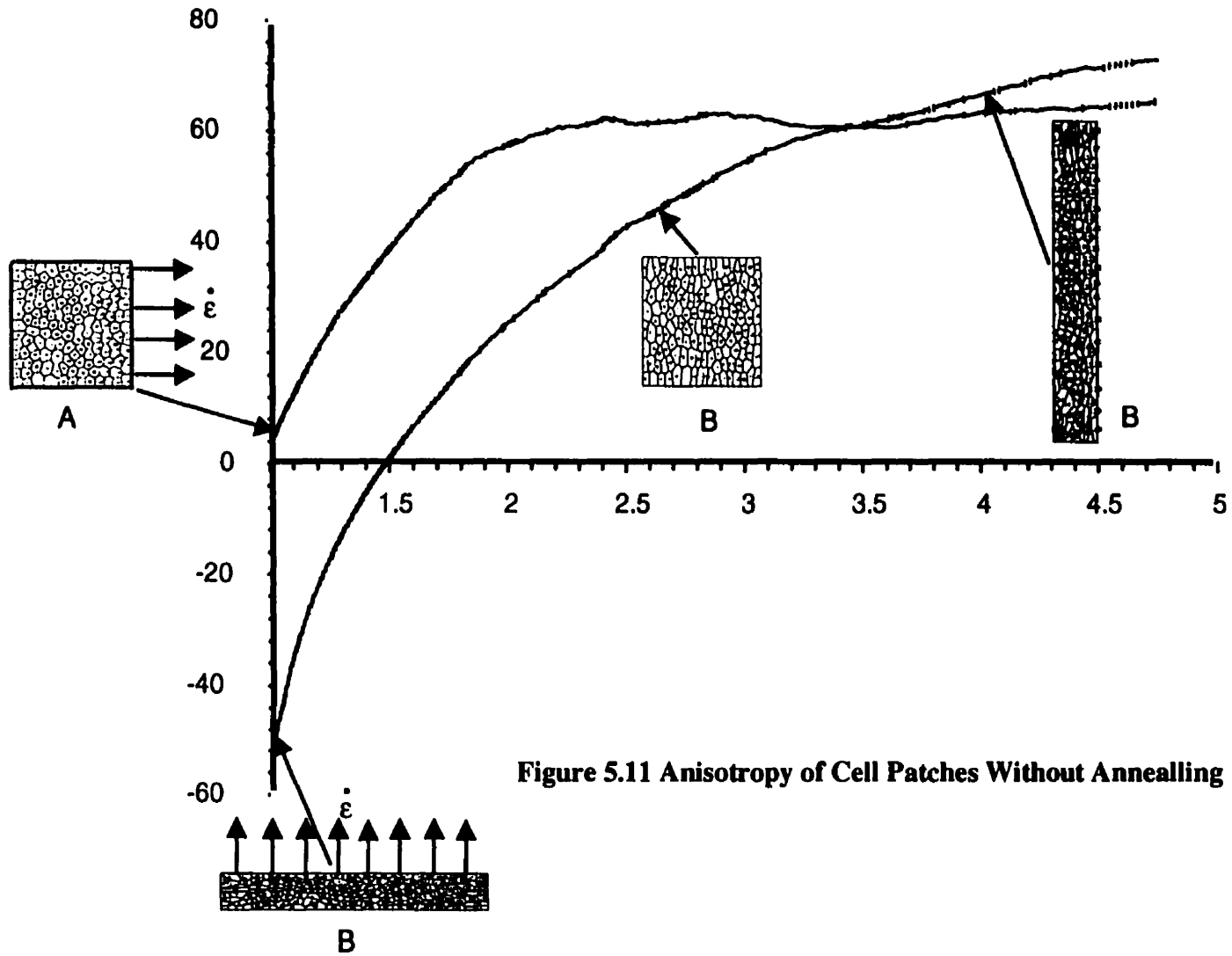


Figure 5.11 Anisotropy of Cell Patches Without Annealing

Chapter 5 - Cell Rearrangement and Bulk Mechanical Properties

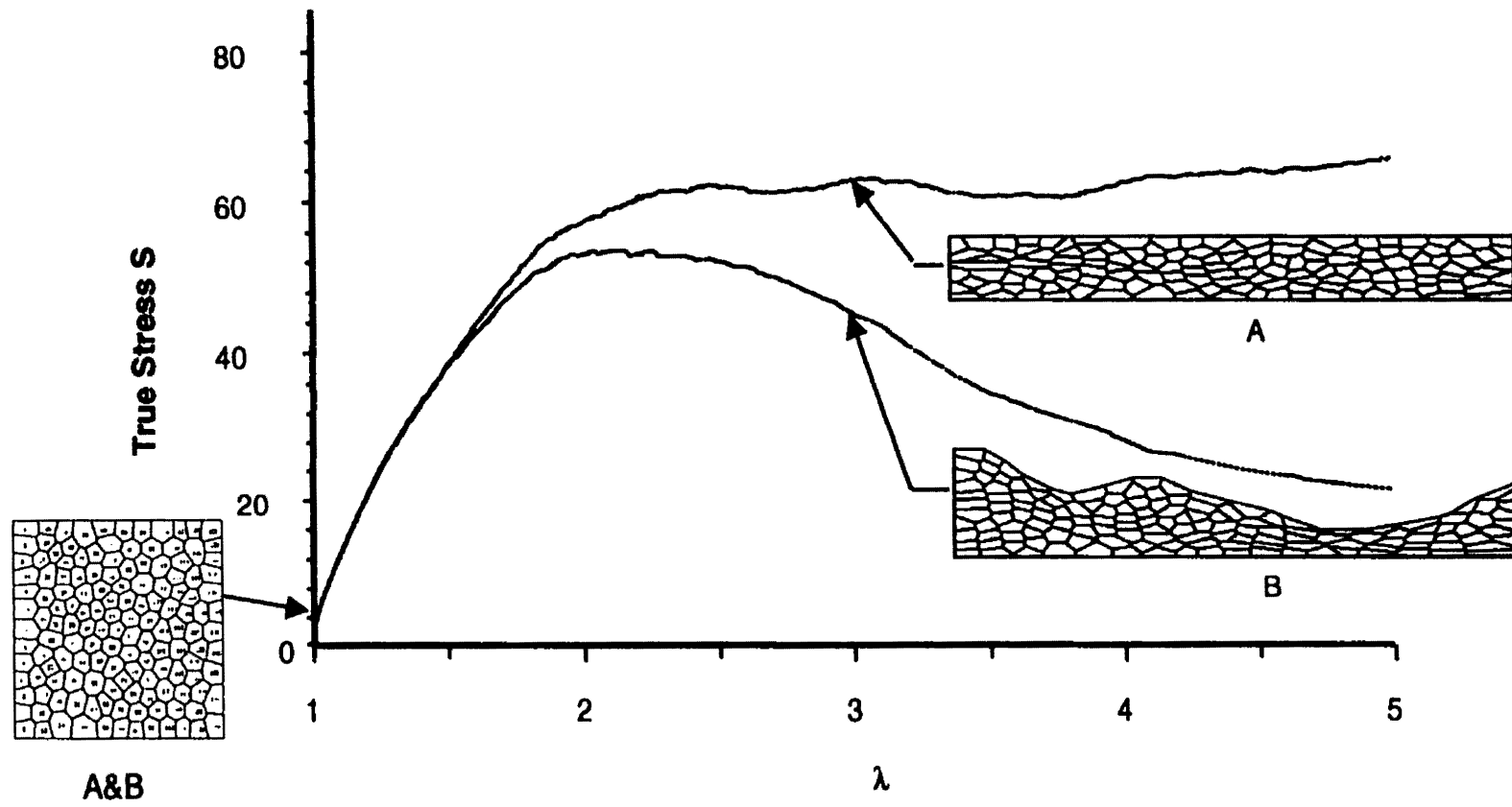
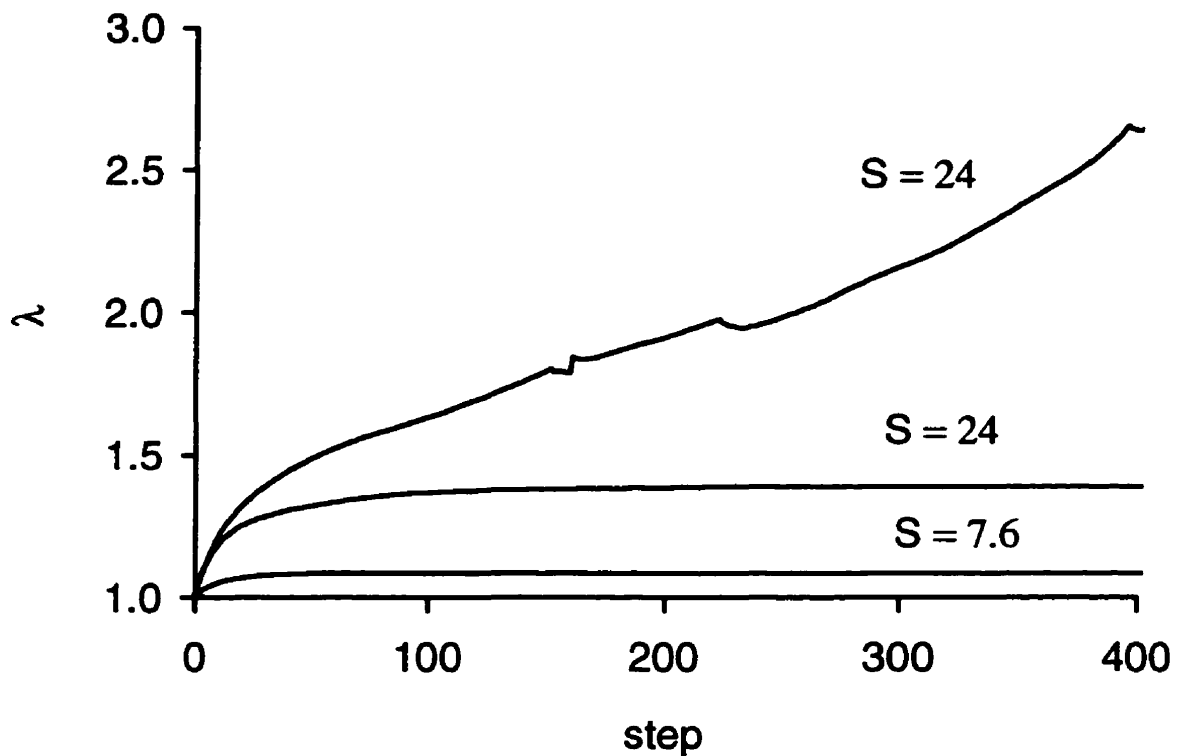


Figure 5.12 Necking Phenomena

increasing degree since local narrowing or necking occurs in Patch B. In this aspect, the behaviour of the living tissue is analog to that of metal when it exhibits necking during a tensile test.

#### 5.4.4 Cell Sheet Subjected to a Constant Lateral Force (Case 7)

Figure 5.13 shows the strains produced by the application of either constant nominal or true stress. Under the action of a modest true stress, the patch and its cells elongate until a shape predicted by Equation 5.8 (with  $\dot{\epsilon}$  set to zero) is reached. Under a



**Figure 5.13 Elongation Rate of a Cell Sheet Subjected to Constant Lateral Stress**

constant nominal stress, the strain rate (associated with the slope of the curve in Figure 5.10) is slowed briefly (to point A) because of cell elongation, and then increases more and more quickly as the patch narrows and the true stress increases without bound.

### **5.5 Discussion**

The factors that are found to be important to the behaviour of epithelial cell sheets are the cytoplasm viscosity, the patch strain rate and the strength of the microfilament forces. These determine the onset and rate of cell rearrangement, and the characteristic cell shape as expressed by  $\kappa$ . Cell rearrangement is found to be an important factor in the behaviour of cell sheets.

As the force parameter  $Q$  is made larger (by increasing the microfilament force or by reducing the rate of elongation, for example), the cells tend to remain more rounded, and cell rearrangement occurs sooner. The force required to produce a certain rate of elongation also increases significantly with  $Q$  because cell rounding increases the resistance to deformation by cell elongation. In contrast, as  $Q$  is made smaller, less rounding occurs, until in the limit as  $Q$  approaches 0, the sheet deforms as a viscous mass, and no cell rearrangement occurs. This is the situation that produce the least resistance to sheet elongation.

Analytical expressions allow the intra-cellular cell pressure  $p$  and applied stress  $S$  to be calculated from the microfilament forces and cell shape parameter  $\kappa$ . At the moment  $\kappa$ , which depends on the deformation history of the sheet, must be found using numerical simulations or physical experiments.

The simulations also demonstrate that the behaviour of a cell sheet can be established using relatively few cells. Under the circumstances and range of deformations investigated here, 143 cells are sufficient that boundary effects, statistical variations from

patch to patch, and non-continuum effects such as individual neighbour changes do not significantly affect the results. In some cases, these conclusions are drawn, in part, from the many additional simulations and tests that were carried out but could not be reported here due to the space limitations.

During embryo morphogenesis, to form a certain organ usually involves the significant deformation of the tissue. In order to accommodate these distortion, cells usually slide along their boundaries and resulting the rearrangement of the topology. This change was carefully observed and cells are traced (Burnside and Jacobson; 1968; Wilson, et al., 1989; Schoenwolf, 1991). The simulations demonstrate this cell rearrangement in detail.

The gross patterns of deformation examined here are often referred to as convergent extension or convergence and extension. In the simulations presented here, anisotropic external forces produce the extension in one direction, and convergence or narrowing in the other. Here, cell intercalation is a passive response driven by cell rounding due to boundary connection. As noted by Keller et al. (1991), intercalation of cells might drive convergence and extension in certain situations. We note that such intercalation would have to occur preferentially in the direction of narrowing, but are not clear as to what mechanism might produce such anisotropic intercalation. Convergence and extension might also be driven by preferentially oriented microfilament bundles (Kalnins, et al., 1995). The theoretical analysis presented herein could be used to analyze that situation and to provide estimates of the resulting stresses and pressures. Measurement of sheet thickening or thinning might also be useful in identifying which of several possible mechanisms is actually at work.

These simulations provide an important step towards the development of “super elements” that can model patches of tissue consisting of many cells. Such elements would

derive their properties from the statistical morphology of the actual cells and the properties of their cytoskeletal and other mechanically-important structures.

The simulations can be used to estimate stresses, pressures and cell shapes for a sheet with given mechanical properties and deformations. Alternatively, given cell shape, viscosity and strain rate, either the simulations or analytical formulations might be used to calculate intracellular pressures and stresses. The results reported here can be applied to situations where a bi-axial stress or other complex stress state exists using principal stress and strain concepts and by decomposing stresses and strains into hydrostatic and deviatoric components (Malvern, 1969).

In conclusion, it is apparent that finite element methods have opened up yet another area of biomechanics inquiry, namely how the morphology and properties of sub-cellular structural components give rise to the behaviour of sheets of epithelial cells.

# Mechanisms of Cell Sorting and Tissue Spreading

# 6

## 6.1 Reaggregation of Dissociated Cells

When dissociated cells of different kinds are put together, they tend to re-group so that like cells are together. This phenomenon is known as cell sorting. Since the beginning of this century, this vital behaviour of cells has become one of the most studied subjects of *in vitro* cell biology (Wilson, 1907; Townes and Holtfreter, 1955; Weiss and Taylor, 1960; Steinberg, 1962; Armstrong, 1989 for review). Wilson's experiments of re-constructing sponges from dissociated cells indicated that cell sorting is species-specific. Later observations made by Weiss and Taylor (1960), and Steinberg (1962b) revealed that cell sorting is also organ-specific.

Subsequent experiments showed that when two fragments of different embryonic tissues were placed in contact with each other, both pieces rounded up, followed by a series of tissue movements (Steinberg, 1962c; Armstrong, 1978), in which one would normally spread around the surface of the other and eventually envelope it. This phenomena is known as tissue spreading. Furthermore, the configuration achieved in this way was the same as that arrived at when dissociated cells of these same kinds of tissue

were intermixed and allowed to sort out (Steinberg, 1962a,b,c). This indicates that heterotypic cell populations of similar composition would gravitate toward a common final state regardless of their initial configuration (Figure 6.1). It appears that a unique equilibrium state can be ultimately reached through cell movements within the heterotypic cells aggregate. It was also discovered that the order of the engulfment agrees with the order of the adhesiveness

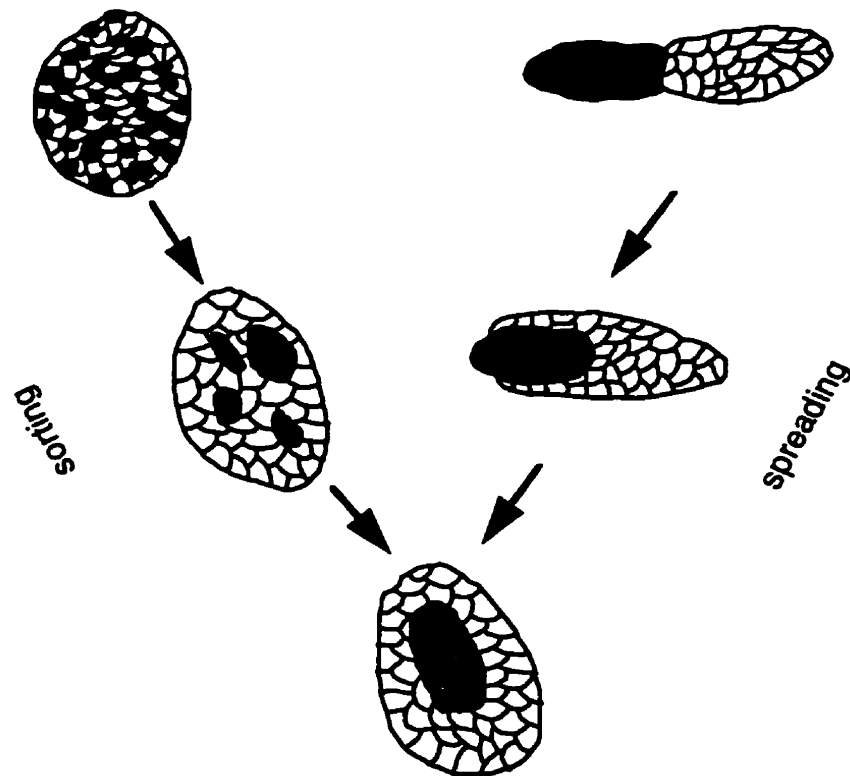


**Figure 6.1 Tissue Reconstruction Through Cell Sorting and Tissue Spreading (after Steinberg, 1970)**

of the tissues involved. Figure 6.2 demonstrates this relationship. Three different types of tissue A, B and C are placed in contact with each other. The order of the adhesiveness associated to each tissue is  $A > B > C$ . After a period of time, tissue A will be enclosed by tissue B, while tissue C forms an outer layer to engulf A and B.

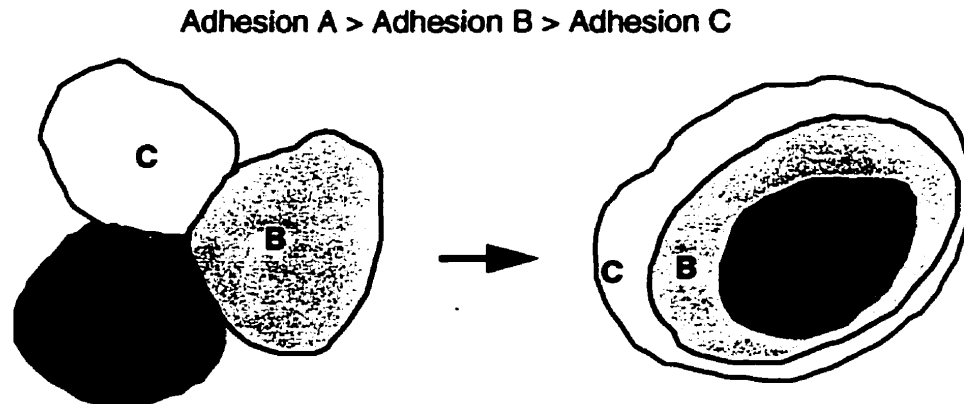


**Figure 6.2 Hierarchy of Final State of Tissue Engulfment**

### **6.2 Postulated Cellular Basis for Cell Sorting and Tissue Spreading**

Cell sorting and tissue spreading are one of the most interesting and important phenomena for the studies of the behaviour of cells during embryo morphogenesis. Consequently, it has been the subject of many hypotheses regarding which cellular properties might drive cell sorting and determine the engulfing preference of the coaggregated tissues (Trinkaus, 1970; Armstrong, 1989 for review). Among them, the most successful and widely accepted theory is the "differential adhesion hypothesis" (DAH) proposed by Steinberg (1963; 1970).

### 6.2.1 The Differential Adhesion Hypothesis (DAH)

Cell adhesion has been recognized as an essential feature of cell specificity and as mediating almost every aspect of embryo morphology (Edelman, 1985; Harris, 1994b; Steinberg, 1996 for review). It is one of the molecular bases of multi-cellular organogenesis and embryo histology (Gumbiner, 1996).

Steinberg postulated that there are three cardinal properties of cells from different embryonic tissues: (a) cells cohere to each other and form an intermingled aggregate when they are put together; (b) cells from different tissues possess different adhesiveness or different interfacial free energy; (c) there exists a final state of any multicellular aggregate which minimizes the total free energy of the system. In this respect, biological cells behave very much like the immiscible liquid. Steinberg called his theory the *differential adhesion hypothesis* (DAH). Since its first appearance, the DAH has been supported by various experimental (Phillips and Steinberg, 1969; Thomas and Yancey, 1988; Steinberg and Takeichi, 1993; Foty and Steinberg, 1995), and numerical studies (Sulsky *et al.*, 1984; Graner, 1993; Glazier and Graner, 1992, 1993; Chen and Brodland, 1997). It is widely accepted as explaining the mechanisms of cell sorting, tissue spreading, and other cellular phenomena including reversible inhibition of cell sorting and tissue spreading (Steinberg and Wiseman, 1972).

According to the DAH, for any aggregate of motile, mutually adhesive cells, the most stable configuration should be governed by the volumes of the member cell populations and the intensities of the adhesions formed at the various possible cell-cell and cell-media interfaces. This configuration can be approached as cells move to increase their areas of mutual adhesion and exchange weaker adhesions for stronger ones. The final state is achieved when the sum of all cellular binding energies is maximized. Because of the analogy between the cell aggregate and the immiscible liquid, interfacial free energy or tissue interfacial tension is introduced to quantify the intensity of cell adhesions.

Figure 6.3 illustrates how the reversible works of cohesion ( $W_{a-a}$  and  $W_{b-b}$ ) and adhesion ( $W_{a-b}$ ) determine the final configuration of a heterotypic cell aggregate, which contains cell type a and type b. According to this figure, to complete the cell sorting and to achieve the final configuration with cell type b population engulfing cell type a population, the following inequalities must be satisfied (Foty and Steinberg, 1995):

$$0 < W_{b-b} < W_{a-b} < (W_{a-a} + W_{b-b})/2 < W_{a-a} \quad (6.1)$$

Denoting the interfacial tension of cell tissue a by  $\sigma_{a-a}$ , the interfacial tension of cell tissue b by  $\sigma_{b-b}$ , and the interfacial tension between tissues a and b by  $\sigma_{a-b}$ , the reversible works are related to the interfacial tensions by:

$$\begin{aligned} W_{a-a} &= 2 \sigma_{a-a}; \\ W_{b-b} &= 2 \sigma_{b-b}; \\ W_{a-b} &= \sigma_{a-a} + \sigma_{b-b} - \sigma_{a-b}. \end{aligned} \quad (6.2)$$

Interfacial tensions of different tissues are measured, in relative terms (Phillips and Steinberg, 1969, 1977, 1978) and later, by the absolute values (Foty et al., 1994). These tests also prove that cells adopt their preferred associations and positions among the intermixed heterogeneous cell population in the sequence precisely predicted by the DAH.

### 6.2.2 Other hypotheses

The effectiveness of the DAH in explaining observed phenomena does not imply that there is only one explanation of the real cell sorting mechanism. More than half a dozen other theories have been proposed (for review, Armstrong, 1989). The following section is a brief description of three alternative hypotheses: (1) the differential surface contraction hypothesis, (2) the specific adhesion hypothesis and (3) the differential

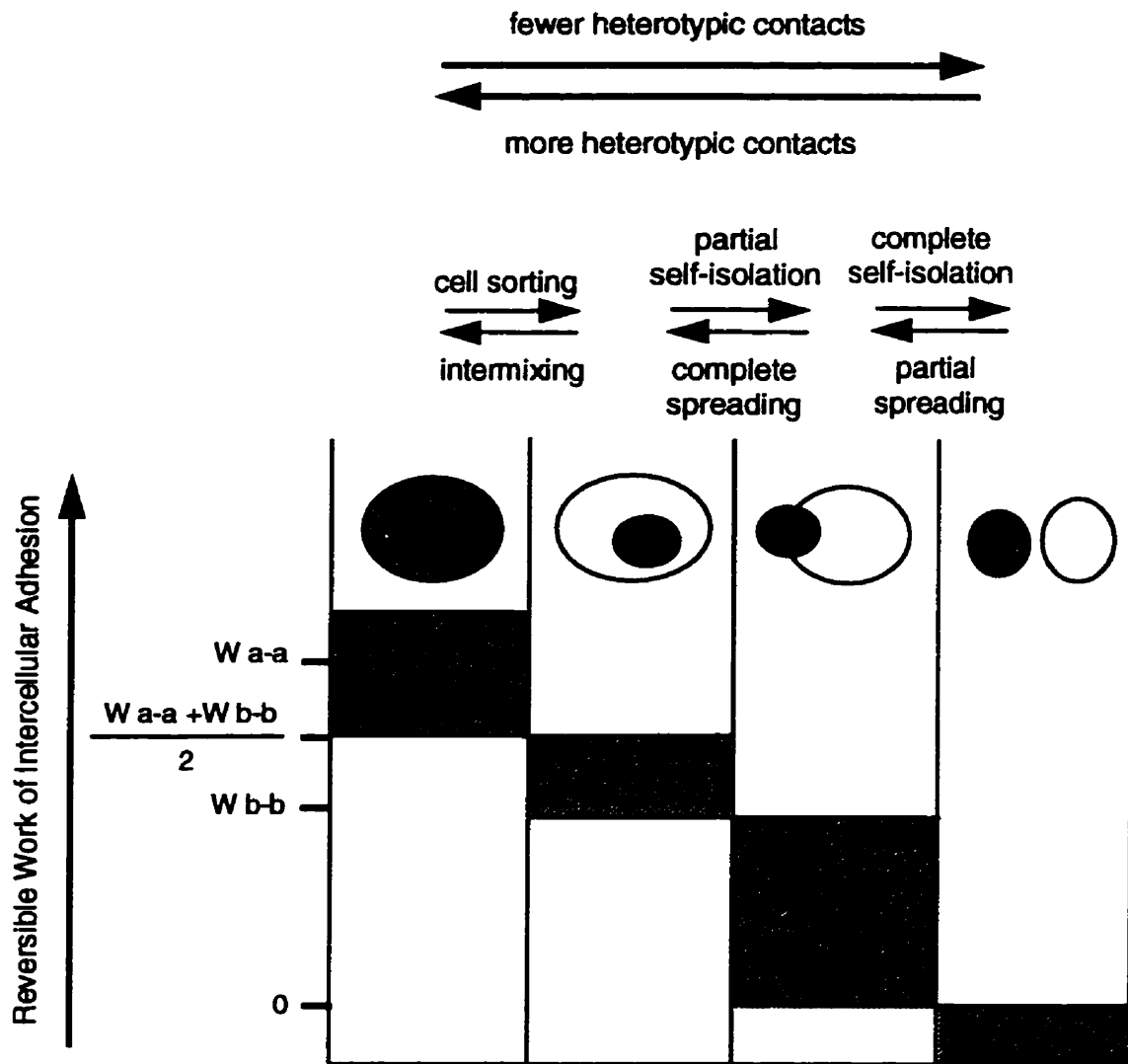


**Figure 6.3 Relationship Between the Reversible Works of Cohesion and Cell Sorting**

(The shaded area represents values of  $W_{a-b}$  .

After Foty and Steinberg, 1994)

chemotaxis hypothesis.

### **The Differential Surface Contraction Hypothesis (DCH)**

Noting that cytoskeletal components such as circumferential microfilament bundles played a crucial role in many organ formation processes including invagination and neurulation, Harris (1975) suggested that in a heterogeneous cell aggregate, the difference in surface contraction, which is caused by cyto-components inside cells, could be a major driving force behind tissue engulfment and histotypic cell sorting *in vivo*. In order for this to be valid, two basic assumptions have to be made:

- (a) the cell surface contraction becomes the greatest when it is exposed to the media and the least when it is adjacent to a cell of the same histological type, and at a medium level when it contacts another cell of a different histological type;
- (b) cells from different tissues exert different surface contraction when they contact the medium.

It is proposed that the more contractile tissue of any given binary combination should segregate to the interior. This hypothesis does not deny the existence of differential adhesions among different histological cells. It only challenges the DAH's exclusion of important roles of other cytoskeletal components.

### **The Specific Adhesion Hypothesis (SAH)**

The specific adhesion hypothesis proposes that intercellular adhesion evinces a significant degree of tissue specificity, with the adhesion between two homotypic cells stronger than that between two heterotypic cells (Moscona, 1960). When dissociated cells cohere to form a mixed reaggregate, the damaged surfaces of cells engendered by the dissociation start to be repaired, and tissue specific cell adhesions re-express on the surface. This is when the sorting out commences. This version of adhesion re-expression

obtained favorable evidences from studies in cell molecular structures on tissue specificity and it is believed that cadherin cell adhesion molecules serve as a determinant in the cell sorting (Marrs and Nelson, 1996 for review).

This hypothesis shares a common basis with the DAH since they both acknowledge differences in cell adhesions among different types of cells. The underlying conflict of these two theories, however, lies in the condition in which complete cell sorting occurs. The DAH postulates it is when  $W_{a-b}$  is stronger than  $W_{b-b}$ , whereas in the SAH,  $W_{a-b}$  is the weakest. Another short-coming of the SAH is that it does not predict the order of engulfment in the final state.

#### **The Differential Chemotaxis Hypothesis (DCHH)**

The notion of chemotaxis implies that the direction of movement of cells may be influenced by the presence in the medium of substances which are in solution. It has been long known that different cells have different chemotactic responses (Harris, 1961; Edelstein, 1971). Advances in molecular cell biology greatly enriched our understanding of cell chemotaxis from the cell surface molecule point of view (Gumbiner, 1996 for review). The differential chemotaxis hypothesis envisions cell sorting as the response of cells to the chemotactic gradient established in a cell aggregate (Townes and Holtfreter, 1955). In the *Dictyostelium discoideum* cell sorting experiment made by Ohmori and Meada (1986), differences in chemotactic sensitivities between cells grown with and without glucose (G(+)) cells and G(-) cells) are measured, confirming the presence of differential chemotaxis when cell sorting out. However, there is no implication of differential chemotaxis is the sole driving force of cell sorting, since differential cell adhesions are also detected at the same time.

This principle can be generalized to all hypotheses. Efforts have been made to verify these hypotheses experimentally and numerically in the past few decades (Armstrong, 1989 for review). Even though one hypothesis might obtain better proof than the others from one kind of experiments or one type of simulation modelling, it does not invalidate the others from being true in explaining the mechanisms of cell sorting and tissue spreading, since multiple driving forces may well govern cell movements in the same phenomenon. In other words, the specific mechanism which plays the dominant role may change with embryo development stages, or under different circumstances.

### 6.3 Computer Simulations of Heterotypic Cell Aggregates

While cell sorting, tissue spreading, and other behaviour of cell aggregates such as checker-board pattern formation and dispersal are observed and documented intensively *in vitro*, their kinetics are still largely unknown. To better understand this matter, heterotypic cell aggregates are simulated using the finite element cell model elucidated in the previous chapters. In this study, two kinds of cells are considered, one is more adhesive than the other. More adhesive cells are denoted with dark shading while less adhesive cells are shown white. In addition, it is possible for cells to be different in other mechanical properties such as contractile force  $F_c$  and viscosity  $\mu$ . The initial configuration is generated using a free-edge Voronoi tessellation. A portion of the cells are assigned to the stronger adhesion in a random fashion, and the rest of the cells are assigned to a lesser adhesion. This cell aggregate is then suspended on a plane, with or without the culture medium. *In vivo*, a cell aggregate should be free of any constraints of motion. In the simulation model, however, for the sake of numerical stability, two vertices of the aggregate have to be restrained in order to eliminate the free-body motion of the system. This minimum constraint does not affect the overall behavioural pattern of the aggregate. Influences from the surrounding medium or the substrate are incorporated into

the model by specifying the force between a cell and the media. There is no other external stimuli present in the simulation. When the simulation is set to motion, cell movements and various cellular activities occur according to the properties of the cells and their interactions.

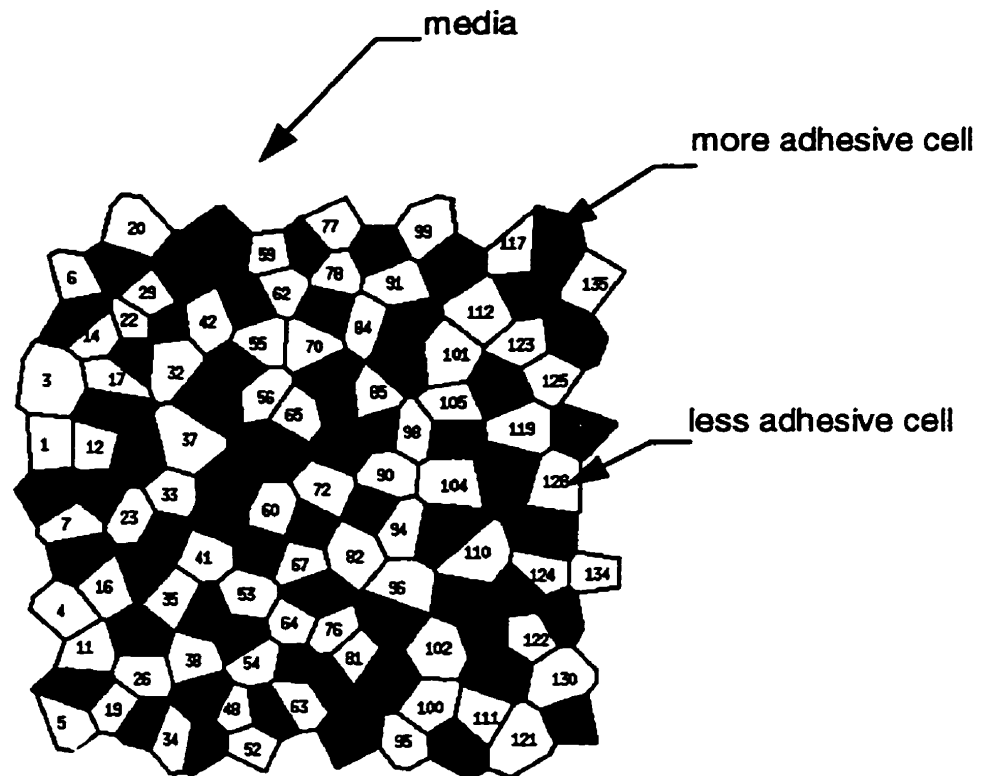
### 6.3.1 Definition of Parameters in a Heterotypic Cell Aggregate

Shown in Figure 6.4 is a typical heterotypic cell aggregate consisting of two kinds of cells. It is assumed that cells of the same kind possess similar sub-cellular micro-components such as cytoplasm, circumferential microfilament bundles, microtubules inside each cell. It is further assumed that on the cell membrane, different expressions of the receptors, and different proteins of adhesion molecules make the cell-cell or cell-media adhesion of dark cells different from white cells. As stated in chapter 2, the adhesion on the interface of two adjacent cells intend to increase their common boundary. this is mechanically equivalent to a force  $F_{Adh}$  which opposes the contractile force  $F_C$ . For simplicity, instead of assigning separate values to  $F_C$  and  $F_{Adh}$ , a resultant force  $F$  is defined as:

$$F = F_C - F_{Adh}, \quad (6.3)$$

and has different values for different types of interfaces.

In a heterotypic cell aggregate, there are five types of interfaces: interfaces between white - white cells; dark - dark cells; white -dark cells (or dark - white cells); white cell - medium and dark cell - medium. Therefore, five parameters  $F_{d-d}$ ,  $F_{w-w}$ ,  $F_{d-w}$ ,  $F_{d-m}$ , and  $F_{w-m}$  have to be defined, each of which represents the force along the





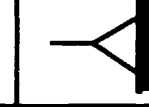


**Figure 6.4 A Heterotypic Cell Aggregate**

respective interface. Table 6.1 lists symbols representing these five interfacial types and their respective forces.

Note that each of these parameters can be positive for a net contractile force, or negative for a net tensile force. Each set of these parameters induces certain kinds of cell activities, ranging from cell dissociation or dispersal to cell sorting and tissue spreading. The transition from one kind of behaviour to another is determined by the relationship

**Table 6.1 Interfacial Types in a Heterotypic Cell Aggregate**

<b>Interface Type</b>	white cell - white cell	dark cell - dark cell	white cell - dark cell	white cell - media	dark cell - media
<b>Symbol</b>					
<b>Force Parameter</b>	$F_{w-w}$	$F_{d-d}$	$F_{d-w}$	$F_{d-m}$	$F_{w-m}$

between these five parameters. These relationships are systematically investigated in this chapter through a variety of simulations.

### 6.3.2 Rounding and Protruding Behaviour of Cells

Most living cells can be characterized either as rounding or protruding. A cell displays predominantly protruding behaviour when spreading over a adhesive substratum, and rounding behaviour when it is suspended in a solution or dropped on a non-adhesive substratum (Lauffenburger and Horwitz, 1996). However, in some cases, one part of a cell is rounding and another part is protruding. The rounding and protruding behaviour of cells are the characteristics of the net forces exerting on' cell interfaces. A monotypic cell sheet shown in Figure 6.5 (a) is simulated to demonstrate this rounding and protruding of cells. The top and bottom edges of the sheet are restrained vertically, while the right and left edges are restrained horizontally. There is only one type of interface in this aggregate, namely white-white interface. Firstly, a net tensile force is assigned to every interface. The rounding behaviour of cells within the sheet is shown in Figure 6.5 (b). Secondly, a net elongation force is assigned to each interface and protruding behaviour of cells are observed (Figure 6.5 (c)).

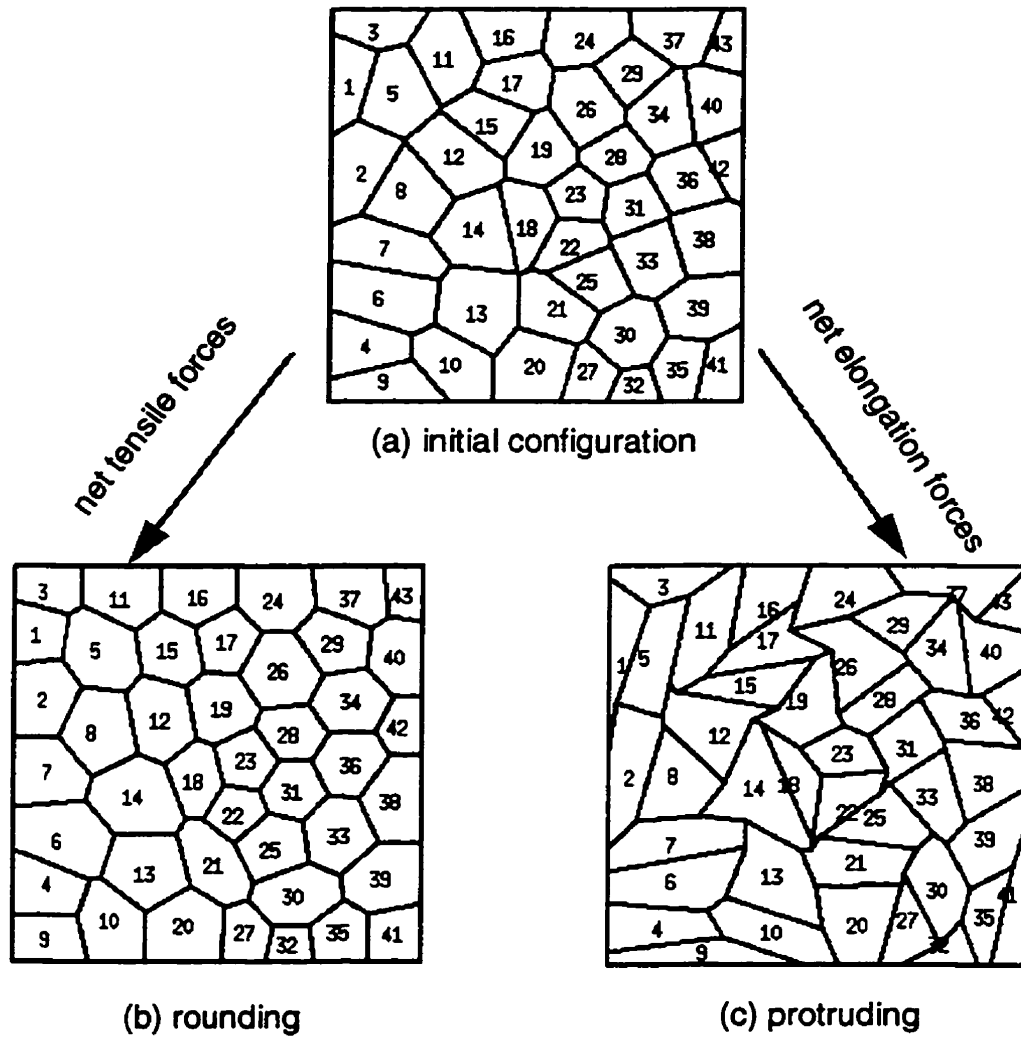


Figure 6.5 Rounding and Protruding Behaviour of Cell Sheets

The rounding of a cell maintains its shape whereas protruding provokes the active exploration of neighbours around the cell. Evidently, the contractile forces are responsible for the rounding of individual cell as well as the global profile of the aggregate, and tensile forces generate protruding of cells. Rounding and protruding are two basic elements of shape changes of a cell. Any complicated behaviour of cells can be dissected into these two elements.

#### 6.4 Simulations of Cell Sorting

Figure 6.6 (a) shows 135 cells with 62 dark cells and 73 white cells randomly put together. It is assumed that cells are able to cohere to each other to form a simple-connected aggregate, which means there is no gap between any two cells. At the beginning, dark cells and white cells are randomly mixed. One vertex in cell 1 and one in cell 5 are anchored to satisfy the minimum requirement of system stability. Two kinds of simulations are carried out. In the first kind of simulations, force parameters remain constant throughout the simulation. In the second kind, some of these force parameters are subjected to random temporal variations.

##### 6.4.1 Cell Sorting without Random Variations

The interface forces are in the ratios  $F_{d-d} : F_{w-w} : F_{d-w} : F_{d-m} : F_{w-m} = 400 : 1400 : 3000 : 6000 : 4000$ . Notice that the hierarchy of the interfacial forces is:

$$0 < F_{d-d} < F_{w-w} < F_{d-w} < F_{w-m} < F_{d-m} \quad (6.5)$$

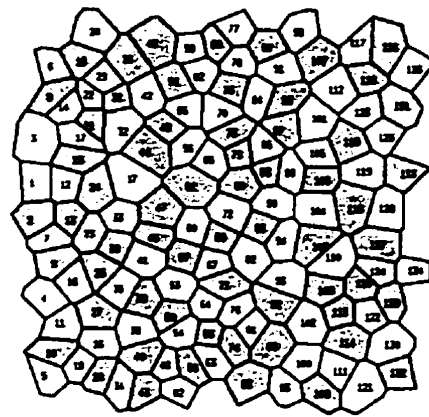
Then the simulation is set to motion. The topological changes within the aggregate as well as shape changes of individual cells are recorded in terms of simulation time  $\tau$ , which equals to the time interval multiplied by iterative steps. Spontaneous cell movements and rearrangements actively take place in a short period of time. Dark cells, such as cell 36, typically form protrusions (Figure 6.6 (b)) due to the interfacial force

differences. When these protrusion happen to contact other dark cells, their even weaker forces cause their common boundaries to increase in length (cell 36 and 18 in Figure 6.6 (b)) and chains of dark cells are formed, while the profile of the aggregate starts to round up. By the time of  $\tau = 5$ , the biggest cluster of dark cells, which happens to be located in the middle section of the aggregate, tends to decrease its boundary with white cells as well as its boundaries with the medium, because of the stronger forces between dark cells and white cells (Figure 6.6 (c)). Substantial cell rearrangement has occurred. White cells positioned between dark cells *in situ*, such as cell 56 and 65 are pushed away from dark cells and clusters of dark cells begin to take a rounded shape. While cell movements proceed, the boundaries of dark cells on the periphery continue to shorten since dark cells are assumed to possess stronger contractile forces when they are exposed to the medium. When the boundary length is short enough, dark cell 107 is pulled away from the edge (Figure 6.6 (d)). Eventually, the biggest cluster of dark cells moves into the interior of the aggregate (Figure 6.6 (e)). As clusters of dark cells form, protrusions are less likely to span from one cluster to the other. Cell movements greatly slow down when the size of the cluster increases and the aggregate approaches its equilibrium state. By the time of  $\tau = 565$ , clusters of dark cells all round up in the interior of the white cell population (Figure 6.6 (f)). After a prolonged time, very little changes occur in the aggregate and further cell sorting virtually stop. Therefore, Figure 6.6 (f) is considered as the final state of the aggregate.

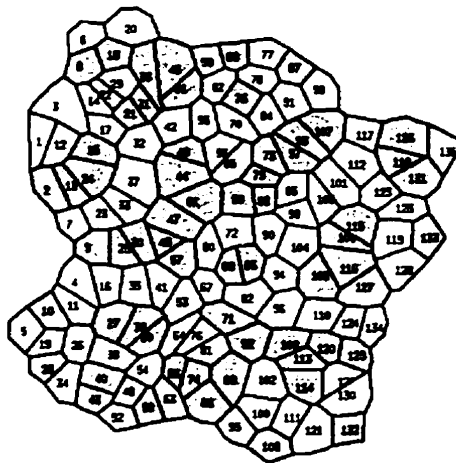
#### 6.4.2 Cell Sorting with Random Variations

Random variations of the cell surface properties have been reported previously. It is believed that the random variations can increase the cell motility and enhance cell sorting performance. The same initial configuration and same force parameters are used in the following simulation, except the dark-white cell interfacial force  $F_{d-w}$  and dark cell - medium force  $F_{d-m}$  change a percentage of their values after a certain number of simulation steps (RAND\_STEP). Each dark cell is assigned a random number. This number is the percentage by which  $F_{d-w}$  and  $F_{d-m}$  in that cell are going to change. In

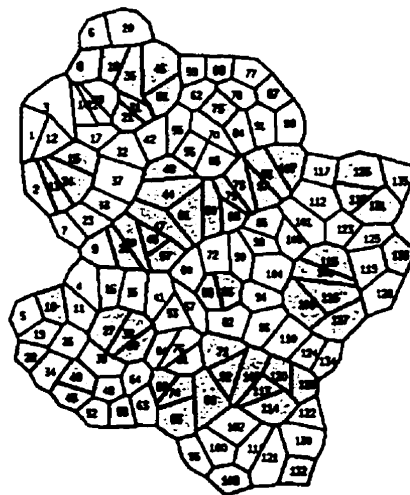
order for the changes to take effect, the same set of number is used within RAND\_STEP simulation steps. Then a new set will be generated. In the simulation presented in Figure 6.7, RAND\_STEP = 70 is found to be a practical number. RAND\_STEP has to be big enough to allow the changes to develop, yet can not be too big, or it may lead to local instabilities, in which, a cell can not maintain the volume-constancy due to strong protrusive activity. Generally, with random variations, cells exhibit more active motility and faster rearrangement. Dark cells are in a more protrusive state. Notice in Figure 6.7, only by the time  $\tau = 2$ , some clusters of dark cells have formed (Figure 6.7 (a)). More significantly, in the biggest dark cell cluster, cell 9 and 107 have already been pulled inside the tissue, whereas in the case without random variations, this event takes place much later, around  $\tau = 30$  (Figure 6.6 (e)). By the time  $\tau = 13$ , two bigger clusters of dark cells move into the interior of the tissue (Figure 6.7 (e)), forming a very similar configuration to the final state of the aggregate without random variations (Figure 6.6 (f)). However, the clusters of dark cells are still separated and complete sorting is not achieved.



(a)  $\tau = 0$

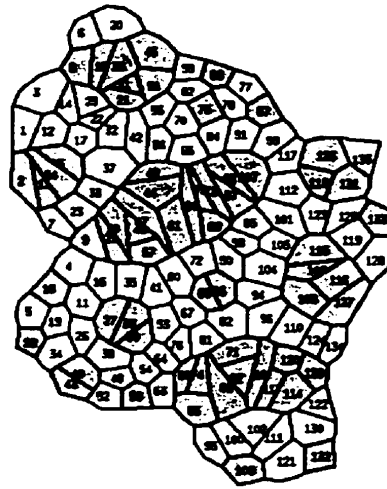


(b)  $\tau = 2$

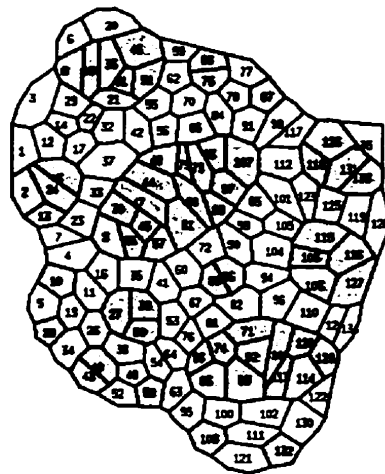


(c)  $\tau = 5$

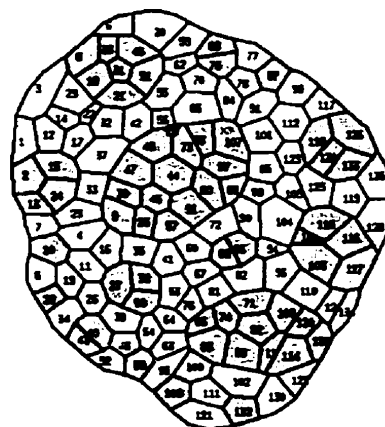
**Figure 6.6 Simulations of Cell Sorting without Random Variation**



(d)  $\tau = 23$



(e)  $\tau = 37$



(f)  $\tau = 565$

**Figure 6.6 Simulations of Cell Sorting without Random Variation (Continued)**

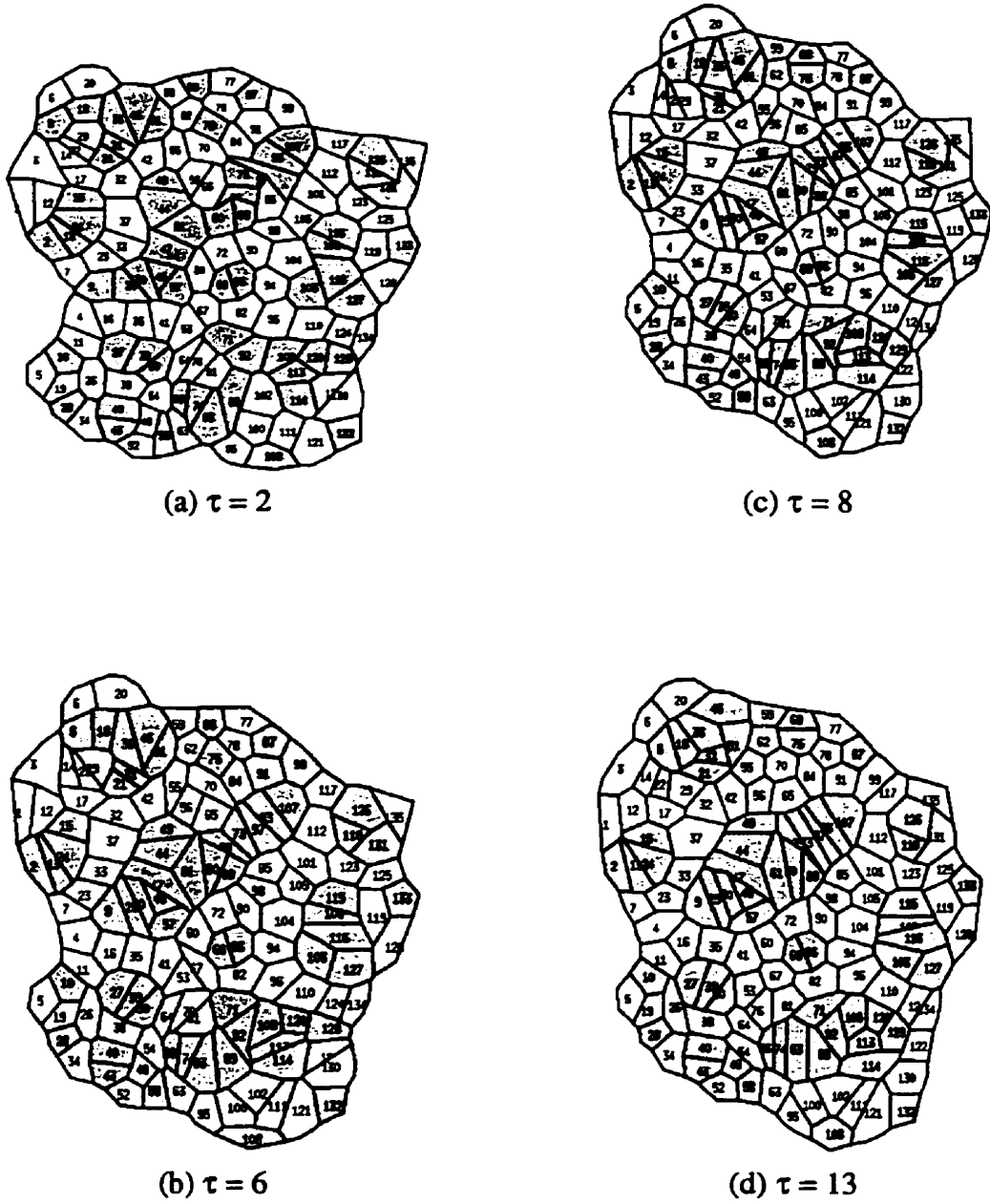


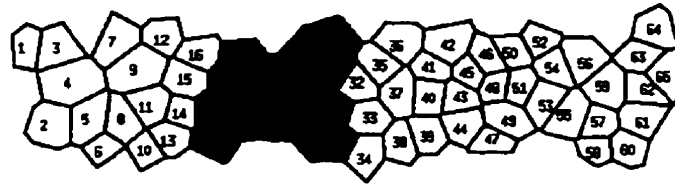
**Figure 6.7 Simulation of Cell Sorting with Random Variation**

### 6.5 Simulations of Tissue Spreading

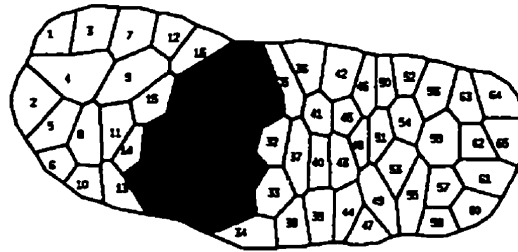
Two kinds of tissues made of the similar dark cells and white cells as in the previous simulations are placed together side by side as shown in Figure 6.8 (a). It is assumed that these three pieces of tissues fuse to each other to form a continuous aggregate. Similarly, one vertex from cell 1 and another from cell 2 are anchored to eliminate the free-body motion of the system, and there is no other external stimuli otherwise. When the aggregate is set to motion, each piece of tissue starts to round up due to the contractile forces on the periphery. Since dark cells are assigned stronger forces on the periphery, they tend to move inwards of the tissue, while white cells such as 16 and 36 crawling over dark cells on the edge (Figure 6.8 (b)). After a fairly long time (Figure 6.8 (c),  $\tau = 150$ ), a monolayer of white cells is formed along the upper part of the edge, engulfing the dark cells. An equilibrium state is reached when a layer of white cells completely engulf the cluster of dark cells (Figure 6.8 (d)). The newly reconstructed tissue has a round shape. This sequence of tissue spreading mimics the behaviour of biological tissue spreading *in vitro* (Steinberg, 1963) to a very significant degree, suggesting that cell sorting and tissue spreading share the same mechanism.

### 6.6 Other Cell Activities Cells Studied by Simulations

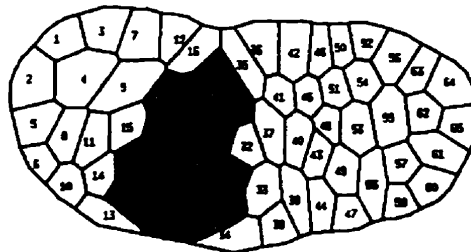
Beside cell sorting and tissue spreading, there are other important cell activities may be explained using the same mechanisms, depending on the developing stages and their histological position. This phenomena include dissociation of tissues, or so called cell dispersal and checker-board formation (Glazier and Graner, 1993)



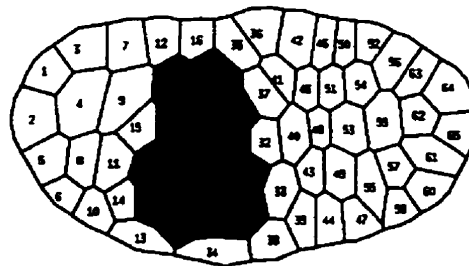
(a).  $\tau = 0$



(b)  $\tau = 7.5$



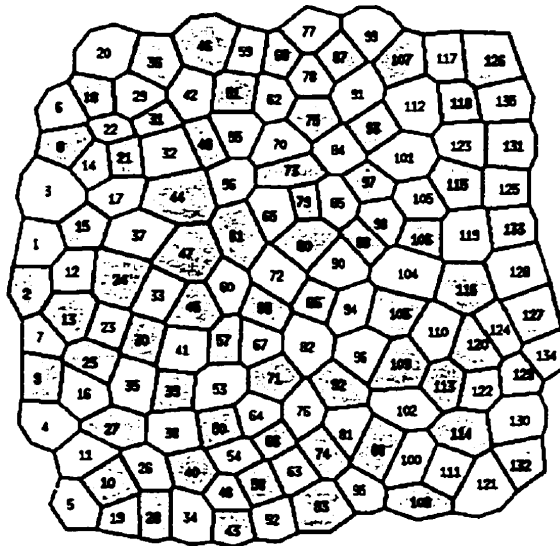
(c)  $\tau = 150$



(d)  $\tau = 500$

**Figure 6.8 Tissue Spreading Simulation**

During sexual maturation of the avian, cells of its oviduct epithelium are found to rearrange in a pattern very similar to the checker-board, in which dark cells are surrounded by white cells and *vice versa* (Honda *et al.*, 1984; Honda and Yamanaka, 1986). This phenomenon is known as checker-board formation. Within the same initial heterotypic aggregate, the checker-board pattern can be achieved by setting the unlike cell interfacial force  $F_{d-l}$  to the lowest value. Figure 6.10 is the simulation result when the interface forces are in the following ratios  $F_{d-d} : F_{l-l} : F_{d-l} : F_{d-m} : F_{l-m} = 1000 : 1000 : 300 : 3000 : 3000$ . It is obvious that dark cells tend to separate from dark cells, white cells from white cells. The result is a check-board pattern.



$$\tau = 14$$

**Figure 6.9 Simulation of Checker-board Formation**

## **6.7 Discussion**

These simulation show that differences in interfacial properties of a heterotypic cell aggregate can drive cell rearrangement and cell sorting.

This is a generalization of the hypotheses outlined at the beginning of this chapter. In a monotypic cell aggregate, only tensile forces are able to produce the protrusive behaviour in cells, as demonstrated in Figure 6.5. However, in a heterotypic aggregate, protrusive behaviour is observed in the presence of differential contractile forces on the cell surface. The implication of the term “difference in interfacial properties”, can be ambiguous. From a mechanical prospective, this interfacial property means that the forces acting on the interfaces of adjacent cells and interfaces of cells and medium vary, as is the case in the finite element cell model used in this work. Essential aspects of cell sorting, tissue spreading and other behaviour of cells including check-board formation and cell dispersal can be explained using this simulation model.

It is found that the simulation results fully agree with predictions made by the differential surface contraction hypothesis (DCH). The parameters that produce cell sorting in sections 6.4 and 6.5 are consistent with the two basic assumptions made by Harris (1975) (See p.100 of this thesis), the predicted requirements for cell sorting coincide with the parameters used in the simulation of cell sorting presented in. The major drawback of the DCH, however, is that it does not predict complete sorting, nor do the simulations in the present work. The expected complete sorting pattern has never been fully achieved, in spite of numerous attempts made with possible combinations of force parameters.

The fundamental issue here is what it exactly is mean by “interfacial forces” and what qualitative relationship between the five force parameters for complete sorting to

happen. On the one hand, the interfacial forces can be interpreted as the contractile forces exerted by CMBs, membrane forces, etc. It is possible that cells from different tissues or of different origins alter slightly their micro-components according to the histological position or developmental stages. On the other hand, one has good reasons to believe the differences in interfacial forces used in this model are caused by the differential cell adhesions and the five force parameters  $F_{d-d}$ ,  $F_{d-w}$ , .... are analogous to the reversible works  $W_{a-a}$ ,  $W_{a-b}$ , .... used in Steinberg's elicitation of the DAH. If this is the case, the numerical values of the reversible works used in Glazier and Graner's model (1993, 1992) should be able to proportionally project into the five forces parameters. To verify this postulation, a simulation is carried out. In the same initial configuration used in the cell sorting simulation (Figure 6.6 (a)), the following ratio of forces are assigned to cell interfaces:  $F_{d-d} : F_{w-w} : F_{d-w} : F_{d-m} : F_{w-m} = 200 : 1400 : 1100 : 1600 : 1600$ . These values are proportional to those of reversible works in Glazier and Graner's model. They also satisfy the inequalities in equation 6.1:

$$0 < F_{d-d} < F_{d-w} < (F_{d-d} + F_{w-w})/2 < F_{w-w} \quad (6.5)$$

According to DAH, these values should produce complete cell sorting. But the simulations in this work yields a very different equilibrium state, as shown in Figure 6.10. Since the contractile force between dark and white cells are relatively weak, a chain of dark cells can not round up to form a cluster. There is no sign that a complete sorting could ever be reached.

In conclusion, in a heterotypic cell aggregate, differential contractile forces between different type of cell interfaces are sufficient to drive cell sorting, tissue spreading, cell dispersal and checker-board formation. The type of cell activities induced depends on the relationships between these interfacial forces. The correlation between the

relationships of five force parameters and the resulting cell activities are summarized in Figure 6.11

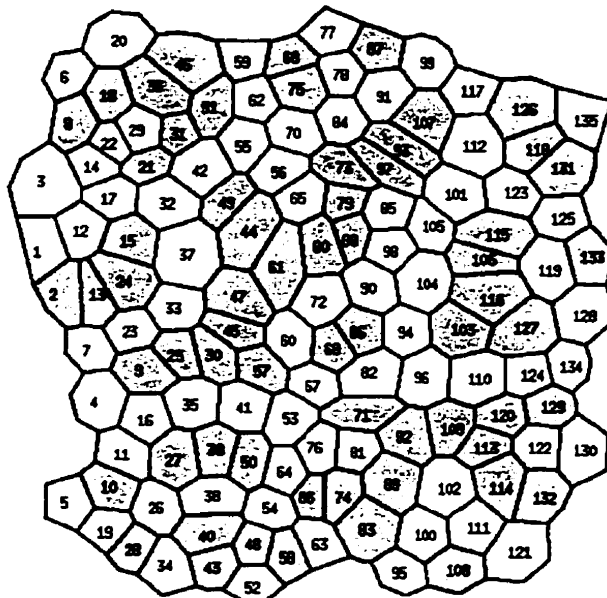
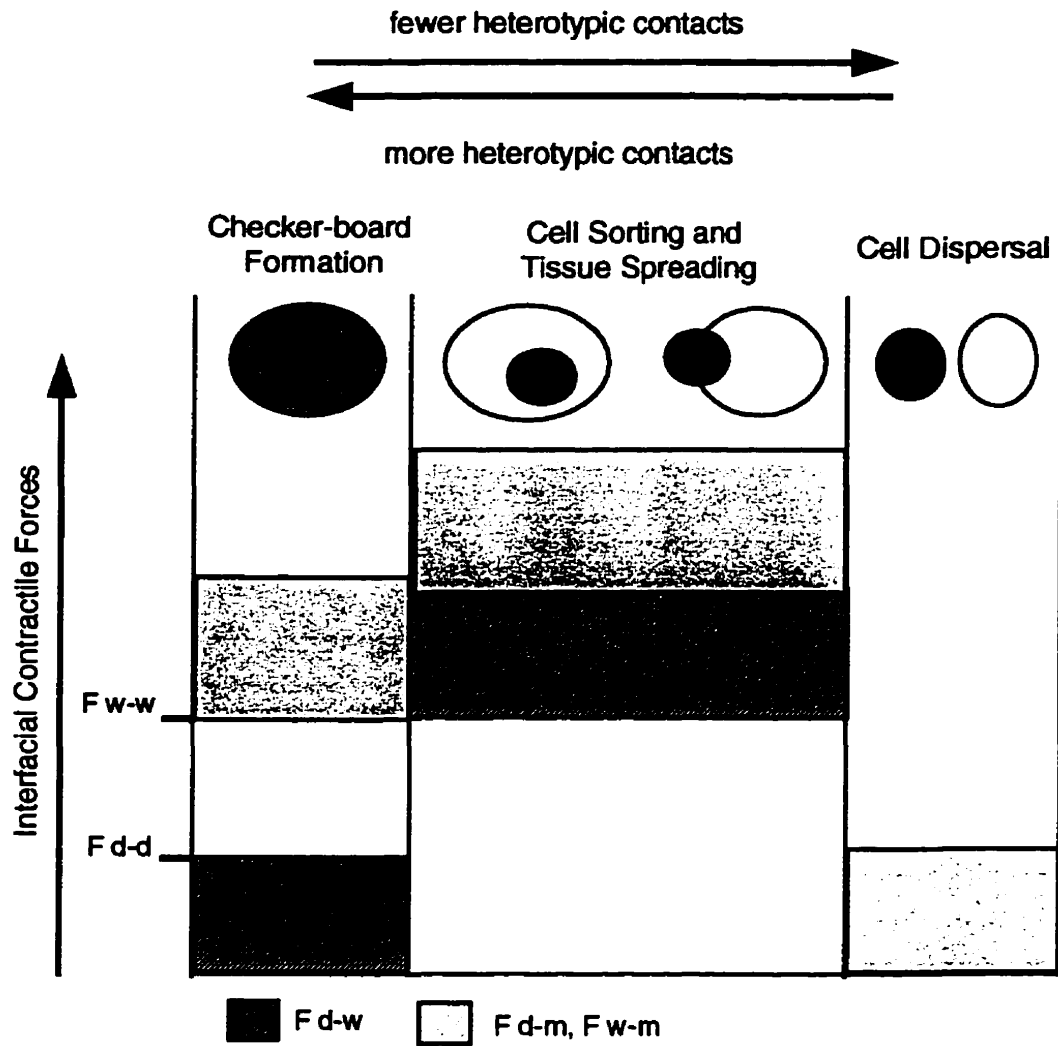


Figure 6.10 Simulation Result Using DAH Values



**Figure 6.11 Correlation Between Interfacial Forces and Cell Activities**

# **Conclusions and Future Prospects**

# **7**

The cell finite element formulation presented in this thesis makes realistic computer simulations of basic cell behaviour possible. These simulations can be a very powerful tool for testing hypotheses about the forces that drive specific cell phenomenon.

When used to complement experimental studies that establish macro- and micro-morphologies, measure forces, detail the kinematics of cell shape changes, movements and topological rearrangements, and perturb normal activities surgically or using teratogens, they make possible quantum advances in scientific understanding.

Simulations of monotypic cell sheets provide, for the first time, a quantitative understanding of how bulk mechanical properties of an embryonic tissue derive from cell components and cell rearrangement during the course of deformation. The mechanical effects of cell micro-structural properties such as forces exerted by CMBs, microtubules and adhesion molecules on the cell surface, and the viscosity of cytoplasm on regulation of cell shapes and bulk stress-strain rate relationships are investigated in a systematic way. The simulation results establish a direct connection between cell micro-mechanics and the tissue macro-mechanics.

Simulations of heterotypic cell aggregates serve a somewhat different purpose. A great deal about the kinematics of cell activities including cell rearrangement, sorting, tissue spreading and checker-board formation has been learned as a result of these computer simulations.

Perhaps more significantly, these simulations of cell activities show that a complex sequence of cell movements and shape changes can be produced by a set of simple driving force. External controls are not always necessary. Instead, the differences in interfacial forces between cells of different kinds are sufficient to produce protrusion and rounding of cells and determine the preferred positions for a specific type of cell. These simulations also suggest that different sets of forces may act in parallel, though not all may be apparent. Thus, redundant force generators may remain undetected during normal morphogenesis.

It is reasonable to expect that computer simulations will become a standard research tool, and that during the next several decades, they will be used to study all manner of morphogenetic processes.

Ongoing advances in computer hardware and software will allow simulations of large number of cells, approaching the real number of cells involved in a biological organ or whole embryo. They will also make possible simulations that bridge larger ranges of the scales shown in Figure 1.4.

In time, computer models that might be called “virtual embryos” will be developed. These will allow “virtual experiments” to be carried out. Such virtual embryos will be especially useful for studies of human morphogenesis.

In summary, the future of computer simulations of cell activities and embryo morphogenetic processes looks very bright. Much remains to be learned about these

remarkable developmental processes, and computer simulations are proving to be an ideal means to study them.

## References

### References

- Alberts, B., Bray, D., Lewis, J., Raff, M., Roberts, M. and Watson, J., 1989 *Molecular Biology of the cell*, 2nd ed., Garland Publishing, Inc., New York.
- Armstrong, P. B.; 1978, "Modulation of tissue affinities of cardiac myocyte aggregates by mesenchyme", *Dev. Biol.* **64**, 60
- Armstrong, P. B.; 1989, "Cell sorting out: the self-assembly of tissues *in vitro*", *Crit. Rev. Biochem. Molecul. Biol.* **24**, No. 2, 119-149.
- Ashkin, A., Schütze, K., Dziedzic, J. M., Euteneuer, U. and Schliwa, M.; 1990, "Force generation of organelle transport measured *in vivo* by an infrared laser trap", *Nature.* **348**, 346-348
- Balinsky, B.I. and Fabian, B.C., 1981 *An Introduction to Embryology*, 5nd ed., Saunders College Publishing, Inc., Philadelphia, Pa.
- Bershadsky, A. D. and Vasiliev, J. M., 1993, "Mechanisms of regulation of pseudopodial activity by the microtubule system", In: *Cell Behaviour: Adhesion and Motility*.(ed. Jones, G., Wigley, C. and Warn, R.), Society for Experimental Biology, 353-373
- Bertolotti, R., Rutishauser, U. and Edelman, G. M., 1980, "A cell surface molecule involved in aggregation of embryonic liver cells", *Proc. Natl. Acad. Sci. USA*, **77**, 4831-4835
- Bordzilovskaya, N.P., Dettlaff, T.A., Duhon, S.T. and Malacinski, G.M., 1989, "Developmental-stage series of axolotl embryos" *Developmental biology of the axolotl*, Armstrong, J.B. and Malacinski, G.M. (eds), Oxford University Press, New York, 201-219
- Bowyer, A., 1981, "Computing Dirichlet tessellations", *The Computer J.* Vol. **24**, No. 2, 1981, 162-166
- Brodland, G.W. and Clausi, D.A., 1995, "Cytoskeletal mechanics of neurulation: insights obtained from computer simulations," *Biochem. Cell Biol.*, Vol. **73**, No.7&8 545-553
- Brodland, G.W. and Clausi, D.A., 1994, "Embryonic tissue morphogenesis modeled by FEM," *ASME J. Biomech. Eng.*, Vol. **116**, May 146-155

- Brodland, G.W. and Shu, D.W., 1992, "Are intercellular membrane forces important to amphibian neurulation?", In *Dynamical phenomena at interfaces, surfaces and membrane*, (ed. G. Forgacs and D. Beysens), New York: Nova Science publishers.
- Brodland, G.W., Scott, M.J., MacLean, A.F., Globus, M., Vethamany-Globus, S., Veldhuis, J.H. and Del Maestro, R., 1996, "Morphogenetic movements during axolotl neural tube formation tracked by digital imaging", *Roux's Arch Dev Biol*, **205**, 311-318
- Brodland, G. W., 1997, "Computer modelling of morphogenesis: recent advances and future prospects", *Proc. of the Sixteen Canadian Congress of Applied Mechanics CANCAM 97*, Vol. 2, June 1-6, Québec, Canada, 85-95
- Brodland, G. W. and Gordon, R., 1990, "Intermediate filaments may prevent bulking of compressively loaded microtubules", *J. Biomech. Eng.* **112**, 319-321
- Burnside, M.B., 1973, "Microtubules and microfilaments in amphibian neurulation", *Am. Zool.*, **13**, 989-1006
- Burnside, M.B. and Jacobson, A.G., 1968, "Analysis of morphogenetic movements in the neural plate of the newt *taricha torosa*", *Devel Biol.* Vol **18**, 537-552
- Brun, R.B. and Garson, J.A., 1983, "Neurulation in the Mexican salamander (*ambystoma mexicanum*): a drug study and cell shape analysis of the epidermis and the neural plate", *J. Embryol. Exp. Morph.* Vol **74**, 275-295
- Carlson, B.M., 1981, *Patten's Foundations of Embryology*, 4nd ed., McGraw-Hill Book Company, New York.
- Carter, S. B., 1967, "Haptotaxis and the mechanism of cell motility," *Nature* **213**, 256-261
- Chen, H. H. and Brodland, G.W., 1997, "Finite element simulation of differential adhesion-driven cell sorting and spreading", *Proc. of the Sixteen Canadian Congress of Applied Mechanics CANCAM 97*, June 1-6, Québec, Canada, 1013-1023
- Clausi, D.A. and Brodland, G.W., 1993, "Mechanical evaluation of theories of neurulation using computer simulations," *Development* **118**, 1013-1023
- Cowin, P., Franke, W. W., Grunk, C., Kapprell, H-P. and kartenbeck, J.; 1985, "The desmosome-intermediate filament complex", In *The Cell in Contact* (ed. Edelman, G.M and Thiery, J), 427-460.

- Curtis, A. S. G., 1969, "The measurement of cell adhesiveness by an absolute method", *J. Embryol. Exp. Morphol.*, **79**, 305-325
- Curtis, A. S. G. and Lackie, J. M., 1991, *Measuring Cell Adhesion* ed., John Wiley & Sons Inc.
- Curtis, A. S. G., 1991, "Measurement from breaking and changing adhesions" In *Measuring Cell Adhesion*, (ed. Curtis A. S. G. and Lackie, J. M), John Wiley & Sons Inc.
- Davidson, L.A., Koehl, M.A.R., Keller, R. and Oster, F., 1995, "How do sea urchins invaginate? Using biomechanics to distinguish between mechanisms of primary invagination", *Development* **121**, 2005-2018
- Edelman, G.M., 1985, "Specific Cell Adhesion in Histogenesis and Morphogenesis," In *The Cell in Contact* (ed. Edelman, G.M and Thiery, J), 139-168
- Edelstein, B. R., 1971, "Cell specific diffusion model of morphogenesis", *J. Theor. Biol.*, **30**, 515
- Erickson, C. A., 1988, "Control of pathfinding by the avian trunk neural crest", *Development Suppl.* **103**, 63-80
- Friedlander, D. R., Mège, R-M, Cunningham, B. A., and Edelman, G. M., 1989, "Cell sorting-out is modulated by both the specificity and amount of different cell adhesion molecules (CAMs) expressed on cell surfaces", *Proc. Natl. Acad. Sci. USA*, **86**, 7043-7047
- Forgacs, G., 1995, "Biological specificity and measurable physical properties of cell surface Receptors and their possible role in signal transduction through the cytoskeleton", *Biochem. Cell Biol.*, **73**, 317-326
- Foty, R. A., Forgacs, G., Pflieger, C. M. and Steinberg, M. S., 1994, "Liquid properties of embryonic tissue: measurement of interfacial tensions", *Phys. Rev. Letters*, **72**, No. **14**, 2298-2301
- Foty, R. A. and Steinberg, M. S., 1995, "Liquid properties of living cell aggregates: measurement and morphogenetic significance of tissue interfacial tensions", In: *Interplay of Genetic and Physical Processes in the Development of Biological Form.*(ed. Beysens, D., Forgacs, G. and Gail, F.), World Scientific Pub. Co. Pte. Ltd., 63-73

- Fukui, Y., 1993, "Toward a new concept of cell motility: cytoskeletal dynamics in amoeboid movement and cell division", *Int. Rev. Cytol*, **144**, 85-127
- Galou, M., Gao, J., Humbert, J., Mericskay, M., Li, Z. L., Paulin, D. and Vicart, P., 1997, "The importance of intermediate filaments in the adaptation of tissues to mechanical stress: evidence from gene knockout studies", *Biol. Cell*, **89**, 85-97
- Glazier, J. A., 1989, *Ph.D dissertation.*, University of Chicago.
- Glazier, J. A. and Graner, F., 1993, "Simulation of the differential adhesion driven rearrangement of biological cells", *Physical Rev. E.*, **47**, 2122-2154
- Gordon, S.R. and Essner, E., 1987, "Investigations on circumferential microfilament bundles in rat retinal pigment epithelium," *European Journal of Cell Biology*, Vol. **44**, 97-104
- Graner, F. and Glazier, J. A., 1992, "Simulations of biological cell sorting using a two-dimensional extended potts model", *Physical Rev. Letters.*, **69**, 2013-2016
- Graner, F., 1993, "Can surface adhesion drive cell-rearrangement? Part I: biological cell-sorting", *J. theor. Biol.*, **164**, 455-476
- Grebecki, A., 1994, "Membrane and cytoskeletal flow in motile cells with emphasis on the contribution of free-living amoeba", *Int. Rev. Cytol*, **148**, 37-79
- Grumet, M. and Edelman, G. M., 1994, "heterotypic binding between neuronal membrane vesicles and glia cells is mediated by a specific neuron-glia cell adhesion molecule", *J. Cell Biol.*, **98**, 1746-1756
- Gumbiner, B. M., 1996, "Cell adhesion: the molecular basis of tissue architecture and morphogenesis", *Cell*, Vol. **84**, 345-357
- Harris, H., 1961, "Chemotaxis", *Expl. Cell Res. Suppl.*, **8**, 199-208
- Harris, A.,K., 1976, "Is cell sorting caused by differences in the work of intercellular adhesion? a critique of the Steinberg Hypothesis", *J. theor. Biol.*, **61**, 267-285
- Harris, A.,K., 1987, "Cell Motility and the Problem of Anatomical Homeostasis," *J. Cell Sci. Suppl.* **8**, 121-140
- Harris, A.,K., 1994a, "Cytokinesis: the mechanism of formation of the contractile ring in animal cell division", In *Biomechanics of Active Movement and Division of Cells.*(Ed: Akkas, N), NATO ASI Series, **84** 37-86

- Harris, A.,K., 1994b, "Multicellular mechanics in the creation of anatomical structures," In *Biomechanics of Active Movement and Division of Cells.*(Ed: Akkas, N), NATO ASI Series, **84** 87-129
- Heldman, A. W. and Goldschmidt-Clermont, P. J., 1993, "Cell Signalling and Motile Activity", In: *Cell Behaviour: Adhesion and Motility.*(ed. Jones, G., Wigley, C. and Warn, R.), Society for Experimental Biology, 317-324
- Hifler, S.R. and Hifler, E.S., 1983, "Computer simulation of organogenesis: An approach to the analysis of shape changes in epithelial organs," *Developmental Biology*, Vol. **97**, 444-453
- Hiramoto, Y., 1969, "Mechanical properties of the protoplasm of the sea urchin egg" *Expl. Cell Res.*, **56**, 201-208
- Hiramoto, Y., 1982, "Rheological properties of echinoderm eggs during cell division," *Biol.* **19**, 71-78
- His, W., 1888, *Proc. R. Soc. Edinburgh* **15**, 287-298
- Honda, H., Kodama, R., Takeuchi, T., Yamanaka, H., Watanabe, K. and Eguchi, G., 1984, "Cell behavior in a polygonal cell sheet", *J. Embryol. exp. Morph.* **83**, Supplement 313-327
- Honda, H. Ogita, Y. Higuchi, S. and Kani, K. 1982, "Cell movements in a living mammalian tissue: long-term observation of individual cells in wounded corneal endothelia of cats", *J. Morph.* **174**, 25-39
- Honda, H. and Yamanaka, H., 1986, "Transformation of a polygonal cellular pattern during sexual maturation of the avian oviduct epithelium: computer simulation", *J. Embryol. exp. Morph.* **98**, 1-19
- Hynes, R. O. and Lander, A. D., 1992, "Contact and adhesive specificities in the association, migration and targeting of cells and axons", *Cell.* **69**, 303-322.
- Ingber, D. E., Dike, L., Hansen, L., Karp, S., Liley, H., Maniotis, A., McNamee, H., Mooney, D., Plopper, G., Sims, J. and Wang, N., 1994, "Cellular tensegrity: exploring how mechanical changes in the cytoskeleton regulate cell growth, migration, and tissue pattern during morphogenesis", In: *Mechanical Engineering of the Cytoskeleton in Development Biology.*(ed. Gordon, R.), Academic Press, 173-224

- Ingber, D. E., 1997, "Tensegrity: the architectural basis of cellular mechanotransduction", *Annu. Rev. Physiol.*, **59**, 575-599
- Ishikawa, H., 1986, "Ultrastructural Organization of the stress fiber", In: *Cell Motility: Mechanism and Regulation*. (ed. Ishikawa, H., Hatano, S. and Sato, H.), Alan R. Liss, Inc., New York, 451-460.
- Itasaki, N., Nakamura, H., Sumida, H. and yasuda, M., 1991, "Actin bundles on the right side in the caudal part of the heart tube play a role in dextro-looping in the embryonic chick heart," *Anat. Embryol.*, **183**, 29-39
- Jacobson, A.G., 1980, "Computer modeling of morphogenesis," *Amer. Zool.*, **20** 669-677
- Jacobson, A.G., Odell, G. M. and Oster, G. F., 1984, "The cortical tractor model doe epithelial folding application to the neural plate", In *Molecular Determinants of Animal Form*, Alan R. Liss Inc. 143-166
- Jacobson, A.G., 1985, "Adhesion and movement of cells may be coupled to produce neurulation" *The Cell in Contact*., Ed. Edelman, G.M. and Thiery, J., John Wiley & Sons, Inc. 49-65
- Jacobson, C.O., 1962, "Cell migration in the neural plate and the process of neurulation in the Axolotl larva," *Zool. Bidrag, Uppsala Bd.*, **35**, 433-448
- Jesuthasan, S., 1997, "Neural crest cell migration in the zebrafish can be mimicked by inert objects: mechanism and implication of latex bead movement in embryos", *J. Exp. Zool* **277**, 425-434
- Kalnins V.I., Sandig, M., Hergott, G.J. and Hagai, H., 1995, "Microfilament Organization and Wound Repair in Retinal Pigment Epithelium", *Biochem. Cell Biol.*, **73**, 709-722
- Kaneda, I., kamitsubo, E. and Hiramoto, Y.; 1990, "The mechanical structure of the cytoplasm of the echinoderm egg determined by "gold particle method" using a centrifuge microscope", *Develop. Growth & Differ.* **32**, 15-22
- Keller, R.E. and Speith, J., 1984, "Neural crest cell behaviour in white and dark larvea of *Ambystoma mexicanum*: Time-lapse cinemicrographic analysis of pigment cell movement *in vivo* and in culture.", *J. Exp. Zool.* **229**, 109-126
- Keller, R. and Hardin, J., 1987, "Cell behaviour during active cell rearrangement: edivence and spectulations", *J. Cell Sci. Suppl.*, **8**, 369-393

- Keller, R.E. and Trinkaus, J. P., 1987, "Rearrangement of enveloping layer cells without disruption of the epithelial permeability barrier as a factor in *Fundulus emipoly*", *Devl. Biol.*, **120**, 12-24
- Keller, R., Shih, J. and Wilson, P., 1991, "Cell motility, control and function of convergence and extension during gastrulation in *Xenopus*", In *Gastrulation*. (Ed. Keller, R., Clark, W. H. Jr. and Griffin, F.), Plennm Press, New York, 101-119
- Khan, S. and Sheetz, M. P., 1997, "Force effects on biochemical kinetics", *Annu. Rev. Biochem.*, **66**, 785-805
- Lackie, J. M., 1986, *Cell movement and cell behaviour*, Allen & Unwin, London
- Lauffenburger, D. A. and Horwitz, A. F., 1996, "Cell migration: a physically integrated molecular process", *Cell* **84**, 359-369
- Lawson, M. A. and maxfield, F. R., 1995, "Ca<sup>2+</sup> - and calcineurin-dependent recycling of an integrin to the front of migrating neutrophils", *Nature*, **377**, 75-79
- Lee, H. And nagele, R. G., 1988, "Intrinsic forces alone are sufficient to cause closure of the neural tube in the chick", *Experientia.*, **44**, 60-61
- Li, Z. L., Mericskay, M., Agbulut, O., Butler-Browne, G., Carlsson, L., Thornell, L. E., Babinet, C. and Paulin, D., 1997, "Desmin is essential for the tensile strength and integrity of myofibrils but not for myogenic commitment, differentiation, and fusion of skeletal muscle", *J. Cell. Biol.*, **139**, 129-144
- Luby-Phelps, K., 1994, "Physical properties of cytoplasm", *Curr. Opin. Cell Biol.*, **6**, 3-9
- Maniotis, A. J., Chen, C. S. and Ingber, D. E., 1997, "Demonstration of mechanical connections between integrins cytoskeletal filaments, and nucleoplasm that stabilize nuclear structure", *Proc. Natl. Acad. Sci. USA*, **94**, 849-854
- Marrs, J. A. and Nelson, W. J., 1996, "Cadherin cell adhesion molecules in differentiation and embryogenesis", *Int. Rev. Cytol.* **165**, 159-205
- Mitcgison, T. J. and Cramer, L. P., 1996, "Actin-based cell motility and cell locomotion", *Cell* **84**, 371-379
- Mogilner, A. and Oster G., 1996, "Cell motility driven by actin polymerization", *Biophysical Journal* **71**, 3030-3045

- Moscona, A. A., 1960, "Patterns and mechanisms of tissue reconstruction from dissociated cells" In *Developing Cell Systems and Their Control*, Ed. Rudnick, D., Academic Press, New York, 45
- Moury, J. D. and Schoenwolf, G. C., 1995, "Cooperative model of epithelial shaping and bending during avian neurulation: autonomous movements of the neural plate, autonomous movements of the epidermis, and interactions in the neural plate/epidermis transition zone" *Developmental Dynamics* Vol. 204, 323-337
- Nagele, R.G. and Lee, H.Y., 1979, "Ultrastructural changes in cells associated with interkinetic nuclear migration in the developing chick neuroepithelium", *J. Exp. Zool* 210, 89-106
- Nardi, J.B.; 1981, "Epithelial invagination: Adhesive Properties of Cells Can Govern Position and Directionality of Epithelial Folding", *Differentiation*. 20, 97-103
- Needham, D. and Hochmuth, R. M.; 1990, "Rapid flow of passive neutrophils into a 4 mm pipette and measurement of cytoplasmic viscosity", *J. Biomech. Eng.* 112, 269-276
- Noble, P. B. and Levin, M. D.; 1986, *Computer-assisted analyses of cell locomotion and chemotaxis*, CRC press, Inc. Boca Raton, Florida
- Odell, G.M., Oster, G.F., Alberch, P. and Burnside, B., 1981, "The mechanical basis of morphogenesis, I. epithelial folding and invagination" *Developmental Biol.* Vol. 85, 446-462
- Ohmori, T. and Meada, Y.; 1986, "Implications of differential chemotaxis and cohesiveness for cell sorting in the development of *Dictyostelium*", *Develop. Growth and Differ.*, 28 (2), 169-175.
- Opas, M., 1995, "Cellular adhesiveness, contractility, and traction: stick, grip, and slip control", *Biochem. Cell Biol.*, 73, 311-316
- Oster, G.F., 1987, "The physics of cell motility", *J. Cell Sci. Suppl.*, 8, 35-54
- Preston, T. M., King, C. A. and Hyams, J. S., 1990, *The cytoskeleton and Cell Motility*, Chapman and Hall, New York
- Phillips, M.H. and Steinberg, M.S., 1969, "Equilibrium measurements of embryonic chick cell adhesives, I. shape equilibrium in centrifugal fields," *Proc. Natl. Acad. Sci. USA.*, 64, 121-127

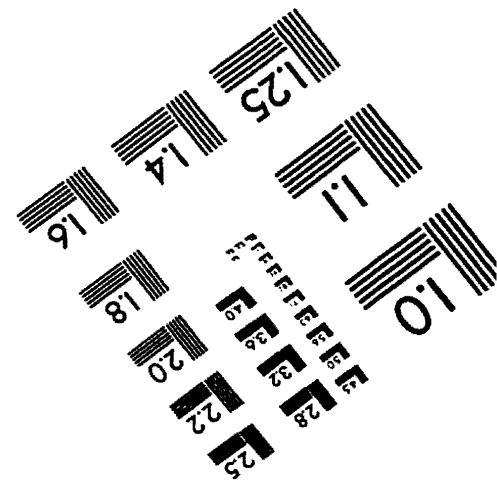
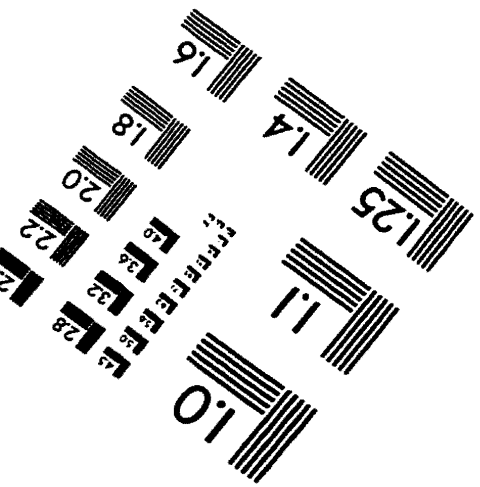
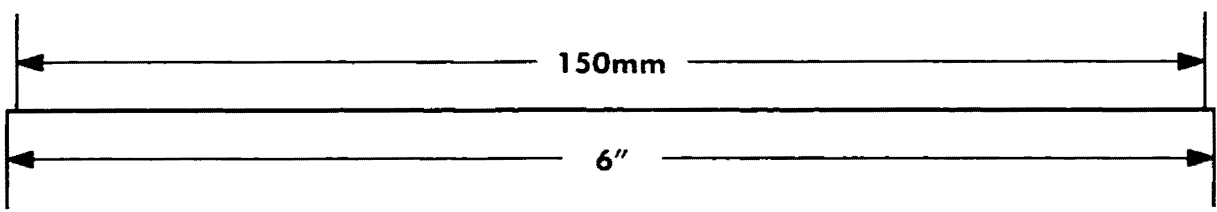
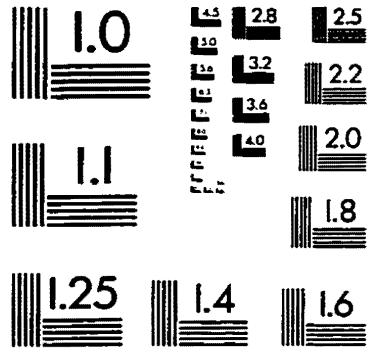
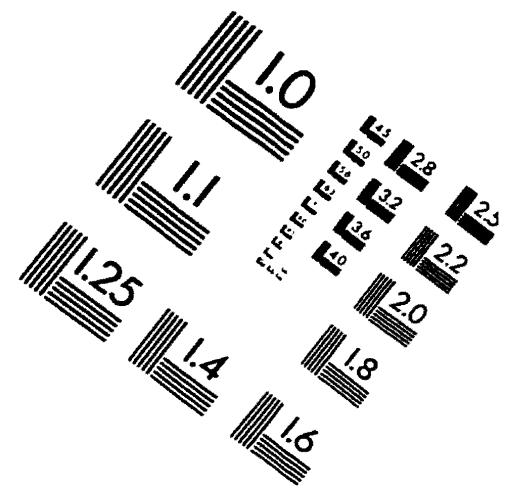
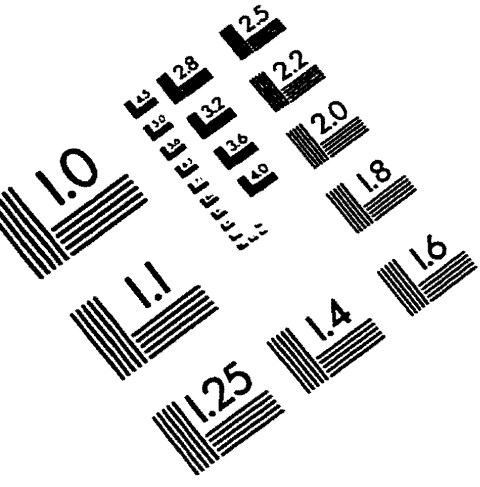
- Phillips, H.M. and Steinberg, M.S., 1977, "Embryo tissue as elasticoviscous liquids II. direct evidence for cell slippage in centrifuged aggregates," *Devel. Biol.*, **59**, 124-134
- Phillips, H.M. and Steinberg, M.S., 1978, "Embryo tissue as elasticoviscous liquids I. rapid and slow shape changes in centrifuged cell aggregates", *J. Cell Sci.*, **30**, 1-20
- Phillips, H.M. and Steinberg, M.S., 1984, "Physical analysis of tissue mechanics in Amphibian gastrulation " *J. Amer. Zool.* , **24**, 657-672
- Rakic, P., 1985, "Contact Regulation of Neurinal Migration" In *The Cell in Contact.*, Ed. Edelman, G.M. and Thiery, J., John Wiley & Sons, Inc. 67-91
- Rappaport, R., 1977, "Tensiometric studies of cytokinesis in cleaving sand dollar eggs," *J. Exp. Zool.*,**201**, 375-378
- Revel, J-P., Yancey, S. B. and Nicholson, B. J.; 1985, "Biology of gap junction molecules and development", In *The Cell in Contact* (ed. Edelman, G.M and Thiery, J), 411-425
- Roth, S. and Weston, J. A., 1967, "The measurement of intercellular adhesion", *Proc. Natl. Acad. Sci. USA*, **58**, 974-980
- Roush, W., 1995, "Cell movement tale told by bacterial tail protein," *Science*, **269**, 30-31
- Ruoslahti, E and Öbrink, B., 1996, "Common Principles in Cell Adhesion", *Expl. Cell Research.*, **227**, 1-11
- Rutishauser, U., Thiery, J. -P., Brackenbury, R., and Edelman, G. M., 1976, "Mechanisms of adhesion among cells from neural tissues of the chick embryo", *Proc. Natl. Acad. Sci. USA*, **73**, 577-581
- Rutishauser, U., Thiery, J. -P., Brackenbury, R., and Edelman, G. M., 1977, "Adhesion among neural cells of the chick embryo. III. Relationship of the surface molecule CAM to cell adhesion and the development of distotypic patterns", *J. Cell Biol.*, **79**, 371-381
- Sausedo, R. A. and Schoenwolf, G.C., 1994, "Quantitative analyses of cell behaviors underlying notochord formation and extension in mouse embryos," *Anat. Rec.*,**239**, 103-112

- Schmidt, C. E., Horwitz, A. F., Lauffenburger, D. A. and Sheetz, M. P., 1993, "Integrin-cytoskeletal interactions in migrating fibroblasts are dynamic, asymmetric, and regulated", *J. Cell Biol.*, **123**, 977-991
- Schoenwolf, G.C. and Alvarez, I. S., 1989, "Roles of neuroepithelial cell rearrangement and division in shaping of the avian neural plate," *Development*, **106**, 427-439
- Schoenwolf, G.C. and Smith, J. L., 1990, "Mechanisms of neurulation: traditional viewpoint and recent advances," *Development*, **109**, 243-370
- Schoenwolf, G.C., 1991, "Cell movement driving neurulation in avian embryo," *Development Supplement*, **2**, 157-168
- Schoenwolf, G.C., Folsom, D. and Moe, A., 1988, "A reexamination of the role of microfilaments in neurulation in the chick embryo", *Anat. Rec.*, **220**, 87-102
- Shyy, J. Y. J. and Chien, S., 1997, "Role of integrins in cellular responses to mechanical stress and adhesion", *Curr. Opin. Cell Biol.*, **9**, 707-713
- Small, J. V., Herzog, M. and Anderson, K., 1995, "Actin filament organization in the fish keratocyte lamellipodium", *J. Cell Biol.*, **129**, 1275-1286
- Spratt, N.T., Jr. 1946, "Formation of the primitive streak in the explanted chick blastoderm marked with carbon particles", *J. Exp. Zool.*, **103**, 259-304
- Stein, M. B. and Gordon, R., 1982, "Epithelia as bubble rafts: a new method for analysis of cell shape and intercellular adhesion in embryonic and other epithelia", *J. theor. Biol.*, **97**, 625-639
- Steinberg, M.S., 1962a, "On the mechanism of tissue reconstruction by dissociated cells, I. population kinetics, differential adhesiveness, and the absence of directed migration" *Proc. Natl. Acad. Sci. USA.*, **48**, 1577-1582
- Steinberg, M.S., 1962b, "On the mechanism of tissue reconstruction by dissociated cells, II. time-course of events" *Science.*, **137**, 762-763
- Steinberg, M.S., 1962c, "On the mechanism of tissue reconstruction by dissociated cells, III. free energy relations and the reorganization of fused, heronomic tissue fragments" *Proc. Natl. Acad. Sci. USA.*, **48**, 1769-1776
- Steinberg, M.S., 1970, "Does differential adhesion govern self-assembly processes in histogenesis? equilibrium configurations and the emergence of a hierarchy among populations of embryonic cells," *J. Exp. Zool.*, **173**, 395-434

- Steinberg, M.S. and Wiseman, L.L., 1972, "Do Morphogenetic Tissue Rearrangements Require Active Cell Movements? The Reversible Inhibition of Cell Sorting and Tissue Spreading by Cytochalasin B" *J. Cell Biol.*, **55**, 606-615
- Steinberg, M.S., 1975, "Adhesion-guided multicellular assembly: a commentary upon the postulates, real and imagined, of the differential adhesion hypothesis, with special attention to computer simulations of cell sorting" *J. theor. Biol.*, **55**, 431-443
- Steinberg, M.S. and Takeichi, M., 1993, "Experimental specification of cell sorting, tissue spreading, and specific spatial patterning by quantitative differences in cadherin expression" *Proc. Natl. Acad. Sci. USA.*, **91**, 206-209
- Steinberg, M. S., 1996, "Adhesion in Development: An Historical Overview", *Dev. Biol.*, **180**, 377-388
- Sullivan, S. J., Daukas, G. and Zigmond, S. H., 1984, "Asymmetric distribution of the chemotactic peptide receptor on polymorphonuclear leukocytes", *J. Cell Biol.*, **99**, 1461-1467
- Sulsky, D., Childress, S. and Percus, J. K., 1984, "A model of cell sorting", *J. Theor. Biol.*, **106**, 275-301
- Swaminathan, R. Bickness, S. and Verkman, A. S.; 1996, "Cytoplasmic viscosity near the cell plasma membrane: transitional diffusion of a small fluorescent solute measured by total internal reflection-fluorescence photobleaching recovery", *Biophys. J.* **71**, 1140-1151
- Taber, L. A., Hu, N., Pexieder, T., Clark, E. B. and Keller, B. B, 1993, "Residual strain in the ventricle of the stage 16-24 chick embryo", *Circ. Res.*, **72**, 455-462
- Taber, L. A., Lin, I-E. and Clark, E. B., 1995, "Mechanics of cardiac looping", *Dev. Dynamics*, **203**, 42-50
- Taber, L. A. and Perucchio, R., 1996, "Computational models for cardiac looping", *ASME 1996 Advances in Bioengineering*, BED **33**, 411-412
- Takeichi, M., Yoshida-Noro, C., Shirayoshi, Y. and Hatta, K., 1985, "Calcium-dependent cell-cell adhesion system: its molecular nature, cell type specificity, and morphogenetic roles" *The Cell in Contact.*, Ed. Edelman, G.M. and Thiery, J., John Wiley & Sons, Inc. 219-232.

- Thomas, W. A. and Yancey, J., 1988, "Can retinal adhesion mechanisms determine cell-sorting patterns - a test of the differential adhesion hypothesis", *Development*, **103** (1), 37
- Thorpe, N.O., 1984, *Cell Biology*, John Wiley & Sons, USA, 600-635
- Townes, P. S. and Holtfreter, J., 1955, "Directed movements and selective adhesion of embryonic amphibian cells," *J. Exp. Zool.*, **128**, 53-120
- Trinkaus, J. P., 1970, *Cells into Organs*, Englewood Cliffs, New Jersey: Prentice Hall
- Valberg, P. A. And Albertini, D. F., 1985, "Cytoplasmic motions, rheology, and structure probed by a novel magnetic particle method", *J. cell. Biol.*, **101**, 130-140
- vanMierop, L. H. S., oppenheimer-Dekker, A. and bruins, C. L. D., 1978, *Embryology and teratology of the heart and the great arteries*, Leiden university Press, The Hague.
- Weliky, M. and Oster, G., 1990, "The Mechanical basis of cell rearrangement," *Development*, **109**, 373-386
- Weiss, P. and Taylor, A. C., 1960, "Reconstitution of complete organs from single-cell suspensions of chick embryo in advanced stages of differentiation," *Proc. Natl. Acad. Sci. U.S.*, **46**, 1177-1185
- Weber, K. and Osborn, M., 1981, "microtubule and intermediate filament networks in cells viewed by immunofluorescence microscopy", In *Cytoskeletal Elements and plasma Membrane Organization*, (ed. Poste, G), North-Holland Publishing Co. Amsterdam, 1-53
- Wilson, H. V., 1907, *J. Exptl. Zool.*, **5**, 245
- Wilson, P. A., Oster, G. and Keller, R., 1989, "Cell rearrangement and segmentation in *Xenopus*: direct observation of cultured explants," *Development*, **105**, 155-166
- Wolpert, L. and Gingell, D., 1968, "Cell surface membrane and amoeboid movement", In *Aspects of Cell Motility*, The University Press, Cambridge, 169-198
- Zackson, S. L. and Steinberg, M. S., 1987, "Chemotaxis or adhesion gradient? pronephric duct elongation does not depend pm distant sources of guidance information," *Devel. Biol.* **124**, 418-422

# IMAGE EVALUATION TEST TARGET (QA-3)



APPLIED IMAGE, Inc  
 1653 East Main Street  
 Rochester, NY 14609 USA  
 Phone: 716/482-0300  
 Fax: 716/288-5989

© 1993, Applied Image, Inc., All Rights Reserved